Theses and Dissertations

2008

Development of a LIBS system for prediction of ash fusion temperature in coal-fired power plants

Ricardo X. Moreno
Lehigh University

Follow this and additional works at: http://preserve.lehigh.edu/etd

Recommended Citation

Moreno, Ricardo X.

Development of a LIBS System for Prediction of Ash Fusion Temperature in Coal-Fired Power Plants

September 2008

Development of a LIBS System for Prediction of Ash Fusion Temperature

in Coal-fired Power Plants

by

Ricardo X. Moreno

Presented to the Graduate and Research Committee

of Lehigh University

in Candidacy for the Degree of

Master of Science

in

Mechanical Engineering and Mechanics

Lehigh University

July 1st, 2008

This thesis is accepted and approved in partial fulfillment of the requirements for the Master of Science.

_7-3-08_

Date

Dr. Edward K. Levy

Thesis Advisor

Dr. Carlos E. Romero

Thesis Co-Advisor

Dr. Gary Harlow

Chairperson of Department

ACKNOWLEDGEMENTS

LIST OF CONTENTS

LIST OF TABLES

LIST OF FIGURES

ABSTRACT

Almost half of the electric power generated in the U.S. is derived from coal, with coal-fired utility boilers. The fact that coals with different characteristics than those that the boilers were designed to work with are fired in the boilers, represents a challenge to the engineers in charge of boiler operations. Operational actions have to be taken in order to avoid and/or mitigate major slagging events inside the boiler, which significantly lower the efficiency of the boiler and can cause internal damage, which can lead to an eventual unexpected shut-down of the unit (with associated financial losses). Information on coal elemental composition, and some other characteristics of the coal, like ash fusion temperatures, can help make decisions on these operational actions. The coal-ash fusion temperature is a parameter widely used as a slagging propensity index of coal. However, this type of information is not typically provided to the boilers operators in a timely manner.

This thesis reports development of laser-induced breakdown spectroscopy (LIBS) spectral-based models for determination of the coal-ash elemental composition and the coal-ash initial deformation temperature. Both laboratory and field testing were carried out. An artificial intelligence (AI) based model was developed, through an artificial neural network (ANN) approach, to predict coal-ash initial deformation temperature, based on LIBS intensity measurements and a coal database. It was found that LIBS analyses can produce coal composition results that correlate well with the American Society for Testing and Materials (ASTM) analyses results, for magnesium,

1

sodium, silicon, and titanium. While further development needs to be carried out for better correlation with iron, potassium, calcium, and aluminum, the lack of accuracy in the prediction of these elements does not preclude accurate prediction of fusion temperature. The ANN model for coal-ash initial deformation temperature prediction was tested in the field with real coals fired at a 630 MW$_g$ coal-fired utility boiler. It was found that the LIBS-based model predicts fusion temperature with an average uncertainty of ±133 °F as compared to the ASTM analyses, and has a reproducibility of ±58 °F. These results are satisfactory, given that the inherent uncertainty of the ASTM ash fusion temperature test data can be as high as 176 °F.

CHAPTER 1

Introduction

Over forty eight percent of electric power generated in 2007 in the U.S. was derived from coal [1]. Coal is a complex assembly of organic and inorganic material, the structure and composition of which vary considerably according to rank and geographic locality [2]. The inorganic component can exist as a separate phase or as inorganic elements chelated or ionically bound to the organic component. Mineral matter is often detrimental to many of the processes that utilize coal, including the direct production of electric energy. For example, the high pyritic content of certain coals is an obvious source of sulfur dioxide (SO_2) pollution in combustion. Nowadays, most energy derived from coal is produced using combustion furnaces which emit significant amounts of pollutants including greenhouse gases, SO_2, nitrogen oxides (NO_x), and heavy metals. Beside these problems inherent to coal, slagging of heat transfer surfaces due to ash deposition represents a serious problem for coal-fired utility boilers. Slagging refers to deposits within the furnace which take place in the hottest parts of the boiler, in areas directly exposed to flame radiation (waterwalls and spaced pendant superheaters), and is mainly derived from the mineral matter in the coal.

Molten ash deposits stick to the tubes and wall surfaces, thus, reducing heat transfer and thermal efficiency. This results in reduced steam temperatures, increased fuel firing rates, increased fan power (to overcome larger pressure drops in the convective pass), and high rates of corrosion. Heavy slag deposits in the waterwall

3

regions of coal-fired boilers can reduce local radiation heat transfer by as much as fifty percent, resulting in increased furnace exit flue gas temperatures (FEGT) and higher rates of thermal NO_x formation [3]. With partial blockage between convective pass tube banks, increased gas velocities can result, which are often associated with erosion. Additionally, corrosion underneath slag deposits can occur, as well as major incidents of internal boiler damage can also occur, due to fused ash material falling to the bottom of the boiler [4]. Overall, slag related reduction in boiler thermal efficiency and increase in stack emissions can result in substantial revenue losses and power cost increases. These problems are sufficiently serious, in terms of their cost implications, to justify considerable research and development efforts to improve understanding of the behavior of inorganics in coal-fired boilers. These efforts should improve the possibility of predicting and quantifying the effects of feedstock changes. However, both boiler manufacturers and utility boiler operators agree that a reliable prediction of ash deposition and its effects continues to be a difficult task.

The problems described in the proceeding paragraphs are exasperated due to stringent SO_2 and NO_x emission limits, which have forced coal-fired plants that fire Eastern U.S. bituminous coals to fire coals and fuel blends with different characteristics than the design coals. As a consequence, there has been a recent growth in the use of foreign coals and the use of Western U.S., low-sulfur, low-rank coals to replace high-sulfur Eastern U.S. bituminous coals. Typically, the average nitrogen and sulfur bound content of these coals and blends is lower, the gross calorific is lower, the ash loading is smaller and the moisture content is higher than the traditional Eastern U.S. bituminous coals. Slagging problems are aggravated with the use of these off-design low-rank coals because FEGT levels are higher when firing low-rank coals in

4

comparison to more traditional Eastern U.S. bituminous coals. This increase is, in part, due to the more reflective nature of the low rank ash that deposits on the waterwalls. In addition, the ash fusion temperatures of the off-design coals are lower. Slagging becomes prevalent when the flue gas temperature exceeds the coal-ash fusion temperature, thus, allowing soft, sticky, plastic deposits to form on tubes and walls.

The behavior of mineral matter is difficult to predict under the complex conditions which arise in a coal-fired utility furnace and its associated heat transfer equipment. Numerous empirical indices, which have had some success in predicting slagging propensity, have been developed for assessing the slagging potential of coal. A commonly used descriptor for the prediction of high-temperature deposition behavior, based on laboratory coal-ash analysis, is the base-to-acid ratio, where base and acid are simply the sums of the weight percentages of the basic and acidic oxides.

Many boiler manufacturers and utility operators have developed their own indices to provide criteria to various aspects of boiler design and operation. All these indices are based on laboratory coal-ash analyses and/or fusion temperatures. Coal yard and boiler operators are rarely equipped to cope with variability in coal composition introduced naturally by geological circumstances or by coal blending resulting from seasonal adjustments in coal supply and reclaim. The best available option is the off-line measurement of coal properties, in the laboratory, and reporting to the operators some simple index that provides limited information on the coal and its properties. These measurements are carried out irregularly and rarely available to the boiler operator in a timely manner. Hence, there is a need for the development of

technology, capable of monitoring coal slagging-related composition and determining a slagging potential indicator, in real time.

There are two different commercially available real-time coal analyzers in the market. These analyzers mainly work on a nuclear source-based principle or based on X-Ray fluorescence (XRF) technology. The nuclear-based instruments typically utilize a Prompt Gamma Neutron Activation Analysis (PGNAA) to provide continuous monitoring of coal composition. This technology is fundamentally designed for conveyor belt-mount applications, for use in material sorting and blending, and raw material proportioning. The main drawback of the nuclear-based instrument is the need of an isotope source, and the permitting, handling and replenishing associated with a nuclear source. Additional drawbacks of the nuclear instruments include their high initial cost, large footprint, specific design for coal yard installations, and requirements for calibration and automatic compensation for nuclear source decay. Furthermore, yearly maintenance costs are high due to the radiation source used.

The XRF technology-based instruments have not been as extensively deployed in coal-fired power plants as nuclear-based instruments. The XRF technology can only measure elements with atomic numbers greater than 11 (like sodium), which means that it needs elaborate algorithms for a full report of coal and ash composition. The main drawback of the XRF technology is the reported difficulty in detecting carbon, hydrogen and nitrogen in the coal, and it's requirements for calibration. Typically, a monthly calibration service is recommended.

The use of Laser-induced Breakdown Spectroscopy (LIBS) represents an alternative method to meet the needs of the power generation industry. LIBS is a

6

technology based on laser interaction with a matrix. When a pulsed laser beam of high density is focused on a certain material, it generates plasma from that material, termed laser induced plasma (LIP). This phenomenon has led to applications in many fields of science from thin film deposition to elemental analyses of gaseous, liquid, and solid samples [6]. The LIBS technology is based on emission spectroscopy, which can be used for elemental analysis of targets from which the plasma is generated, as well as for determination of temperature, electron density and atom density in the LIP.

The LIBS technology applied to elemental coal composition analysis has been studied, mainly, by two research groups. One of the groups is the Cooperative Research Centre for Clean Power From Lignite, in Mulgrave Victoria, Australia [7, 8]; and the other one is a joint group formed by the Sandia National Laboratories, Combustion Research Facility, in Livermore, California; and the Applied Laser/Optics Group, Physics Department, New Mexico State University, in Las Cruces, New Mexico [9, 10]. These groups have used the LIBS technology to determine coal composition of a variety of North American and Australian bituminous and lignite coals.

The objective of this study is to investigate the feasibility of using a combination of LIBS-derived coal elemental composition determination and ash fusion temperature correlation. Determination of ash fusion temperature was carried out through an Artificial Neural Network (ANN) approach. An ANN is an interconnected group of artificial neurons that uses a mathematical or computational model for information processing. An ANN typically changes its structure based on external or internal information that flows through the network, using different training algorithms, becoming an adaptive system. In more practical terms, an ANN is a non-linear data

modeling tool, commonly used to establish correlations between input and output parameters in systems and/or processes that are usually very complicated to model using a traditional numerical modeling approach.

This thesis reports work performed to investigate the applicability of the LIBS-ANN technology to coal-fired utility boilers for determining the coal elemental composition and, more importantly, the ash fusion temperature of the coal as a useful slagging index. A LIBS-based laboratory configuration was assembled. Sixteen coals, from different locations, and with different elemental composition and slagging potential were collected, creating a coal bank. The coal inventory was tested with the LIBS system in the laboratory, and the data collected were used to develop calibration curves for coal elemental composition determination and ANNs, to predict the initial deformation temperature of the coal-ashes. The system showed LIBS elemental composition measurement uncertainty in the range of ±18 percent, and below, for all elements of interest (Al, Ca, Mg, Na, Fe, Si, Ti, and K). The uncertainty in the LIBS measurements for elemental composition detection, as compared to the American Society for Testing and Materials (ASTM) standardized measurements, was of the order of ±14 percent, for all elements of interest except for potassium and magnesium, which were not detected with that degree of uncertainty. However, for the coal-ash initial deformation temperature prediction, the root mean square error, between LIBS and ASTM measurements, was ±133 °F and the prediction repeatability was ±58 °F, with 99 percent confidence level.

The LIBS-ANN approach was taken to a power station and tested at a 650 MW coal-fired utility boiler, using three different coals. These coals have different historical

slagging potential and different elemental composition. The results obtained from the plant testing were very encouraging, since the system was able to identify the coal-ash initial deformation temperature for each coal. The information determined by the LIBS-ANN system can be provided in a timely manner to boiler operators and then used to optimize pertinent operating parameters to mitigate the coal slagging impact. The benefits obtained from the LIBS-ANN technology could be very significant in the coal-fired power industry, resulting in lower emissions, enhanced thermal efficiency, increased revenues, and reduced power costs.

CHAPTER 2

Literature Review

A literature review pertinent to this project and in the area of coal-fired boilers slagging control must include a description of coal, a definition of slagging, slagging propensity and slagging indices; the ASTM methodology for elemental coal analysis, and non-intrusive techniques for elemental coal analysis. In addition to the definitions and methodology descriptions mentioned in the previous sentences, this chapter describes in more detail the principles and functionality of the LIBS technology. A review of previous work carried out in research related to the one of this thesis and the respective results are also mentioned and briefly described in this chapter.

Coal is a highly variable, heterogeneous, fossilized material that formed from ancient plant material exposed to elevated temperatures and pressures after burial. Vegetation grew in great swamps in the equatorial climate, which accumulated the organic debris hundreds to thousands feet depth. Detrital minerals washed into the swamps and were incorporated as sediment into the accumulating organic remains of the great ferns and related plants. With time, the debris was buried and underwent anaerobic decay and compaction from the overlying mass of cover. It is roughly considered that one foot of coal resulted from ten feet of original organic debris. These plants bio-accumulated heavy metals as part of their metabolism, which were further concentrated during the coal formation process [12]. In addition to the major elements of carbon, oxygen, hydrogen, nitrogen, and sulfur, coal also contains varying levels of

trace elements such as sodium, mercury, chlorine, etc. Coal occurs in association with various types of inorganic minerals. Some elements such as sulfur occur in both the organic and inorganic coal fractions. The inorganic minerals, deposited along with the plant material, are inherent and make up, typically, 5 to 10 percent of the coal. It is principally these incombustible materials that form the "ash" that remains after combustion of the coal [13]. Strictly, coal does not contain ash. The "ash" is, however, a convenient and widely used term which quantifies the solid residue that remains after the coal is burned. The term mineral matter refers to inorganic constituents in coal and is all of the elements that are not part of the organic coal substance (carbon, hydrogen, nitrogen, oxygen, and sulfur).

A large number of distinct mineral phases have been reported in various coals. Although, lists of mineral in coal may contain as many as 50 to 60 minerals, most fall into one of five groups:

(1) Alumino-silicates (clay minerals) – These are the most common inorganic constituents of coal and of the strata associated with coal seams. Many different clay minerals have been reported within and associated with coals, but the most common clay minerals are kaolinite and mixed-layer Illite-montmorillonite. Kaolinite-rich clay is commonly found within coals in most of the coal basins of the world. They are generally called either tonstein or kaolin-tonstein.

(2) Sulfide minerals – The dimorphs pyrite (FeS_2) and marcasite (FeS_2) are the dominant sulfide minerals in coal; pyrite is the more abundant. Pyrite and marcasite have different crystal forms; pyrite is isometric and marcasite is

orthorhombic. These two minerals are readily observed and, to some degree, easily removed, as well as being especially interesting because they contribute significantly to the total sulfur content that causes boiler tube fouling, corrosion, and pollution by emission of sulfur dioxide (SO_2).

(3) Sulfate minerals – The sulfate minerals identified in coal do not generally comprise a significant portion of the mineral matter in fresh, unoxidized coal samples. However, the Iron disulfides oxidize rapidly after the coal is mined, and a number of hydrated sulfates ($FeSO_4 \cdot xH2O$) have been reported in weathered coals and in coal refuse banks. The sulfates gypsum ($CaSO_4 \cdot 2H_2O$) and barite (Ba_2SO_4) are found in fresh coal. Most of the sulfates that form on weathering (oxidation) of pyrite are various hydrated states of ferrous and ferric sulfate.

(4) Carbonate minerals – The major cations found in the carbonate minerals in coals are calcium, magnesium, and iron. The member calcite ($CaCO_3$) is dominant in some coals, whereas siderite ($FeCO_3$) is dominant in others. Calcite and ankerite (a mixed crystal composed of Ca, Mg and Fe carbonates) are abundant in some coals.

(5) Silicate minerals – Quartz is the dominant form in which silica is found in coals, and it is everywhere. There is some distinction between clastic grains of quartz introduced by wind or water and authigenic quartz deposited from solutions. Quartz is also a major component of clay and siltstone partings in coal that are of detrital origin.

(6) Other minerals – A large number of minerals, in addition to those already discussed, have been reported to occur in coal. Not all have been positively

identified, and often it is impossible to determine from the reports whether the mineral was intimately associated with the seam. Most of these other minerals are of limited significance in coal utilization, but few are worth noting. As an example, authigenic apatite [calcium fluorochlorohydroxyphosphate, $Ca_5(PO_4)_3 \cdot F \cdot Cl \ OH$] has been found in coal produced in widely separated areas of the world.

Generally speaking, in practice, the chemical composition of coal-ash is typically made up of silicon, calcium, aluminum, iron, magnesium, and sulfur oxides, along with carbon and various trace elements. These elements are found in the ash because of their high melting points and the short time the ash particles actually remain in the furnace during combustion. The mineral quartz (SiO_2) survives the combustion process and remains as quartz in the coal-ash. Other minerals decompose, depending on the temperature, and form new minerals. The clay minerals lose water and many melt, forming alumino-silicate crystalline and non-crystalline (glassy) materials. Elements such as iron, calcium, and magnesium combine with oxygen in the air to form oxide minerals, such as hematite (Fe_2O_3), lime (CaO), and perticlase (MgO).

Conventional coal combustion for electric power generation involves pulverizing the raw coal into small particles and injecting it into the boiler's furnace, where it is burned in a long luminous flame at temperatures in the order of 2,700 °F or greater. Temperatures this high melt 70 to 90 percent of the mineral phases, leaving fused mineral impurities (coal-ash). Approximately, one fifth of the ash particles fall to the bottom of the furnace. The rest of the fused matter is transported further up the furnace. Some of the matter solidifies into crystalline and non-crystalline glassy phases

that are carried out of the furnace with the flue gas, typically referred to as fly ash. However, some of the matter remains fused when touching some of the furnace heat exchanging surfaces and then solidify, creating a layer of "ash deposits" on these surfaces, which are highly detrimental for the electric generating process.

Ash deposits formed from the combustion of coal have plagued with problem the steam production, and more specifically the electric power generation industry from the start. As power plant size increased, so have the problems associated with ash deposits. There are two basic forms of ash deposits: molten ash and alkali salts. The molten deposits are called slag and occur primarily in the furnace area of the boiler (the hottest parts), and areas directly exposed to flame radiation (waterwalls and spaced pendant superheaters). The alkali salts are called fouling and generally occur in the convection or cooler portions of the boiler and duct work, they are bonded together by sulfate salts. This thesis work is focused specifically on slagging problem control in utility boilers.

Typically, deposits may consist of one or more types of slag [15]:

(1) Metallic – These slags have a metallic luster and are usually associated with combustion of pyrite-rich coals under reducing conditions. The high specific gravity of the metal generally allows it to separate from slag, and to remain isolated at any subsequent oxidizing atmosphere.

(2) Amorphous – These slags are dark, solid, glassy, and generally show a conchoidal fracture. Amorphous slags are usually found in the higher temperature regions of the boiler.

14

(3) Vesicular – These are glassy slags with trapped bubbles (a sponge-like appearance). These slags are also associated with higher temperature regions in the furnace; they can also be found associated with sintered type deposits in the hotter regions of the convection pass. Trapped gas bubbles may be distorted due to viscous flow.

(4) Sintered – These are deposits that are composed of partially fused particles. They are gritty in texture, are typically found in the upper furnace and convection passes, and may be associated with vesicular slags.

Most slagging deposits form from coals that have pyrite as a major component. The iron from the pyrite reacts with the alumino-silicates (clays) to form low melting point or low viscosity molten deposits. There are no distinct melting points for coal-ash like with ice or other pure compounds, thus, when melting is mentioned, it is used to represent a decrease in viscosity, rather than a melting point. When coal-ash melts, it occurs in both a large scale and a microscopic scale. On the large or bulk scale, the ash behaves like a glass. As the temperature of the material increases, its viscosity decreases. At temperatures less than 2000 °F, the ash may appear solid, or at least stiff. On a microscopic scale several minerals may have already melted, but their concentrations are low compared to other minerals with higher melting temperatures. As the temperature is increased, the ash becomes less viscous or more liquid like. Many reactions can then occur between the minerals as they melt and become more fluid. As the molten components mix, they become more like molten glass. This molten material starts to dissolve the non molten materials like quartz and other minerals. In this way, the melting temperature of minerals such as sandstones and shales are lowered by other minerals such as pyrite and limestone.

15

There are a number of undesirable effects associated with the deposition of ash on heat transfer and other surfaces within the boiler. Some of the main effects have been summarized by Couch (1994):

- Reduction of heat transfer due to solid or liquid deposits. This leads to a reduction in the amount of heat exchanged between the combustion gases and the circulating water-steam. It, therefore, leads to an increase in gas temperature (as it is not being cooled effectively), which readily leads to an increase in the rate or amount of deposition. This also results in continually changing conditions in the boiler.
- The formation of sticky surfaces which then collect other particles.
- The fouling of surfaces in the convective section of the boiler by the condensation of volatile species.
- The formation of large clinkers on heat transfer tubes. These can weigh several tons and can physically distort the tubes (possibly leading to premature failure) and be a substantial hazard when attempts are made to remove these deposits during a shut-down.
- Increased rates of corrosion and erosion which can either be direct effects of the deposition or due to the sootblowing, which is necessary.
- Large slag falls during operation.

Deposition can and does take place in various parts of the boiler. The effects are different, depending on where deposition occurs, and in many situations it may be possible to control deposition by sootblowing. Sootblowing is a process in which steam, water or air are used, through lances, to dislodge and clean the surfaces within the

16

boiler. It is where there is a long-term accumulation which is not easily removed, or where there is a very rapid short-term accumulation, that there are potential problems.

The main locations of deposition are shown in Figure 2-1, and the numbers refer to those in the figure [4]:

(1) Ash hopper bridging is a major cause of unplanned outage. It is usually caused either by slag running down the boiler walls and solidifying or by large sintered deposits falling off the tube platens high up in the boiler and falling into the hopper. The incidence of bridging is largely unpredictable, but coals with high iron content and low ash fusion temperatures are particularly susceptible. High heat content resulting in high flame temperature can also have an effect. Slag bridges may be removed by thermal shock (from a load reduction or water lancing), by mechanical prodding or, ultimately during a shut-down. In severe cases the bridge may have to be removed with the help of explosives.

(2) Accumulations on the hopper slope may be due to other accumulations higher up in the boiler coming loose and dropping down. This may damage the tubes. If an ash slab on the slope breaks loose, it may slide down and bridge over the hopper exit.

(3) Burner "eyebrows" can form above or below the burner mouth. These can distort the flow pattern from the burner, and in severe cases cause quarl damage and flow blockage. They can develop into large lumps of slag hanging onto the burner tip. The problem is difficult to diagnose and correct.

(4) Wall slag can occur where coals with a low ash fusion temperature and/or high heating value are burned. The interaction between burner type and boiler

17

Figure 2-1. Arrangement of Heat Transfer Surfaces, and Regions of Slagging and Fouling in Typical Boilers (Couch, 1994).

dimensions can be critical, and the degree of swirl on short flame turbulent burners is critical. Minimizing local reducing conditions is critical, by ensuring a sufficient air supply. Particle size is important, and a coarse grind may result in local slagging.

(5) In certain boiler designs, slag can form on internal division walls within the furnace. In some severe cases, the walls have had to be removed.

(6) Sintered/fused ash deposition can cause "birdsnesting" in tube platens. These build-up first on the bottom of the platens, and may be removed fairly easily. Larger accumulations of ash are difficult to remove while the boiler is in operation and can become considerably harder with age. They can eventually bridge across the tube bank and cause a major distortion of flow patterns. This results in erosion and increased pressure drop, and may cause tube distortion. Larger accumulations can eventually fall off, possibly damaging burners and the main boiler hopper.

(7) Convection bank bonded deposits are often the result of condensing alkali metal sulphates. Hard thick deposits can form as other particles stick to the surface. The initial deposits may be difficult to remove, and can be the cause of tube corrosion. Some deposits may be removed by differential expansion during load variations, especially when tubes are made of austenitic steels.

(8) Some boilers have finned economizers or heat pipes, and these are particularly vulnerable to the build-up of bonded dust. High calcium content in the ash can exacerbate this problem, although this may not be true for coals with lignitic rather than bituminous type ash [17]. Debris is carried with the flue gas during sootblowing in the higher temperature region of the boiler. Much of this is

collected in the economizer hopper located at the bottom of the back pass of the boiler in a conventional arrangement. Difficulties in cleaning this material are sometimes encountered.

(9) There are sometimes difficulties with ash deposition at the air heater gas inlet. This may be due to large particles being dislodged elsewhere by sootblowing bypassing the earlier collection hopper. A material known as "popcorn ash" sometimes accumulates in air pre-heaters. It has a low density and may have been deposited temporarily, and then removed by sootblowing or by load changes. It then moves further along with the flue gases.

The reduction of heat transfer that results from deposition has a number of significant effects on the overall performance of an electric power station. In particular, for a given output and level of availability, these effects may include (Couch, 1994):

- Increased maintenance cost.

- A reduction in boiler efficiency, and hence in the amount of fuel needed, and in the amount of carbon dioxide (CO_2) formed.

- Increased risk for occurrence of unplanned shut-downs.

- Increased capital cost, typically for new plants.

The main causes of ash deposits are typically related to a combination of three areas: the use of low-rank, off-design coal, plant design and plant operation. The major fuel related causes for ash deposition are:

- Large pyrite particles that impact the furnace wall before they completely combust.

20

- Clay minerals that contain significant amounts of iron, calcium, sodium or potassium causing them to have low melting temperatures.

- Interaction of pyrite, clays and alkalis with alumino-silicates to form low viscosity melts.

- Extremely fine or organically bound alkalis.

The major operational related causes for ash deposition are:

- Sootblowers not in operation or used improperly.

- Poor pulverization of fuel.

- Improper air to fuel ratio.

- Burners damaged or improperly adjusted.

- FEGTs significantly higher than the ash fusion temperature of coal.

- Changes in operation of boiler or other equipment.

The major design related causes for ash deposition are:

- Furnace size too small for fuel release.

- Inadequate tube material and/or spacing.

- Inadequate sootblowing coverage.

- No means provided to observe slag build-up.

Therefore, any preventive action to avoid and/or mitigate ash deposition effects has to include a combination of knowledge on all three areas: the fuel, the plant design, and the plant operation. In old boilers already built and in service, the ash deposition effect has to be attacked from the fuel and operational point of view. The characteristics of the coal (coal composition, coal-ash composition, and ash fusion

temperature) should be known by the boiler operator in order to take operational actions (adjust operational parameters) to prevent and/or mitigate the ash deposition effects.

Experience has shown (Raask, 1985) that for pulverized-coal-fired boilers ("dry ash" boilers), where ash deposition is highly undesirable, the initial deformation temperature and, sometimes, softening temperature observed in ash fusion tests is an important criterion in boiler layout, regarding heat transfer and flue gas temperatures. Design engineers usually aim at limiting the temperature of flue gas entering the convection superheater section to a value below the initial deformation temperature noted in ash fusion tests.

A slagging index based on fusion temperatures has been proposed [19]. This slagging index uses the initial deformation temperature (IT) and the hemisphere temperature (HT) observed in ash fusion tests:

$$F_s = \frac{4\,IT + HT}{5}$$

Eqn. 2-1

Table 2-1 offers a guidance classification on coal-ash slagging propensity based on the F_s temperature.

Table 2-1: Coal-ash Slagging and Temperature Index (Raask, 1985).

Slagging index (F_s) Temperature, K (°F)	Boiler slagging
< 1,325 (1,926)	Severe
1,325 (1,926) – 1505 (2,250)	High
1,505 (2,250) – 1,615 (2,448)	Medium

On the other hand, coal-ash composition has been also used to establish different slagging indices. The eight principal oxide constituents of sulfate-free ash can be divided into those that are acidic in the pyrochemical sense (SiO_2, Al_2O_3, and TiO_2) and those that are basic (Fe_2O_3, CaO, MgO, K_2O, and Na_2O). Several researchers have used the ratio of the sum of basic oxides to the sum of acidic oxides to assess ash deposition effects (slagging propensity) of bituminous and non-bituminous coal ashes. The ratio of basic to acidic oxides in ash is given by

$$R_{b/a} = \frac{Fe_2O_3 + CaO + MgO + K_2O + Na_2O}{SiO_2 + Al_2O_3 + TiO_2}$$ **Eqn. 2-2**

where the constituent oxides are given as weight percent of the total.

Experience has shown that the lowest fusion temperature occurs when the oxide ratio is lower than 0.55. Most bituminous coals have a pyrochemically acidic ash with the $R_{b/a}$ ratio between 0.2 and 0.4. With these coals, additional amounts of basic oxides, Fe_2O_3, CaO, and Na_2O, in ash would increase the slagging propensity, and a maximum value for the $R_{b/a}$ ratio of 0.5 is sometimes specified for pulverized-coal-fired boilers. For cyclone-fired boilers, $R_{b/a}$ values below 0.27 usually result in a slag that is too viscous to flow readily (Raask, 1985).

The two slagging indices mentioned previously (F_s and $R_{b/a}$) are the most commonly used in the industry to assess ash deposition effects. However, there are many other slagging indices. For example, for low-rank Western U.S. coal ashes, the following index has been proposed:

$$F_x = 0.38\,Na_2O + 0.006\,SiO_2 - 0,008\,CaO + 0.062\,Ash + 0.0037$$ **Eqn. 2-3**

where the oxide constituents are expressed as percent of ash by weight and the ash content is given as percent of dry coal by weight. In the case of sub-bituminous coal ashes of high CaO content, additional amounts of silica would enhance the ash deposition characteristics.[*]

Raask [5] also introduced the use of the total amount of alkalis, $Na_2O + K_2O$, in coal to assess its ash deposition propensity:

$$Na_2O_{eq} \text{ of coal} = (Na_2O + 0.659\, K_2O) \frac{ash}{100}$$

Eqn. 2-4

where Na_2O and K_2O are given in weight percent of ash, and "ash" is given in weight percent of coal. The factor 0.659 before K_2O is the molecular weight ratio of Na_2O to K_2O. Table 2-2 shows Na_2O_{eq} values that have been suggested as a guide for bituminous coal-ash. However, this classification assessment, based on the total alkali metal content of coal, does not apply to many sub-bituminous coal-ashes.

The ratio of basic to acidic oxides (Eqn. 2-2) was modified by Attig and Duzy (1969) by introducing a multiplication factor, the Na_2O content of ash:

$$F_y = \frac{(Fe_2O_3 + CaO + MgO + K_2O + Na_2O)}{SiO_2 + Al_2O_3 + TiO_2} Na_2O = R_{b/a} \cdot Na_2O$$

Eqn. 2-5

and

$$F_y{}' = R_{b/a} \cdot (Na_2O)_{ws}$$

Eqn. 2-6

where F_y and F_y' are the slagging indices when Na_2O and $(Na_2O)_{ws}$ denote the total and water-soluble fraction of sodium in ash, respectively. Table 2-3 shows the values of F_y suggested for bituminous and sub-bituminous coal-ash, and F_y' suggested for lignitic coal-ash, respectively.

Another slagging index was derived by Attig and Duzy (1969), based on the ratio of basic to acidic oxides in ash multiplied by the sulfur content of coal:

$$F_s' = \frac{(Fe_2O_3 + CaO + MgO + K_2O + Na_2O)}{SiO_2 + Al_2O_3 + TiO_2} S = R_{b/a} \cdot S \qquad \textbf{Eqn. 2-7}$$

where S denotes the weight percent of sulfur in dry coal. The slagging enhancement factor of sulfur was introduced on the basis that much of sulfur in slagging coals is present as pyrite and the pyrite residue can be an effective fluxing agent. Table 2-4 shows the values of F_s' suggested for bituminous coal-ashes.

Table 2-2: Sodium Equivalent Criterion for Boiler Slagging With Bituminous Coal-ash (Raask, 1985).

Na_2O_{eq} of Coal (weight percent)	Boiler Slagging
< 0.3	Low
0.3 – 0.45	Medium
0.45 – 0.6	High
> 0.6	Severe

Table 2-3: Slagging Propensity of Coal-ashes Assessed from Base/Acid Ratio and Sodium Content (Raask, 1985).

F_y	F_y'	Boiler Slagging
< 0.2	< 0.1	Low
0.2 – 0.5	0.1 – 0.25	Medium
0.5 – 1.0	0.25 – 0.7	High
> 1.0	> 0.7	Severe

Table 2-4: Slagging Index of Bituminous Coal-ashes from Base/acid Ratio and Sulfur Content (Raask, 1985).

F_s'	Boiler Slagging
< 0.6	Low
0.6 – 2.0	Medium
2.0 – 2.6	High
> 2.6	Severe

Once the importance of the coal and coal-ash characteristics to assess ash deposition effects is understood, the reference method processes used to determine both ash fusion temperature and coal-ash composition should be known. The ASTM fusion temperature test is a documented observation of the ash melting process, described previously in Chapter 2. This test occurs in small cone shaped coal-ash, held together by a binder, and placed in a furnace with increasing temperatures, usually ranging from 1,922 to 3,002 °F (1,050 to 1,650 °C). Figure 2-2 shows the critical temperature points of the ash fusion tests. The ash fusion tests commonly performed in fuel laboratories are the ASTM D-1857 and D-1957, which are basically the same tests under oxidizing (like air) and reducing (CO present) furnace conditions, respectively. An equivalent method is the ISO 540.

The ash fusion temperature test involves observing the profiles of carefully shaped cones. The cones are gradually heated in a furnace under either oxidizing or reducing conditions, until the ash softens and melts. The initial deformation temperature, IT (or ID), is usually a hundred or more degrees Fahrenheit larger than the temperature where the first low melting temperature minerals start to melt. This

temperature is identified with the rounding of the cone tip. The remaining fusion temperatures represent an ever increasing amount of molten material, and a lowering of the viscosity of the glass-like material. The softening temperature, SD, is identified where the height equals the width of the cone. The hemispherical temperature, HT, is identified where the height equals one half of the width of the cone. The fluid temperature, FT, is identified where the height equals one sixteenth of the width of the cone. It should be noted that even at the fluid temperature there may be solid or non-melted minerals such as quartz.

1		cone before heating
2	IT (or ID)	initial deformation temperature
3	ST	softening temperature (H=W)
4	HT	hemispherical temperature (H=½W)
5	FT	fluid temperature
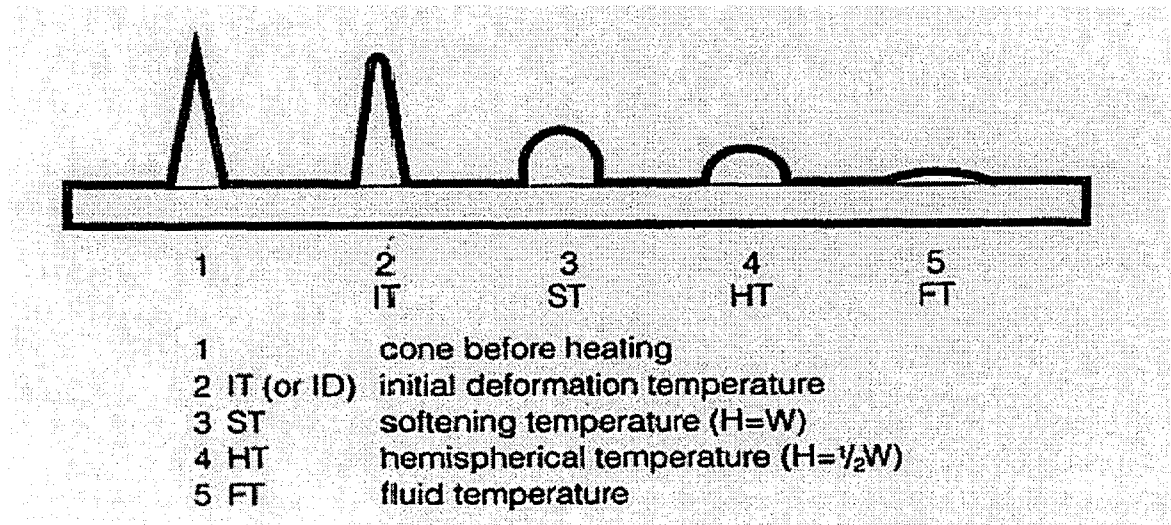
Figure 2-2. Critical Temperature Points of the Ash Fusion Test (Couch, 1994; ASTM).

For carrying out the mentioned ash fusion temperature test, through the method ASTM D-1857 (equivalent to ISO 540) [18], coal samples are prepared in accordance with ASTM D-2013 Method. This method involves the coal passing a 60 mesh (250 µm) sieve, dried, and then heated gradually to a temperature of 1,472 to 1,652 °F (800 to 900 °C) to remove most of the combustible material. The ash is ground in an agate mortar to pass a 200 (75 µm) sieve, spread on a suitable dish, and ignited in a stream

27

of oxygen for approximately one hour at 1,472 to 1,562 °F (800 to 850 °C). Enough coal is used to produce 3 to 5 grams of ash. The ash is mixed thoroughly and moistened with a few drops of dextrin binder and worked into a stiff plastic mass. The mass is then formed into a cone, using a cone mold. The cone is dried, mounted on a refractory base, and heated at a specified rate in a gas-fired or electrically heated furnace under either oxidizing or reducing conditions.

The condition under which the ash fusion temperature test is performed (oxidizing or reducing condition), is very important due to the oxidation behavior of iron atoms. Under reducing conditions the fusion temperatures are lower, since the iron is present as ferrous ions, which have a greater fluxing action than when the iron is in the ferric form, under oxidizing conditions. When the iron is in the ferric form, under oxidizing conditions, the refractory quality of the ash is increased, resulting in higher fusion temperatures. The difference between the oxidizing and reducing fusion temperatures can be of the order of hundreds of degrees.

It is important to mention that these are not precise measurements, and the uncertainty of ash fusion temperature is quoted as being about 131 °F (55 °C) under reducing conditions. In the ASTM standards, repeatability tolerances are large. Tolerances on the measurement for initial deformation temperature range from 86 to 176 °F (30 to 80 °C) for repeatability. All this makes consistent fusion temperature data hard to obtain, even with a relative homogeneity of the laboratory test sample. In practice, two different laboratories can produce fusion temperatures that vary well outside the ASTM guidelines, and yet both laboratories are performing the test satisfactorily. Therefore, correlation of laboratory test results with the actual utilization

of coal is only approximate, due to the heterogeneous mixture of ash that occurs when coal is burned in utility boilers. Despite these differences between laboratory conditions and the complex conditions that exist in a utility boiler, fusion temperatures have been used for years, and are included in most coal delivery contracts. However, the information about the coal-ash composition and coal-ash fusion temperatures is rarely given to boiler's operators in a timely manner. In some cases the information is never provided to the operators, and decisions on operational actions, to prevent and/or mitigate ash deposition impact are usually made based on the operator's personal experience.

The melting properties can be estimated or inferred based on the major and minor ash chemistry. Both, the type and amount of minerals present are important. Unfortunately, it is both difficult and expensive to determine the actual minerals in the coal. Caution is advised when using average numbers for the mineral matter. The average sometimes bears no relationship to reality, where the range can vary from considerably below the average, to considerably above the average.

There have been studies to determine ash fusion temperatures based on the coal-ash chemical composition given by laboratory analyses. An example of these studies is the one made by the joint group formed by the Mining Engineering Department and the Petroleum and Natural Gas Engineering Department, from the Middle East Technical University, in Ankara, Turkey [11]. In this study, non-linear correlations were developed by using the coal-ash chemical composition and coal parameters to determine ash fusion temperature, or fusibility temperature. The analyses made by this group, were performed by using the oxides in coal-ash

calculated on weight and mole basis. Sixteen independent parameters were considered in the regression analyses. Each parameter was treated separately and in combination. The parameters used in this study were silica value, base, acid, R250, dolomite ratio, ash content (% coal), specific gravity of coal, hardgrove grindability index (HGI) of coal, coal mineral matter content, and SiO_2, the sum of Al_2O_3 and TiO_2, Fe_2O_3, CaO, MgO, K_2O, and Na_2O, all in percentage of coal-ash. Non-linear regression analyses carried out by this group showed to be more accurate for the prediction of coal-ash fusion temperatures than linear regression analyses, previously carried out. It also showed that the use of major groups (silica value, base, acid, dolomite ratio, and R250), for predicting coal-ash fusion temperatures does not give results as accurate as using major groups in combination with individual chemical composition of the coal-ash (percentages of SiO_2, Al_2O_3 + TiO_2, Fe_2O_3, CaO, MgO, K_2O, and Na_2O). The major limitation of this technique is that it employs a complex statistical method (the Quasi-Newton estimation method) to determine the correlation coefficients, and the correlations established are usually very sensitive to variations in the characteristics. The capacity of this approach to perform satisfactorily outside of the parametric range used to develop the correlations (extrapolate) is very limited.

Regarding the ASTM analytical techniques used to determine ash chemical composition, the following techniques are available: X-ray diffraction, X-ray fluorescence, scanning electron microscopy, atomic absorption/emission spectroscopy, ICP-atomic emission spectrometry, and electron probe microanalysis.

The test method (ASTM D-3682) covers analysis of the commonly determined major and minor elements (such as silicon, aluminum, iron, calcium, magnesium,

sodium, potassium, and titanium) in laboratory coal ash and in combustion residues from coal utilization processes by atomic absorption/emission spectroscopy. In the test method, the ash sample or combustion residue to be analyzed is standardized by ignition in air at 1,382 °F (750 °C) to a constant weight. The ash is then fused within lithium tetraborate ($Li_2B_4O_7$) followed by a final dissolution of the melt in either dilute hydrochloric acid (HCl) or dilute nitric acid (HNO_3). The solution is analyzed by atomic absorption/emission spectroscopy for applicable elements.

X-ray fluorescence analysis (ASTM D-4326) is a rapid, simple, and reasonably accurate method of determining the concentration of many minor and trace elements in coal. This method is dependent on the availability of suitable standards. Although the major elements in coal (carbon, hydrogen, oxygen, and nitrogen) cannot be analyzed by X-ray fluorescence, most other elements at levels greater than a few parts per million (ppm) are readily determined. In the test method ASTM D-4326, the coal to be analyzed is ashed under standard conditions and ignited to constant weight. The ash is then fused with lithium tetraborate ($Li_2B_4O_7$) or other suitable flux, and either ground and pressed into a pellet or cast into a glass disk. The pellet or disk is then irradiated by an X-ray beam of short wavelength (high energy). The characteristic X-rays of the atom that are emitted or fluoresced upon absorption of the primary or incident X-rays are dispersed, and intensities at selected wavelengths are measured by sensitive detectors. Detector output is usually related to concentration by calibration curves. All of the elements are reported as oxides and include silicon, aluminum, iron, calcium, magnesium, sodium, potassium, phosphorus, titanium, manganese, strontium, and barium.

31

There is a standard test method for determination of major and minor elements in coal-ash by inductively coupled plasma (ICP)-atomic emission spectrometry (ASTM D-6349). In this test method, the sample to be analyzed is ashed under standard conditions and ignited to constant weight. The ash is fused with a fluxing agent followed by dissolution of the melt in a dilute acid solution. Alternatively, the ash is digested in a mixture of hydrofluoric, nitric, and hydrochloric acids. The solution is analyzed by (ICP)-atomic emission spectrometry for the elements. The basis of the method is the measurement of atomic emissions. Aqueous solutions of the samples are nebulized, and a portion of the aerosol that is produced is transported to a plasma torch, where excitation and emission occurs. Characteristic line emission spectra are produced by a radio-frequency inductively coupled plasma. A grating monochromator system is used to separate the emission lines, and the intensities of the lines are monitored by photomultiplier tube or photodiode array detection. The photocurrents from the detector are processed and controlled by a computer system. A background correction technique is required to compensate for variable background contribution to the determination of elements.

Inductively coupled plasma atomic emission spectrometry (ICPAES) measures the intensities of light emitted from each species as they are atomized and ionized in the plasma. As an atomic emission spectrometry (AES) technique, ICPAES has the capability of simultaneous multi-elemental measurement. Atomization is more complete in the ICP system than in the AAS system. Therefore, limit of detection values are generally lower for ICPAES than for AAS.

Atomic absorption spectroscopy (AAS) is used to detect the presence and amount of metal atoms in very dilute solutions. It is widely used in laboratories that analyze the purity of water. The resonant wavelength of choice from a selected spectral lamp passes through the sample vapor. The atomized element absorbs the light energy over time. The concentration is determined through a calibration curve. The sample solution can be atomized by passing an electrical current through a graphite tube which contains the analyte (graphite furnace atomic absorption, AA) or using a flame to atomize the sample (flame AA). The graphite AA technique often offers about 1000-fold sensitivity improvement as compared with flame AA.

LIBS is a technique based on atomic emission spectroscopy, which utilizes a highly energetic laser pulse as the excitation source. LIBS can analyze any matter regardless of its physical state, be it solid, liquid or gas. Even slurries, aerosols, and gels can be readily investigated with LIBS. Because all elements emit light when excited to sufficiently high temperatures, in theory, LIBS can detect all elements, limited only by the power of the laser, as well as the sensitivity and wavelength range of the spectrometer and detector. Operationally, LIBS is very similar to spark emission spectroscopy.

More specifically, LIBS operates by focusing a laser onto a small area at the surface of a specimen. When the laser is discharged it ablates a very small amount of material, in the range of nanograms to picograms, which instantaneously generates a plasma plume with temperatures of about 10,000 to 20,000 K (see Figure 2-3). At these temperatures, the ablated material dissociates (breaks down) into excited ionic and atomic species. At this point the characteristic atomic emission lines of the

elements can be observed. The delay between the emission of continuum radiation and characteristic radiation is of the order of 10 microseconds, this is why, it is necessary to temporally gate the detector [6].

PULSED LASER
(TYPICALLY
5ns PULSE 1064nm)

PLASMA EMMISION

PLASMA
PLUME

SAMPLE
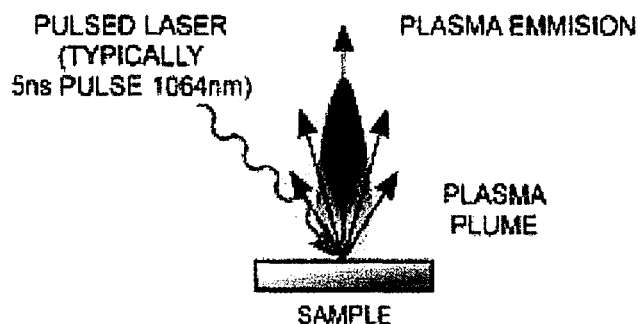
Figure 2-3. LIBS Plasma Plume (www.andor.com).

LIBS is technically very similar to a number of other laser-based analytical techniques, sharing much of the same hardware. These techniques are the vibrational spectroscopic technique of Raman spectroscopy, and the fluorescence spectroscopic technique of laser-induced fluorescence (LIF). Currently, devices are being manufactured which combine these techniques into a single instrument, allowing the atomic, molecular and structural characterization of a specimen, as well as giving a deeper insight into its physical properties.

A typical LIBS system consists of a neodymium doped yttrium aluminum garnet (Nd:YAG) solid-state laser and a spectrometer. This set-up includes a wide spectral range, with a high sensitivity, fast response rate, time gated detector. This set-up is coupled to a computer which can rapidly process and interpret the acquired data.

The main properties of laser light which distinguish it from conventional light sources are intensity, directionality, and coherence. In addition, lasers may operate to

34

emit radiation continuously or it may generate radiation in short pulses. Some lasers can generate radiation with the properties just mentioned in a tunable fashion, over a wide range of wavelengths. Generally, pulsed lasers are used in the production LIPs. It is possible to generate short-duration laser pulses with wavelengths ranging from the infrared (IR) to the ultraviolet (UV), with powers of the order of millions of watts. Such high-power pulses of laser radiation can vaporize metallic and refractory surfaces in a fraction of a second. It should be noted that not only the peak power of the laser, but also the ability to deliver the energy to a specific location is of great importance (Basov & Krokhin, 1964). In LIBS, the power per unit area that can be delivered to the target is more important than the absolute value of the laser power. The power per unit area of the laser beam is termed "irradiance", and is also called "flux" or "flux density."

Another property of laser radiation that is of interest is the directionality of the beam. Laser radiation is confined to a narrow cone of angles which is of the order of a few tenths of a milliradian for gas lasers, to a few milliradians for solid state lasers. Because of the narrow-divergence angle of laser radiation, it is easy to collect all the radiation with a simple lens. The narrow beam angle also allows focusing of the laser light to a small spot. Therefore, the directionality of the beam is an important factor in the ability of lasers to deliver high irradiance to a target. Coherence of the laser is also related to the narrowness of the beam divergence angle and it is indirectly related to the ability of the laser to produce high irradiance. However, coherence is not of primary concern in LIBS [6]. Provided that a certain number of watts per square centimeter are delivered to a surface, the effect will be the same whether the radiation is coherent or not. The frequency spread of gas lasers is of the order of one part in 10^{10} or better. For solid lasers, it is of the order of several megahertz.

Solid state lasers, such as ruby lasers, Nd: glass, and Nd: YAG lasers that produce high powers are generally pulsed with widely different pulse durations and with different methods of pulsing. If the laser is pumped by a flashlamp, pulse widths in the range of 100 to 1000 microseconds are typical. In many cases, the laser emission is not uniform, but consists of many microsecond duration spikes called relaxation oscillations, whose amplitudes and spacing are not uniform. The presence of these spikes in the laser pulse causes heating and cooling of the target and is not suitable for producing a uniform plasma plume [6].

Laser pulse durations in the range of 10 to 1000 nanoseconds can be produced by Q-switching techniques, where laser operation is suppressed and population inversion in the solid rod increases greatly over a normal threshold condition. If the Q-switching component in the laser cavity is changed to a transparent condition, the laser rod, now in a highly inverted state, gets coupled to two mirrors in the cavity and the stored energy is emitted in a pulse of higher power and shorter duration than without Q-switching.

There are a wide variety of different lasers with many different characteristics. Each type has its own properties of wavelength and operating parameters. Even within one type, there are many varieties of design. A large variety of lasers are available, which span an entire spectral range, from extreme UV to the far-IR region. Developments in LIBS use laser wavelengths provided by existing technology. In 1962 a ruby laser at 694 nm was used in LIBS, but its pulse-to-pulse stability was very poor. As a consequence, LIBS was not considered to be a very reliable technique for spectrochemical analysis. The next phase of LIBS development was marked by the

sophisticated pulsed-laser technology of the 1980s, which led to very reliable Nd: YAG lasers in the near-IR, visible, and UV regions. At present, many more laser wavelengths have become available for use on LIBS measurements.

There is a great difference in the behavior of surfaces struck by laser pulses with millisecond duration as compared to those with pulse durations in the nanosecond region. The short pulses of very high power do not produce much vaporization, but instead remove only a small amount of material from the surface, wheras longer, low-power pulses produce deep, narrow holes at the target. For laser pulses of picoseconds (ps) and femtosecond (fs) duration there is no reheating of the plasma due to absorption of laser radiation as in the case of nanosecond (ns) laser pulses (see Figure 2-4). Thus, the volume of plasma produced in the cases of ps and fs laser pulses is much smaller than in the case of ns laser pulses. The plasma plume produced by ns laser pulses gets elongated towards the incident laser beam as a result of reheating.
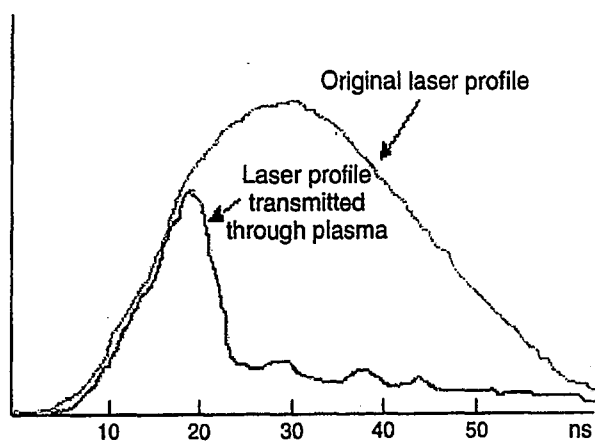
Figure 2-4. Schematic Temporal Profile of Laser Pulse in Absence and in Presence of Gas Breakdown Showing Attenuation of Laser Beam (Singh & Thakur, 2007).

37

The interaction of the laser with a target surface is considerably modified by the presence of material emitted from the surface by ns-pulsed high power laser irradiation. It exerts a high pressure on the surface and changes the vaporization characteristics of the surface. Since the laser flux density is very high, the ejected material can be heated further by absorption of incoming laser radiation. It becomes thermally ionized and opaque to the incident radiation. The absorbing plasma prevents light from reaching the target surface, which is effectively cut off from the incoming radiation for a large fraction of the laser pulse. At the end of the laser pulse, the blow off material becomes hot and it begins to radiate thermally. Some of this radiation may reach the surface, causing further vaporization. The temporal evolution of the depth vaporized by the high-power laser pulse is schematically shown in Figure 2-5.
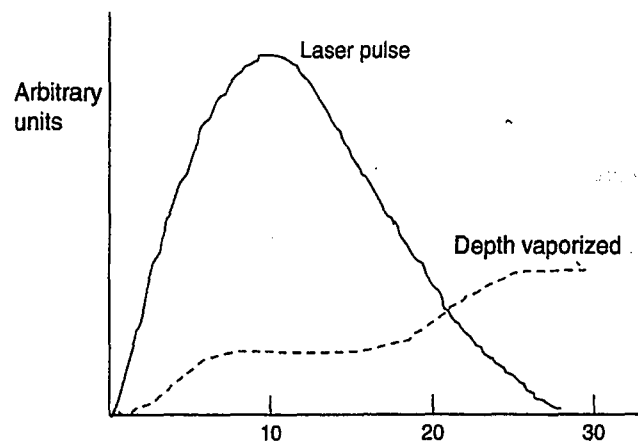
Figure 2-5. Schematic Representation of Depth Vaporized in Metal Target as Function of Time Showing Effect of Shielding by Blow-off Material (Singh & Thakur, 2007).

Multi-elemental detection capability offered by the LIBS technique demands a spectrograph with a wide spectral coverage. In the multi-elemental analysis, sequential measurements of parts of the spectrum of interest are performed, inspecting each time

38

a different sample of the material ablated from the target surface. In principle this procedure limits the LIBS application to homogeneous samples but most of practical samples are heterogeneous. This is the reason why the LIBS spectra vary from shot to shot, as a result of changes in the sample composition as well as due to stochastic fluctuations in the plasma. Therefore, simultaneous measurement of the complete optical spectrum is necessary for getting optimal information for analytical purposes (Rai, Yueh, Singh and Zhang, 2002). Instruments, which allow simultaneous measurements, are Paschen-Runge spectrometers or the more compact Echelle spectrometer. Echelle spectrometers offer excellent spectral resolving power ($\lambda/\Delta\lambda \geq 10,000$ and more) in combination with a spectral coverage of several hundred nanometers. In combination with intensified charge coupled devices, Echelle spectrometers represent a very powerful tool for elemental analysis for LIBS.

Typical Echelle spectrometer have focal length of 25 cm with a numerical aperture 1:10, and a quartz prism positioned in front of the granting separates the different orders of spectra and produces a two dimensional pattern. The flat image plane is 24.85 x 24.5 mm^2. This system provides maximum resolution in the wavelength range between 200 to 780 nm. The linear dispersion per pixel ranges from 0.005 nm (at 200 nm) to 0.019 nm (at 780 nm), which is based on the spectral resolution $\lambda/\Delta\lambda \geq 40,000$. The detector in this system is an intensified charge-coupled device (ICCD) camera. This camera has a charge-coupled device (CCD) array of 1024 x 1024 pixels (24 x 24 μm^2), and a microchannel plate. A fast pulse generator delivers a 5 ns pulse to the intensifier to ensure synchronization of the measurements with the laser pulse. The spectral response in a particular order of diffraction of the Echelle spectrometer is non-linear, when measured using the black body radiation from a

deuterium lamp. Each diffraction order has similar shape but a different sensitivity, which requires a correction factor when the measurement is made in a different spectral range, with different sensitivity. Normally, a black body radiation calibration spectrum is recorded to obtain the intrinsic response of the Echelle/ICCD system, which is then used to normalize the acquired spectrum.

In recent years, the Echelle spectrometer has proved to be very successful in the acquisition of spectral data from which relevant physical or chemical information can be extracted. Calibration curves of various elements have been obtained, the limits of its detection determined, and the excitation and ionic temperatures of LIP, as well as the electron density have been measured. The reproducibility of experimental results shows that the dynamic range of the Echelle detector makes it possible to simultaneously measure the intensities of spectral lines of the major elements and the trace elements in the sample. The detectability of elements at low concentration is facilitated by the very high resolution of this system.

Overall, the integrated LIBS technique has several advantages compared to conventional emission methods. In LIBS, a high-energy pulsed laser beam is used to produce atomic emissions from the focal volume. Hence, it provides time and spatially resolved measurements. It requires only a small amount of sample and minimal sample preparation. Gated detection with an intensified detection system discriminates the background emission and also improves detection limits. With properly selected atomic lines, multiple species can be simultaneously monitored in a spectral region. Furthermore, as a laser spark can be generated in a remote location, it has remote monitoring capability.

Typical limits of detection for LIBS are in the parts per million (ppm) to percentage range. A direct comparison of LIBS detection limits with other analytical techniques is unrealistic because of the dissimilarity in the samples used. In general, LIBS still cannot match the detection limits of most conventional analytical techniques in most cases. However, its ability to directly analyze samples without cumbersome sample preparation has led to its promising application in practical field determination of elemental composition of samples.

Figures 2-10 and 2-11 show a typical LIBS experimental set-up and a typical LIBS fiber-based set-up [20]. Elements that were described in the proceeding text are schematically presented.
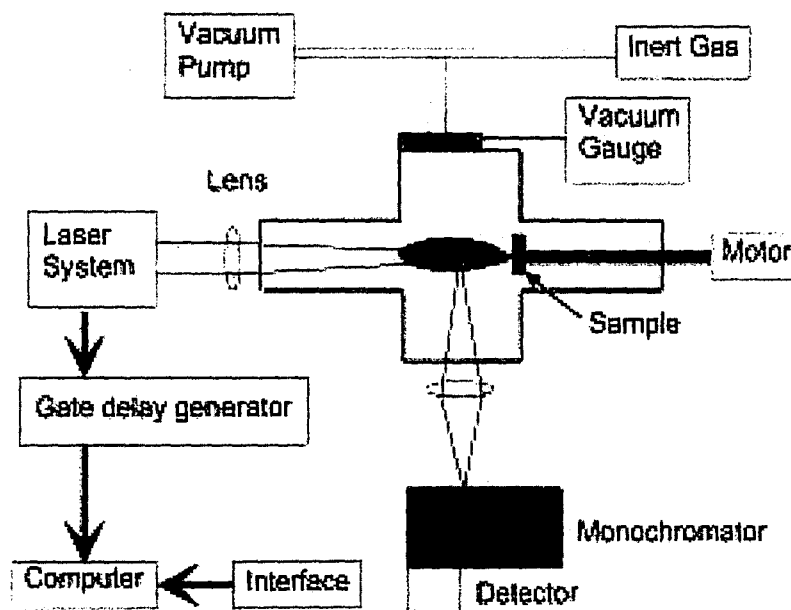
Figure 2-6. Typical LIBS Experimental Set-up.

Figure 2-7. Typical LIBS Fiber-based Experimental Set-up.

Work has been carried out in the area of coal elemental composition determination using LIBS. Two research groups have performed research on this application of the LIBS technique. One of these groups is a consortium formed by Sandia National Laboratories, Combustion Research Facility, in Livermore, California and the Applied Laser/Optics Group, Physics Department, New Mexico State University, in Las Cruces, New Mexico [9, 10]. This group has carried out studies on LIBS and laser spark spectroscopy (which is technically the same principle and apparatus), for the analysis of coals since the late 1980s. They have studied coals of different ranks, geographical origin, and mineral content. However, their main focus has been on Eastern U.S. bituminous coals. Their studies included in situ, real time determination of size, velocity, and elemental composition of coal particulates in combustion environments. Flowing dry nitrogen was used in conjunction with a syringe-type feeder to introduce a stream of particles into the optical system. Particles were

42

Figure 2-7. Typical LIBS Fiber-based Experimental Set-up.

Work has been carried out in the area of coal elemental composition determination using LIBS. Two research groups have performed research on this application of the LIBS technique. One of these groups is a consortium formed by Sandia National Laboratories, Combustion Research Facility, in Livermore, California and the Applied Laser/Optics Group, Physics Department, New Mexico State University in Las Cruces, New Mexico [9, 10]. This group has carried out studies on LIBS and laser spark spectroscopy (which is technically the same principle and apparatus), for the analysis of coals since the late 1980s. They have studied coals of different ranks, geographical origin, and mineral content. However, their main focus has been on Eastern U.S. bituminous coals. Their studies included in situ, real time determination of size, velocity, and elemental composition of coal particulates in combustion environments. Flowing dry nitrogen was used in conjunction with a syringe-type feeder to introduce a stream of particles into the optical system. Particles were

42

introduced along the vertical centerline of a premixed flat-flame burner of circular symmetry through a tube of 1.2 mm inside diameter. The combustion region of the burner was of 50 mm in diameter and surrounded by an annu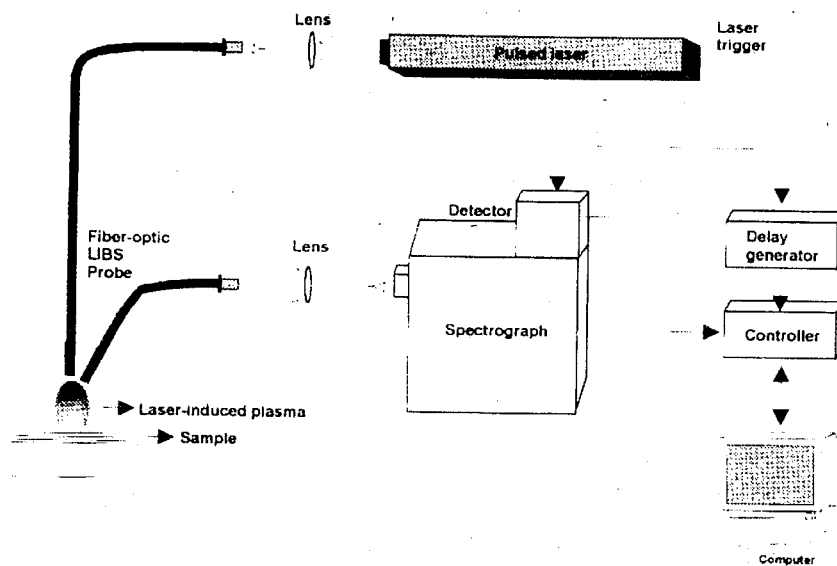lar co-flow region for the purpose of flow regulation and to prevent mixing with the outer atmosphere. The residence time of the particles in the combustion environment was varied by translating the burner vertically with respect to the laser focal volume. A focused Nd: YAG Q-switched laser (Quanta-Ray Model DCR-2) was used to create the plasma on coal particles at 532 nm, yielding 100 mJ of pulse energy. The triggering rate was approximately one event per second. The laser spark was imaged on the entrance slit of a spectrometer by using an independent optical train and detected by using an intensified linear-diode array (photodiodes/amplifier assembly). Spectra were acquired with a 300-groove/mm diffraction grating. A time delay of 1 µs was used following plasma initiation, and a time gate of 1µs was used for the emission spectrum.

The Sandia National Laboratories and New Mexico State University group found a systematic way of studying the emission intensity lines, by examining the relative intensity for two elements for a large number of shots. It was found that by doing this over a relatively narrow spectral bandwidth, the optical system response was reasonably constant, and the observed intensity ratios could be quantitatively related to reference intensities, avoiding the expected large variation in emission intensity lines due to the heterogeneity of coal. The element chosen for normalization was carbon at 247.86 nm. All spectra were previously background-corrected for detector dark current. Relative concentrations on an atomic basis were then obtained by averaging over 500 shots for each coal studied. The elements observed and detected with best accuracy were compared to the average bulk concentrations for the coals tested, as determined

43

by standard analytical methods. These elements were: magnesium at 285.21 nm, calcium at 317.93 nm, aluminum at 309.27 nm, silicon at 288.16 nm, titanium at 336.12 nm, and iron at 259.90 nm. The average repeatability of these tests were 47 percent for magnesium, 13.75 percent for calcium, 9.5 percent for aluminum, 10.5 percent for silicon, 7.75 percent for titanium, and 10.5 percent for iron. Quantitative results to estimate the uncertainty of elements were not available in the publications found from the work carried out by this group.

The Cooperative Research Center for Clean Power From Lignite, in Mulgrave Victoria, Australia [7, 8], has used LIBS in the analysis of a variety of low-ash and high-ash lignite Australian coals, with ash contents ranging from 1.6 percent to 35.0 percent (on a dry basis). The most important results obtained by this group were achieved with an approach that includes crushing the samples received to <100 µm, and loading the samples into sample holders that allow pressing of the sample, using a hydraulic press (Carver), and direct transfer into the analyzer. The laser used was a high-power "mini" Nd: YAG Q-switched laser (New Wave Research), which yields up to 90 mJ of pulse energy in a 7 ns pulse, at a repetition rate of 15 Hz. The laser was focused onto the samples by a short, 38 mm focal length lens. The sample was located on a fast translation stage that moved the sample between laser pulses, exposing a fresh region of the sample to each successive laser pulse. A parallel processing design, comprising multiple spectrographs and CCD (unintensified Sony ILX511) detectors, was a distinguishable feature of this approach. With the use of multiple spectrographs wide spectral coverage was achieved, while maintaining the required resolution. Each separate CCD detector recorded the spectral range from each spectrograph simultaneously in a single laser pulse, overcoming the data transfer bottleneck

encountered in other LIBS designs. A time delay of 1 µs was used following plasma initiation, and a time gate of 5 µs was used for the emission spectrum.

The acquisition cycle involved moving the sample, firing the laser, and storing the resulting spectrum from the spectrometer channel. Typically, up to 300 laser pulses were used during each analysis. The data was processed using peak integration and ratio to normalization parameters. Storing of individual spectra allowed normalization for pulse-to-pulse instability in the plasma, resulting in a superior level of precision in the measurement. For this study, five samples of mine material (low-ash and high-ash samples, covering the range of analyte concentrations encountered in the mine) were used as calibration standards. The calibration samples were characterized using standard methods (typically ash fusion, acid extraction followed by spectrometric analysis of the solute). A calibration curve over the element concentration range was constructed.

Six mineral elements were reported, including magnesium, calcium, sodium, aluminum, silicon, and iron. The average repeatability of the measurements were found to be 3.57 percent for magnesium, 4.51 percent for calcium, 5.44 percent for sodium, 12.63 percent for aluminum, 8.19 percent for silicon, and 2.75 percent for iron. While measurement uncertainty, as compared to standardized analyses was found to be 4.66 percent for magnesium, 8.86 percent for calcium, 5.6 percent for sodium, 27.38 percent for aluminum, 12.45 percent for silicon, and 16.69 percent for iron. The Australian group has continued working on research aiming at ultimately develop an instrument that can be deployed at the mine face.

CHAPTER 3

Laboratory Experimental Instrumentation and Procedure

Laboratory tests were carried out with an experimental LIBS system assembly and a coal inventory containing different types of bituminous and sub-bituminous coals. LIBS experimentation on the coal inventory was performed following a testing procedure. The main goal of the laboratory experimentation was to create a database that could serve as source data for neural network modeling. This chapter includes a description of the coal inventory, the instrumentation, the experimental set-up, and the laboratory test procedures for developing this database.

For experimental purposes, a coal inventory of sixteen coals with different ranks and characteristics was collected from several electric power generation companies, included Allegheny Energy Inc., Dominion, NRG Energy Inc., Constellation Energy Group, DTE Energy Co., and Public Service Electric and Gas Company (PSE&G), as well as from the Pennsylvania State University coal bank. The coal bank includes U.S. coals and imported coals used by different power stations. These coals are from different locations in the U.S., Colombia, Venezuela, Indonesia, and Russia. The coal inventory includes coals that have been reported to have slagging issues, as well as coals that have shown no slagging problems. It includes bituminous and lignitic type of ashes. The ASME Research Committee on Boiler Fouling (Winegartner, 1974) has defined bituminous types of ashes as pyrochemically acidic, and with iron oxide content higher than that of calcium oxide. On the other hand, lignitic types of ashes are

46

highly alkaline and with calcium oxide content higher than that of iron oxide. Alternative definitions are (Raask, 1985):

(1) For bituminous type of ash: $SiO_2 > (Fe_2O_3 + CaO + Na_2O)$

(2) For lignitic type of ash: $SiO_2 > (Fe_2O_3 + CaO + Na_2O)$

The samples collected were grounded to a 60 mesh (250 μm), then riffled and sent to Mineral Labs, Inc., in Salyersville, Kentucky for analysis. Characterization of the coal inventory was made through ASTM analyses by Mineral Labs, Inc. Samples were prepared following ASTM Method 2013 (in terms of coal sample crushing, sieving, and drying). Proximate, ultimate, mineral, and ash fusion temperature analyses were performed on the coals, obtaining information on the composition of major elements in the coals, and their four fusion temperatures. ASTM Method D5142 was followed for moisture, ash content, and volatiles, ASTM Method D4239 for sulfur, ASTM Method D5373 for carbon, hydrogen, and oxygen, ASTM Method D5865 for gross heating value, ASTM Method D6349 for ash mineral, and ASTM Method D1957 for ash fusion temperatures in a reducing environment. Information on coal inventory description and characteristics is presented in detail in Table 3-1. The ash mineral concentrations in weight percentage reported ranged from 30.6 to 61.8 for SiO_2, 14.6 to 28.1 for Al_2O_3, 0.7 to 1.5 for TiO_2, 3.8 to 30.6 for Fe_2O_3, 0.5 to 23.6 for CaO, 0.4 to 4.5 for MgO, 0.2 to 5.6 for Na_2O, 0.4 to 3.3 for K_2O, and 0.7 to 20.3 for SO_3.

Pulverized coal-fired boilers have typical oxygen levels above 3 percent by volume of the flue gas, and combustion should be completed by the time the flue gas reaches the superheater zone, indicating, that an oxidizing atmosphere should prevail. However, in practice, reducing gases can reach higher sections in the furnace, and it is

advisable to take the initial deformation temperature of the ash in a reducing atmosphere as guidance for prevention of severe upper furnace and superheater slagging. Also, since the ash fusion temperatures reported under reducing conditions are typically lower than those reported under oxidizing conditions, the former ones are more critical for slagging prevention purposes. Furthermore, as mentioned in Chapter 2, ash fusion temperature measurements are not precise, with tolerance of up to 176 °F. For these reasons, ash fusion temperatures were determined under reducing conditions. The initial deformation temperatures for the entire coal inventory ranges from 1,755 °F to 2,700 °F.

In collaboration with the Energy Research Company (ERCo), located in Staten Island, NY, an automated LIBS system was assembled using off-the-shelf and custom made components to test the coal inventory. The experimental set-up for the LIBS operation was designed to accomplish: the sparking of the sample with the laser under controlled atmosphere, displacement of the sample to obtain a collection of shots, resolution of the spectral using a spectrometer and photodiodes, and processing of the acquired data using software tools. Figure 3-1 shows a general layout of the LIBS system assembly, showing the components and their connections.

The experimental set-up consists of a sample chamber, a flow meter for Helium inlet control into the chamber, a pressure gauge for chamber pressure monitoring, a vacuum pump for chamber purging and atmospheric control inside the chamber, a Helium tank for pumping into the chamber as inert gas, an excitation Nd: YAG (neodymium-doped yttrium aluminum garnet) laser, an optical spectrometer, a photodiode/amplifier unit, and a controller/processing computer.
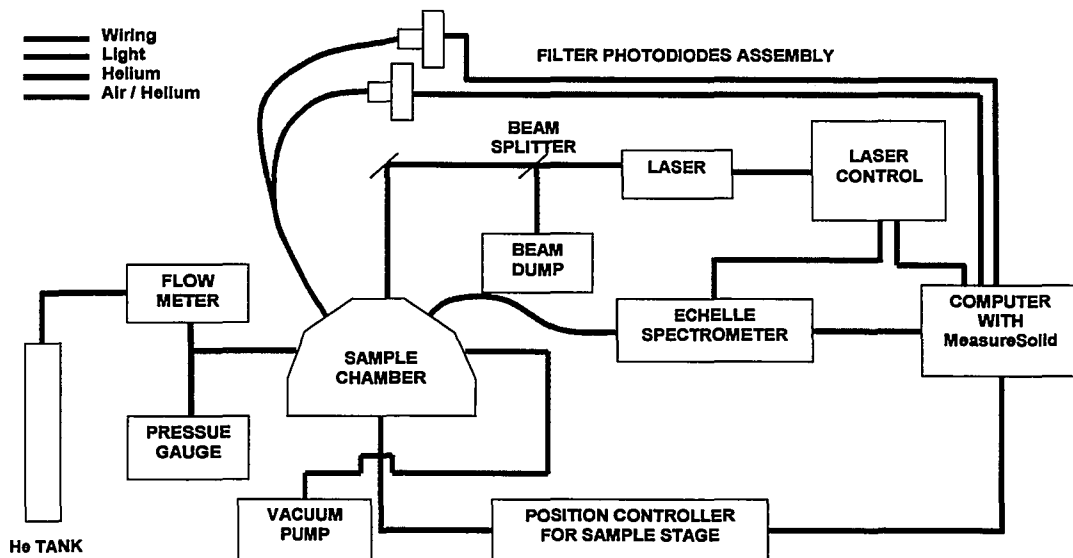
Figure 3-1. LIBS General Experimental Layout.

The laser used in the LIBS system is a Q-switched Nd: YAG laser, a Big Sky Laser model CFR-400, which yields coincident UV, visible, and near IR 7 ns pulses, at a repetition rate of 10 Hz. The UV pulses were not used and were directed down into a beam dump by a 266 nm beam splitter. The visible and near IR pulses are directed down into the chamber by 1,064 nm and 532 nm laser mirrors. Pulse energies of approximately 100 mJ at 1,064 and 180 mJ at 532 nm are used to generate the laser sparks on the sample. An f/4 lens is used to focus the light pulses onto the surface of the coal sample to create the LIBS spark. Figure 3-2 shows the laser pulse generator (power tower) and the head of the laser.

Table 3-1: Coal Inventory Characterization Based on ASTM Analyses.

Coal Sample Code	HAT	HAR	PLE	LOG	RUSS	BPD	DRUM	GUA
Supplier	Allegheny Energy	Allegheny Energy	Allegheny Energy	NRG	Constellation	Dominion	Dominion	Dominion
Power Plant Facility	Hatfield Ferry St.	Harrison St.	Pleasant St.	Logan St.	Brandon Shores St.	Brayton Point St.	Brayton Point St.	Brayton Point St.
Geographical Orign	U.S. East	U.S. East	U.S. East	U.S. East	Russia	U.S. Eastern	Colombia	Venezuela
Rank	Bituminous	Bituminous	Bituminous	Bituminous	Bituminous	Bituminous	Bituminous	Bituminous
Proximate Analysis								
Inherent Moisture (% wt.)	6.68	0.94	1.48	1.73	11.77	5.56	11.90	5.94
Ash (% wt.)	8.64	14.21	9.43	10.52	11.81	9.37	3.90	9.80
Ash - dry basis (% wt.)	9.26	14.34	9.57	10.71	13.39	9.92	4.42	10.42
Volatile Matter (% wt.)	34.87	38.61	41.67	32.75	28.07	39.17	35.77	33.47
Volatile Matter - dry basis (% wt.)	37.36	38.98	42.30	33.33	31.82	41.48	40.60	35.58
Sulfur (% wt.)	2.26	3.69	4.77	1.06	0.58	0.48	0.46	0.74
Sulfur - dry basis (% wt.)	2.42	3.72	4.84	1.08	0.65	0.50	0.52	0.78
Fixed Carbon (% wt.)	49.81	46.24	47.42	54.99	48.34	45.90	48.44	50.79
Fixed Carbon - dry basis (% wt.)	53.38	46.68	48.13	55.96	54.79	48.60	54.98	54.00
Gross Calorific Value (Btu/lb)	12,773	12,929	13,205	13,207	11,431	12,457	11,633	12,628
Mineral Analysis for Ash								
Silica, SiO_2 (% wt.)	46.60	44.65	38.10	52.63	54.86	58.43	46.14	60.37
Alumina, Al_2O_3 (%wt.)	21.40	18.70	18.60	28.08	27.98	23.64	20.75	21.71
Titania, TiO_2 (%wt.)	1.02	0.92	0.86	1.53	1.34	0.90	0.81	0.86
Ferric Oxide, Fe_2O_3 (% wt.)	18.17	18.89	30.57	6.41	3.84	4.51	8.32	6.18
Lime, CaO (% wt.)	3.31	7.29	2.67	2.15	2.01	3.25	6.05	1.83
Magnesia, MgO (% wt.)	0.77	1.11	0.62	0.75	1.37	1.05	1.75	1.34
Sodium Oxide, Na_2O (% wt.)	0.53	0.62	0.40	0.22	0.35	1.00	1.56	0.36
Potassium Oxide, K_2O (% wt.)	2.62	1.07	3.32	3.17	3.21	1.33	2.94	2.64
Sulfur Trioxide, SO_3 (% wt.)	2.61	3.88	2.07	1.98	1.83	1.77	8.81	1.78
Fusion Temperature Analysis								
Initial Deformation Temperature, IT (°F)	2,120	2,040	2,000	2,700	2,700	2,480	2,300	2,420
Softening Temperature, ST (°F)	2,187	2,100	2,040	2,700	2,700	2,520	2,360	2,500
Hemispherical Temperature, HT (°F)	2,247	2,180	2,080	2,700	2,700	2,600	2,400	2,570
Fluid Temperature, FT (°F)	2,303	2,290	2,100	2,700	2,700	2,700	2,510	2,690
Ultimate Analysis								
Total Moisture (% wt.)	6.68	0.94	1.48	1.73	11.77	5.56	11.9	5.94
Carbon (% wt.)	72.56	72.79	74.08	76.84	65.27	70.07	68.07	72.90
Hydrogen (% wt.)	4.83	4.97	5.07	4.97	4.11	4.92	4.57	4.84
Nitrogen (% wt.)	1.35	1.23	1.20	1.45	0.07	1.55	1.37	1.33
Oxygen (% wt.)	3.61	2.11	3.92	3.30	5.17	8.01	9.72	4.42
Sulfur (% wt.)	2.26	3.69	4.77	1.06	0.58	0.48	0.46	0.74
Ash (% wt.)	8.64	14.21	9.43	10.52	11.81	9.37	3.90	9.80
Chlorine (% wt.)	0.06	0.06	0.05	0.13	0.07	0.04	0.01	0.03

Table 3-1: Coal Inventory Characterization Based on ASTM Analyses (Continued).

| Coal Sample Code	CUCU	DECS-2	DECS-18	DECS-1	DECS-9	WEST	WEST/EAST	ADAR
Supplier	Dominion	Coal Bank PSU	Coal Bank PSU	Coal Bank PSU	Coal Bank PSU	DTE-Energy	DTE-Energy	PSE&G
Power Plant Facility	Brayton Point St.	N/A	N/A	N/A	N/A	St. Clair St.	St. Clair St.	Bridgeport St.
Geographical Orign	Colombia	U.S. Illinois	U.S. Kentucky	U.S. Texas	U.S. Montana	U.S. West	U.S. West/East	Indonesia
Rank	Bituminous	Bituminous	Bituminous	Lignitic	Lignitic	Lignitic	Lignitic	Lignitic
Proximate Analysis								
Inherent Moisture (% wt.)	6084.00	10.43	6.81	30.00	24.68	17.21	16.95	14.50
Ash (% wt.)	8.67	14.47	11.42	11.07	4.80	5.04	5.47	1.10
Ash - dry basis (% wt.)	9.31	16.16	12.25	15.81	6.37	6.09	6.59	1.29
Volatile Matter (% wt.)	34.68	34.16	38.38	33.18	33.46	40.04	34.65	37.80
Volatile Matter - dry basis (% wt.)	37.23	38.14	41.18	47.40	44.43	48.36	41.27	44.21
Sulfur (% wt.)	0.68	4.05	3.92	0.69	0.31	0.33	0.45	0.09
Sulfur - dry basis (% wt.)	0.73	4.52	4.21	0.99	0.41	0.40	0.54	0.11
Fixed Carbon (% wt.)	49.81	40.93	43.40	25.75	37.06	37.71	42.93	34.90
Fixed Carbon - dry basis (% wt.)	53.46	45.70	46.57	36.79	49.20	45.55	51.69	40.82
Gross Calorific Value (Btu/lb)	12,650	14,061	14,226	12,812	12,809	10,215	10,255	9,211
Mineral Analysis for Ash								
Silica, SiO_2 (% wt.)	61.79	49.20	41.20	45.60	36.20	30.56	33.03	34.21
Alumina, Al_2O_3 (%wt.)	24.76	19.10	15.60	17.00	18.10	14.60	14.79	17.05
Titania, TiO_2 (%wt.)	1.16	0.89	0.75	1.26	1.20	1.06	1.05	0.69
Ferric Oxide, Fe_2O_3 (% wt.)	4.76	20.40	22.00	4.18	4.90	4.07	5.05	17.59
Lime, CaO (% wt.)	0.52	5.18	8.08	5.50	13.50	23.63	13.23	13.00
Magnesia, MgO (% wt.)	0.38	0.82	0.70	2.68	4.52	3.08	2.82	3.96
Sodium Oxide, Na_2O (% wt.)	0.22	0.71	0.66	0.42	5.55	3.92	3.88	0.21
Potassium Oxide, K_2O (% wt.)	2.83	1.87	1.89	0.60	1.01	0.39	2.81	0.99
Sulfur Trioxide, SO_3 (% wt.)	0.70	1.60	9.40	12.70	13.40	15.60	20.31	11.84
Fusion Temperature Analysis								
Initial Deformation Temperature, IT (°F)	2,700	1,900	1,755	1,840	1,910	2,090	2,000	2,138
Softening Temperature, ST (°F)	2,700	2,035	1,900	2,000	1,990	2,120	2,030	2,192
Hemispherical Temperature, HT (°F)	2,700	2,100	2,000	2,060	2,040	2,140	2,090	2,210
Fluid Temperature, FT (°F)	2,700	2,180	2,040	2,100	2,090	2,160	2,120	2,318
Ultimate Analysis								
Total Moisture (% wt.)	6.84	10.43	6.81	30	24.68	17.21	16.95	—
Carbon (% wt.)	74.85	65.49	69.39	62.53	70.73	60.99	61.61	72.00
Hydrogen (% wt.)	5.39	4.56	5.09	4.75	4.85	4.03	3.99	4.79
Nitrogen (% wt.)	1.53	1.11	1.26	1.23	0.84	0.75	0.78	0.84
Oxygen (% wt.)	2.02	8.16	7.80	14.69	16.80	11.64	10.73	20.73
Sulfur (% wt.)	0.68	4.52	4.21	0.99	0.41	0.33	0.45	0.12
Ash (% wt.)	8.67	16.16	12.25	15.81	6.37	5.04	5.47	—
Chlorine (% wt.)	0.02	0.12	0.16	0.11	0.09	0.01	0.02	—
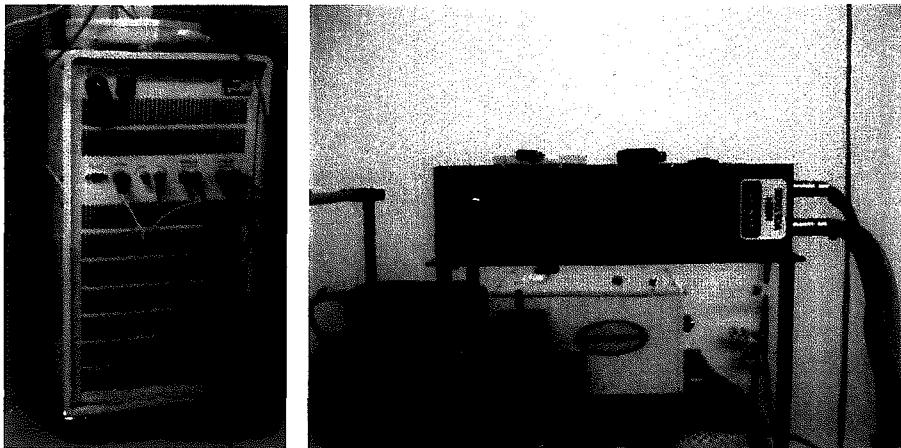
Figure 3-2. Laser Pulse Generator or Power Tower (left) and Laser Head (right).

The sample chamber is composed of two machined aluminum pieces. The chamber encloses a sample cart, coupled to a motorized XY stage (see Figure 3-3). The sample cart is positioned during measurements via a controller activated by the MeasureSolid software. The MeasureSolid software was adapted by ERCo to set the laser firing and spectrometer data collection parameters, control the sample position, and store the spectrometer trace data. The sample chamber allows a controllable non-oxygen atmosphere (helium was used as inert gas) to preserve the sample integrity from the elements in the air and preclude potential coal sample combustion. Further explanation for the use of an inert gas will be made later in this chapter. The top portion of the chamber has ports that allow creating the desired atmosphere inside the chamber, introducing the laser into the chamber, and viewing of the plasma by the optical components for the data collection. Inlet vents are located near the optic ports at the top of the chamber and directed to sweep particulate in the laser spark away from the laser window. The exhaust ports are connected to a 1/6 HP vacuum pump. A

door allows easy access to place the sample in the sample cart. Figure 3-4 shows a picture and a diagram of the sample chamber.
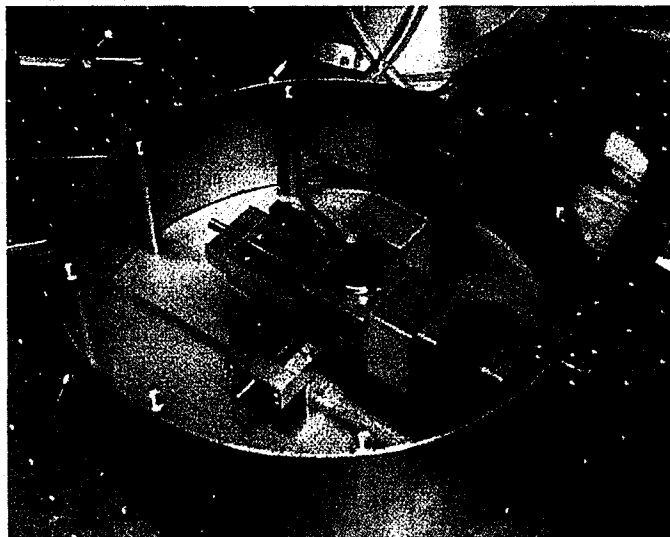

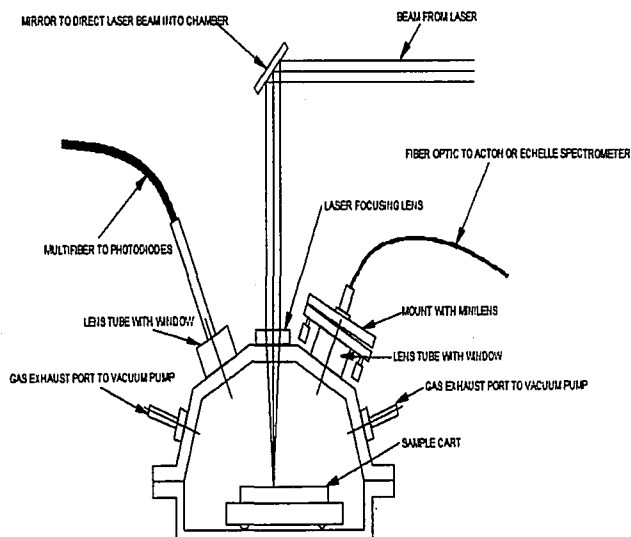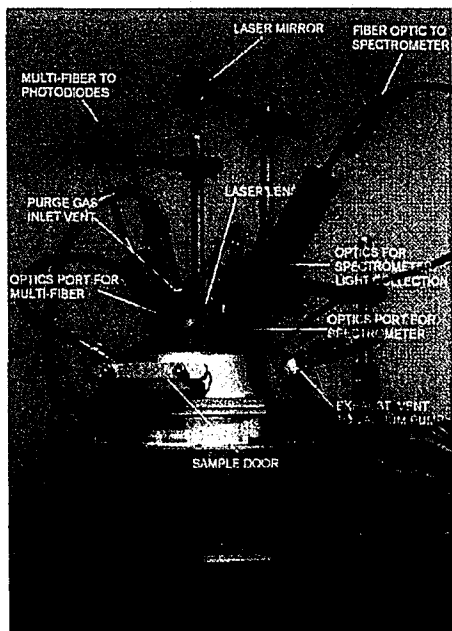**Figure 3-3.** Motorized XY Displacement System for Sample Inside the Chamber.

Figure 3-4. Sample Chamber Picture (left) and Diagram (right).

door allows easy access to place the sample in the sample cart. Figure 3-4 shows a picture and a diagram of the sample chamber.
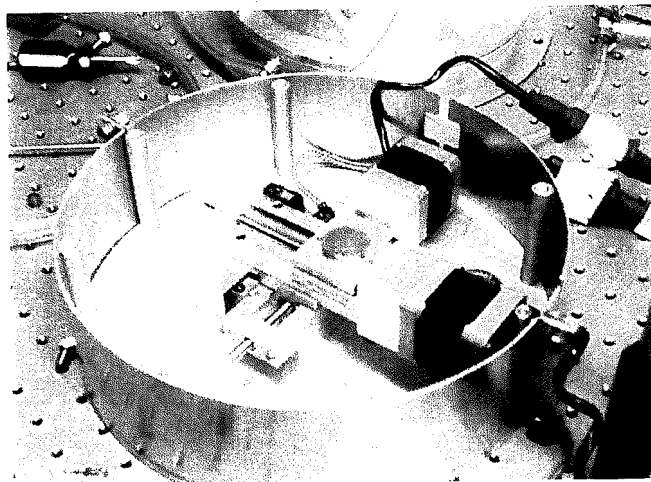

Figure 3-3. Motorized XY Displacement System for Sample Inside the Chamber.
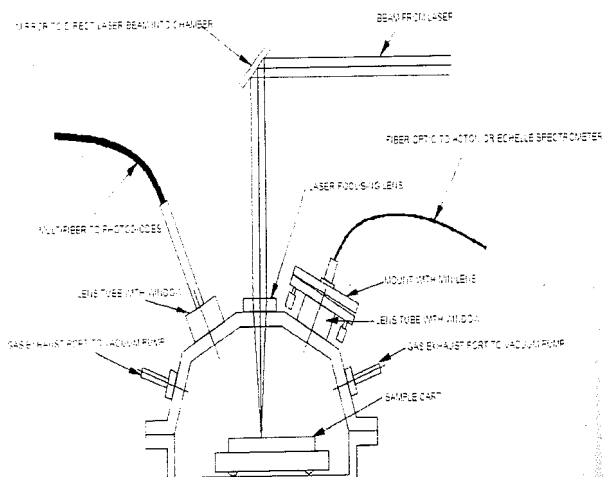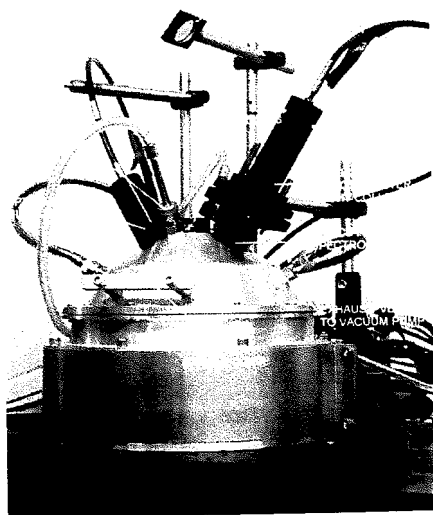

Figure 3-4. Sample Chamber Picture (left) and Diagram (right).

Light collection elements used in the set-up include mini-lenses to focus the emitting light and UV and visible-grade fused-silica optical fibers. An Echelle spectrometer (ESA – 3000 LLA) is used to collect the spectral data. The spectrometer contains an Echelle type grating that allows for high resolution spectra to be collected over a broad wavelength range of 200 to 600 nm. The following elements were measured with the Echelle spectrometer: aluminum, calcium, magnesium, sodium, iron, silicon, and titanium. The timing window for the Echelle spectral collection is set by the MeasureSolid software. Additionally, a photodiode/amplifier unit (ThorLabs – PDA55 – Switchable Gain Amplified Silicon Detector) assembly is used to collect intensity traces for the emission lines of potassium (interference filter centered at 769.9 nm), as well as the background intensity of the plasma (interference filter centered at 821.0 nm). The photodiode/amplifier assembly can be used to collect spectral data for sulfur, hydrogen, nitrogen, carbon, and oxygen. These elements were not considered for this application. Interference filters (Andover Corporation) are used to limit the wavelength of the light reaching the photodiodes to that of the emission line of interest. The light intensity passing through the filter is converted to a voltage signal, which is stored on the computer as a function of time. A trigger from the laser control unit initiates the collection of the data coincidental with the laser spark occurrence.

For the experimental procedure, to improve reproducibility of the results, coal samples used in the experiments were grounded to a 60 mesh (250 μm). Additionally, the coal samples were placed inside a laboratory furnace (Thermolyne, model 30400) at 230 °F (110 °C) for 2 hours for drying (see Figure 3-5). Double-sided sticky tapes were placed on aluminum sample holders for sample fixation. Riffled, powdered, dried up samples, of the order of less than a gram, were spread on the double-sided sticky

tape (see Figure 3-6). This method was selected over other methods, such as pressing the powders into pellets, and provided satisfactory results. The samples were placed inside the chamber and the chamber was sealed. A purging process was performed running the vacuum pump for about 1.5 minutes at a gauge pressure of 27 "Hg, then helium was run at a rate of about 18 SCFH for about 1.5 minutes, to achieve a gauge pressure in the chamber between 20 and 21 in. Hg. This purging process was carried out twice for chamber conditions preparation. The atmospheric conditions inside the chamber for the laser shooting and data acquisition process were determined by the elements to be measured. Half of the elements (iron, magnesium, sodium, and potassium) were measured under sub-atmospheric pressure conditions (gauge pressures between 20 and 21 in. Hg), and the other half (calcium, aluminum, silicon, and titanium) were measured under atmospheric pressure conditions.
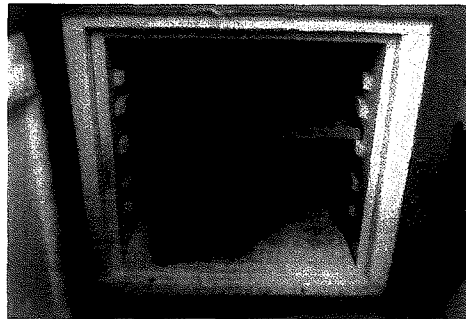

Figure 3-5. Riffled Powdered Coal Samples Placed Inside the Laboratory Furnace for Drying Process.
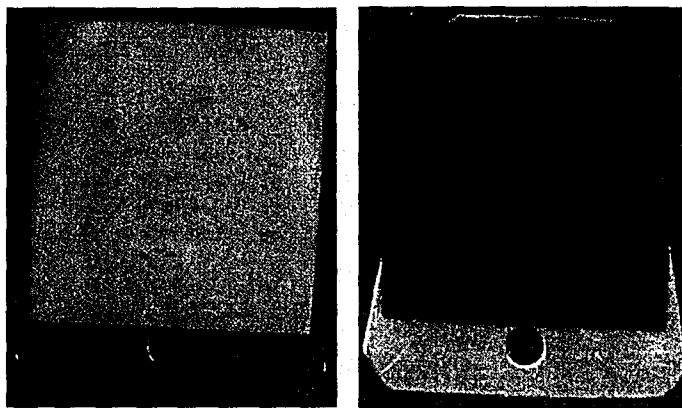
Figure 3-6. Double-sided Sticky Tape Placed on Aluminum Holder (left) and Coal Sample Spread on the Double-sided Sticky Tape (right).

All the elements, regardless of the atmospheric pressure inside the chamber, were measured in the presence of helium as inert gas. The inert gas acts as a buffer gas to prevent rapid oxidation of the free atoms in the plasma. Breakdown of argon and other inert gases occur in the plasma at a relatively high pressure. The argon atmosphere can enhance the analytical signal by re-excitation of atoms, resulting from collision with photon-excited argon. LIP in an argon atmosphere has a higher plasma temperature and longer emission period due to the low thermal conductivity of argon. The higher plasma temperature in the argon atmosphere also produces the highest continuum background. The emission characteristics of LIP from the air atmosphere are similar to that from the argon atmosphere. However, the continuum background is only half of that in the argon atmosphere. Helium has higher thermal conductivity and higher ionization potential than argon. Hence, it has a high-energy coupling efficiency compared with argon or air. Therefore, background from a helium atmosphere is lower and less sensitive to changes in laser energy and pressure [23].

After preparing the sample and the chamber atmosphere, the acquisition cycle per sample included moving the sample by the motorized XY displacement system through the controlling computer (MeasureSolid software), firing the LIBS system (see Figure 3-7 for an example of a LIBS single shot on a sample), and storing the resulting spectrum from both the spectrometer and the photodiodes channels. The MeasureSolid software was used to externally control the gating of the spectrometer and photodiodes, control the sample position, and store the spectrometer trace data. Time-gated optical detection is critical in optimizing signal response in LIBS experiments. Different delay and integration times were tried. The best configuration achieved for the experiments was 900 ns delay time and 1 ms gating time. A total of 60 sparks were shot per sample, in a 6 x 10 matrix (see Figure 3-8). However, only 50 of these shots were used per sample, leaving the first 10 shots as a warm-up process for the system. Once the acquisition cycles were completed, the data were processed automatically by MeasureSolid using averaging of spectral data from all the 50 shots and peak integration, for each particular sample. A file containing the spectrum for each one of the 50 shots for each sample, as well as a file containing the averaged spectrum for all the 50 shots was created and stored by MeasureSolid. This procedure allows normalization for pulse-to-pulse instability in the plasma, resulting in a superior level of precision in the measurement. The arithmetic average of the 50 spectrum collected from each sample, showed good accuracy in general for the elements of interest. The overall time for sample processing, including sample and chamber preparation, LIBS processing, and data archiving was of the order of 15 minutes per sample.

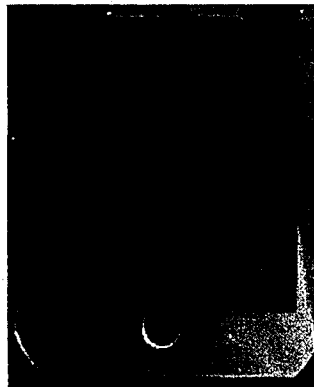**Figure 3-7.** LIBS System Single Shot on Coal Sample.

Figure 3-8. LIBS System Shooting Matrix (Coal Sample Already Run Through The System).

CHAPTER 4

Laboratory Experimental Results

The data collected with the LIBS system in the laboratory were processed and normalized for the development of ANNs. A series of steps was followed to carry out the data processing and normalization. The results of the laboratory experimentation were calibration curves, which were developed for the eight different elements of interest in this application (aluminum, calcium, magnesium, sodium, iron, silicon, titanium, and potassium). This chapter reports a description of the data processing and normalization procedures, as well as the laboratory experimental results.

The data from the LIBS system acquired by the Echelle spectrometer result in a spectrum containing different intensity levels at defined wavelengths. For practical applications, the measured emission intensities need to be related to relative or absolute elemental concentration. Performance of the coal chemical analysis using LIBS spectral strongly depends on the LIBS ability to differentiate the elemental composition in the LIBS intensity vs. wavelength trace. Figure 4-1 shows an example of a typical partial spectrum from the LIBS system made on a pulverized coal sample with the following elemental composition by weight: C=75.1 percent, Si=2.3 percent, Al=1.6 percent, Fe=1.1 percent, and Mn=77 ppm_w. Reference atomic emission line intensity information from the Kurucz's spectral line database was used to perform spectral fitting. Table 4-1 shows a part of the Kurucz's spectral line database, pertinent to the elements used for determination with the LIBS system in this application. The

59

Kurucz's spectral line database contains emission line wavelengths for different elements stretching from the vacuum UV to the near IR (approximately 200 to 780 nm).

The actual contour of spectral lines was closely approximated by the Voigt function profile. The generally accepted representation of the Voigt function in the form of a convolution of a Gaussian and a Lorentzian has the form:

$$V = \frac{a}{\pi} \int_{-\infty}^{\infty} \frac{exp(-t^2)}{a^2 + (x - t)^2} dt \qquad \text{Eqn. 4-1}$$

where a is the impact parameter, and x is the normalized wave number. Several algorithms that differ in accuracy and computational speed have been developed for integrating the Voigt profile. The Drayson algorithm is the most popular. For this application, an accepted equivalent form of the Voigt function was used:

$$V = \frac{a_0 \cdot a_3}{2\pi \cdot \sqrt{\pi} \cdot a_2{}^2} \int_{-\infty}^{\infty} \frac{exp(-t^2)}{\frac{a_3{}^2}{2a_2{}^2} + (\frac{x - a_1}{\sqrt{2}a_2} - t)^2} dt \qquad \text{Eqn. 4-2}$$

where a_0 is the area, a_1 is the center of the wavelength, a_2 is the Gaussian width (>0), and a_3 is the Lonrentzian width (≥0).

The information from the spectral lines showed in Table 4-1 was first supplied to a data processing algorithm. The 50 spectrums collected for each sample, from the 60 shots matrix mentioned in Chapter 3, were first averaged. The spectral lines database was then used to locate the spectral peaks corresponding to each element of interest in the averaged spectrum. Each spectral peak was fit to a Voigt function, which was solved using the Drayson algorithm. A multidimensional minimization routine was used, which minimizes the sum of the squares of the point-by-point differences

between the data and the fit. Additionally, a background correction was performed of the data by subtracting the average intensity level surrounding each spectral line of interest from the resulting area, for each spectral peak. The resulting value for this subtraction (in arbitrary units) represents the LIBS-detected signal for each element of interest.

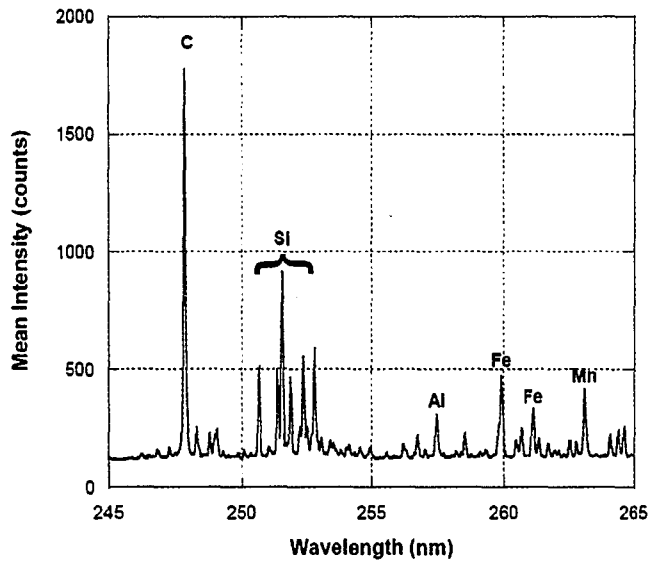**Figure 4-1.** Sample of Partial (245 to 265 nm) LIBS Spectrum for Pulverized Coal.

Table 4-1: Partial Data from Kurucz's Spectral Line Database.

Element (Code Name)	WI [nm] vac<200<air
13.00 Al I	396.15
20.00 Ca II	422.67
19.00 K I	769.90
12.00 Mg II	285.21
11.00 Na I	589.00
26.00 Fe I	259.96
14.00 Si I	288.16
22.00 Ti I	323.44

61

The data acquired by the photodiodes assembly result in a voltage signal trace as a function of time for potassium (at 769.9 nm), and for the background (at 821.0 nm). Figure 4-2 shows an example of a typical voltage signal trace from the photodiodes assembly in the LIBS system made on a pulverized coal sample with a potassium concentration of 0.13 percent by weight.
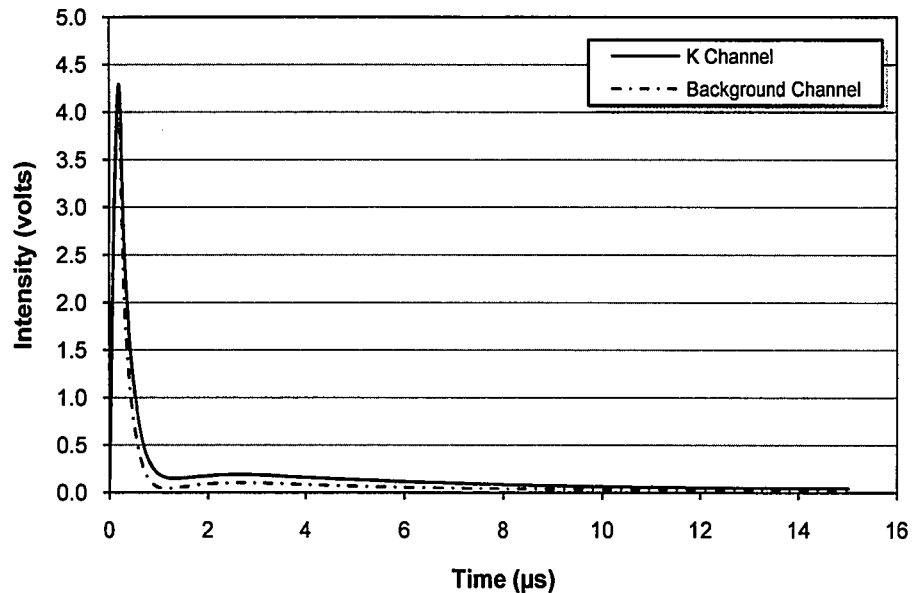
Figure 4-2. Sample of Voltage Trace from Photodiodes Assembly in the LIBS System.

For this application, the voltage signal collected with the photodiodes assembly was used to calculate the dark current, averaging the voltage signal for the last three microseconds on each channel (potassium and background channel). The dark current is the current that flows in the photodetector when there is no optical radiation incident and operating voltages are applied. The dark current was subtracted in the period between 3 and 7 μs on each channel. Potassium to background channel signal ratios (K/BG) were determined in the period between 3 and 7 μs. The value resulting from the sum of these ratios represented the LIBS-detected data for potassium.

The LIBS system response must be calibrated with a set of certain measurements. Calibration is the most difficult issue in the development of LIBS, especially for field measurements. In addition to the variables related to emission spectra, several other variables affect the intensity of the LIBS signal. These variables are: the fluctuation of incident laser energy; the size and density of particles and associated sample matrix; the location of the focus point; and the surface feature and history of ablation by laser shots. The calibration principle used was "comparing like with like". Samples of coals from the coal inventory were used as calibration standards, since they covered an expanded range of elemental concentrations, as mentioned in Chapter 3.

As mentioned in Chapter 3, from all the elements of interest (aluminum, calcium, magnesium, sodium, iron, silicon, titanium, and potassium), half of the elements (iron, magnesium, sodium, and potassium) were measured under sub-atmospheric pressure conditions (gauge pressures between 20 and 21 "Hg), while the other half (calcium, aluminum, silicon, and titanium) were measured under atmospheric pressure conditions. The reason for choosing two different conditions inside the chamber was that experimentally the LIBS system was found to produce better and more consistently stable signals for each half of the elements measured at chosen atmospheric pressure conditions. This procedure resulted in two independent runs for each sample to obtain a complete LIBS-based characterization of a specific coal. Therefore, one run to get the signal for iron, magnesium, sodium, and potassium; and another run to get the signal for calcium, aluminum, silicon, and titanium, would complete one single characterization of the coal sample containing all the elements of interest.

A set of three samples was analyzed with the LIBS system for each coal. This procedure resulted in six independent samples that had to be prepared and run through the system for complete characterization of each coal. The six samples were prepared after splitting the samples with a riffler. Each pair of samples with both atmospheric conditions was analyzed independently, and the results processed separately. The spectral intensity data collected were processed to obtain LIBS intensity ratios. Individual elemental intensity values were normalized by using the calcium emission line, at 422.7 nm, for aluminum, iron, and potassium. The silicon emission line, at 288.2 nm, was used to normalize calcium, magnesium, and sodium. This normalization was done to minimize the impact of the variability of the background emission level in each individual set of measurements. On the other hand, silicon and titanium were left as LIBS intensity signal (counts), since they showed to have less impact from the background variability. Table 4-2 shows a summary of the normalization carried out for each element of interest, using the LIBS intensity signal from the different spectral lines.

Table 4-2: Summary of LIBS-signal Normalization for Elements of Interest.

Element of interest	Normalized LIBS intensity signal
Fe	$(Fe/Ca)_{LIBS}$
Mg	$(Mg/Ca)_{LIBS}$
Na	$(Na/Ca)_{LIBS}$
K	$(K/Ca)_{LIBS}$
Ca	$(Ca/Si)_{LIBS}$
Al	$(Al/Si)_{LIBS}$
Si	$(Si)_{LIBS}$
Ti	$(Ti)_{LIBS}$

It is important to make some relevant distinctions between the measurement of coal composition using LIBS and the chemical reactions that are used in traditional ASTM laboratory analysis before describing the principle of comparison used between both methods. Metal oxides are the parameters directly measured by the ASTM methods, because coal is reduced to ash before the ASTM measurements are performed. The LIBS technique measures only the total number of atoms of each corresponding element in the coal matrix, independent of the compound involved, because this type of light interaction is insensitive to the chemical bonds in matter. Furthermore, coal is not burned before it is measured by the LIBS analyzer and is only sensitive to elemental composition; hence, the oxides cannot be measured directly by the analyzer. Thus, LIBS measurements are insensitive to chemical bonds, and encompass the total atom concentration in the coal matrix.

For the reasons described above, elemental LIBS intensity ratios were compared to equivalent molar ratios calculated from the ash analyses (Table 3-1). The molar percentage for each element in the coal was estimated using the proximate, ultimate and ash mineral analyses by the following equation:

$$x_i = y_j \cdot ash \cdot n_i \cdot \frac{MW_{coal}}{MW_{oxide}}$$

Eqn. 4-3

where x_i is the elemental mole fraction of element i, y_j is the mass fraction of oxide j, ash is the ash weight percentage in the coal, n_i is the number of atoms of element i on the j oxide, and MW_{coal} and MW_{oxide} are the molecular weights of coal and oxide, respectively.

Figures 4-3 through 4-10 show the calibration curves constructed for each elemental ratio. These calibration curves were generated by plotting the measured LIBS intensity ratios versus the corresponding molar ratio estimated from the results of the standardized chemical analyses using Equation 4-1. The LIBS measurements were set-up in such a way that the measured intensities were linearly proportional to the elemental mole percentage. The curves were constructed by making x-y scatter plots. In these plots, the y-axis represents the count rate or emission intensity ratios measured by the analyzer, and the x-axis represents the elemental molar percentage ratios of the elements found through standardized (ASTM) methods. For each element, a linear least squares fit to the data points yields an equation in the form:

$$y = C_0 + C_1 \cdot x \qquad \text{Eqn. 4-4}$$

where y is the intensity ratio measurement, x is the molar concentration ratio, and C_0 and C_1 are coefficients associated with the calibration of the respective element. Through the use of the calibration curves, when an unknown sample is measured, the LIBS-measured elemental intensity ratio for a particular element is converted to an equivalent ASTM-measured elemental molar ratio by using the appropriate calibration equation (shown in Figures 4-3 through 4-10). The individual elemental molar concentration for Si and Ti can be directly found from the calibration curves, since these elements were not normalized with respect to any other. The use of the determined Si molar concentration leads to the determination of Al and Ca molar concentration by:

$$x_i = \left(\frac{I}{Si}\right)_{STANDARD\ Mol\%} \cdot Si_{determined} \qquad \text{Eqn. 4-5}$$

where x_i is the individual elemental mole fraction of element i (Al or Ca), $(I/Si)_{STANDARD}$ $_{Mol\%}$ is the elemental molar ratio determined through the calibration curve for element i (Al or Ca), and $Si_{determined}$ is the individual elemental mole fraction of element Si determined through the calibration curve.

The use of the determined Ca molar concentration leads to the determination of Fe, Mg, Na, and K molar concentration by:

$$x_i = \left(\frac{I}{Ca}\right)_{STANDARD\,Mol\%} \cdot Ca_{determined}$$

<div align="right">Eqn. 4-6</div>

where x_i is the individual elemental mole fraction of element i (Fe, Mg, Na or K), $(I/Ca)_{STANDARD\,Mol\%}$ is the elemental molar ratio determined through the calibration curve for element i (Fe, Mg, Na or K), and $Ca_{determined}$ is the individual elemental mole fraction of element Ca, previously determined through Equation 4-5.

All of the calibration curves exhibited linear responses. No sign of spectral saturation was observed from the data, which may occur at high concentrations of a particular element, due to the ability of the atoms to sink the emitted energy. The error bars shown in the calibration curves represent two standard deviations of each data set for each coal and represent the errors associated with the measurement at each particular concentration. The two standard deviations gives a 95 percent confidence level for future measurements to be within the shown ranges.

Figure 4-3. Calibration Curve for Elemental Iron.

Figure 4-4. Calibration Curve for Elemental Magnesium.

68

Figure 4-5. Calibration Curve for Elemental Sodium.

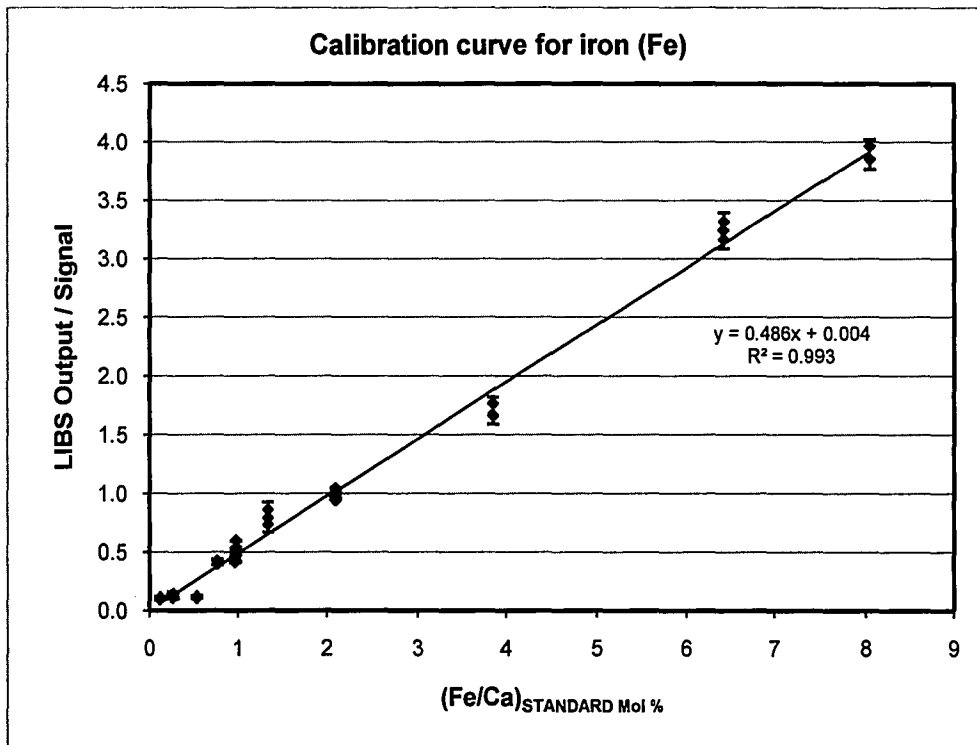**Figure 4-6.** Calibration Curve for Elemental Potassium.

69

Figure 4-7. Calibration Curve for Elemental Calcium.

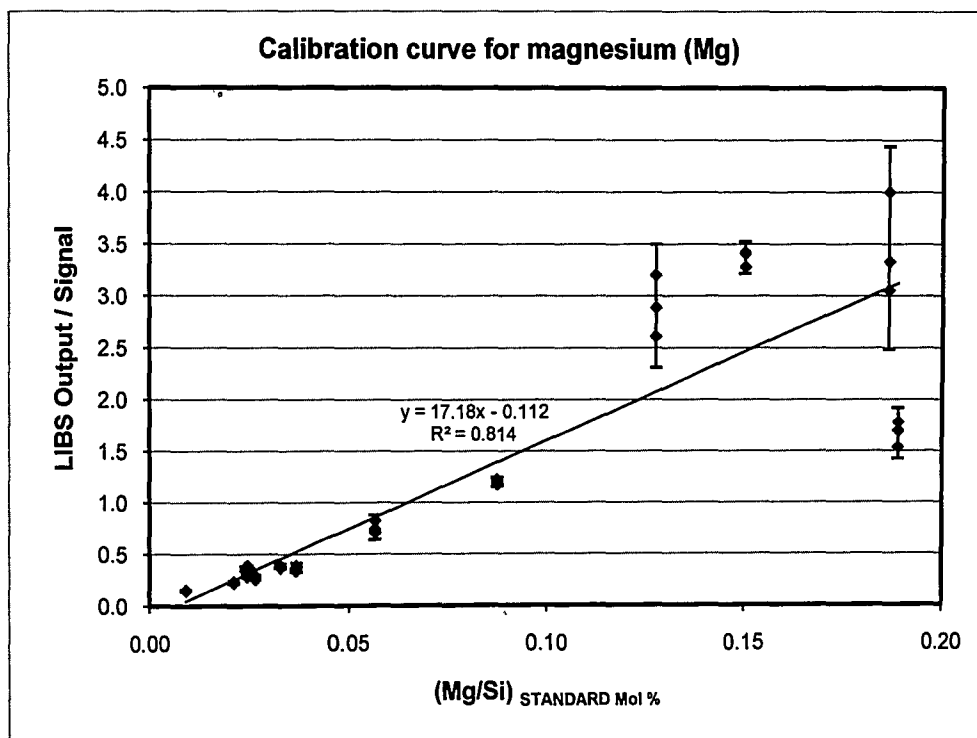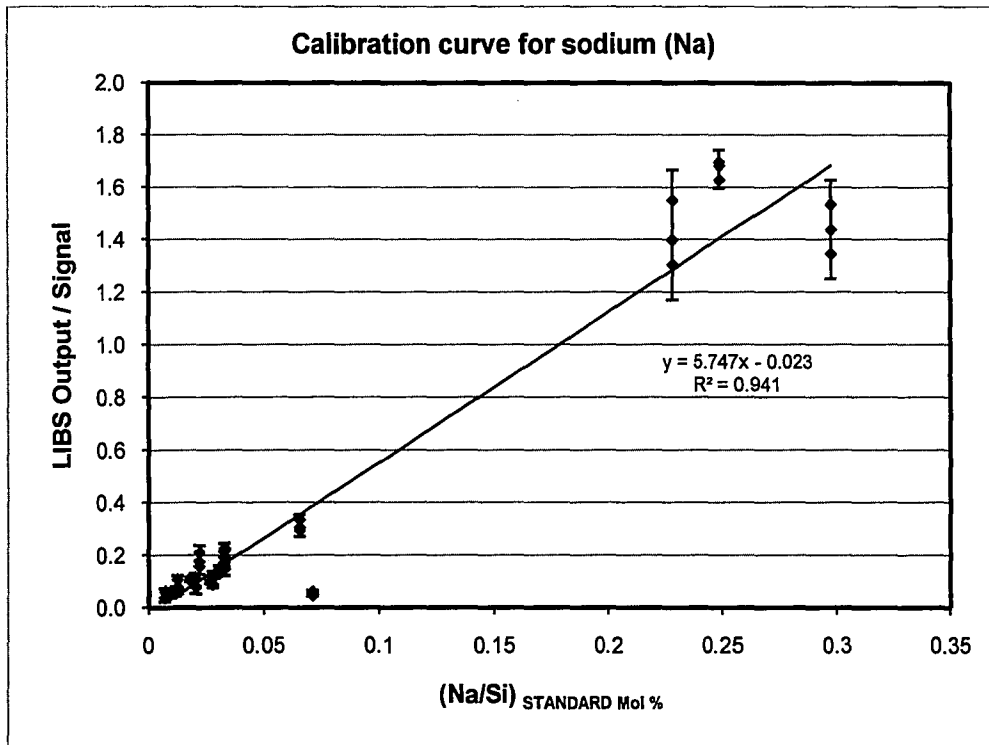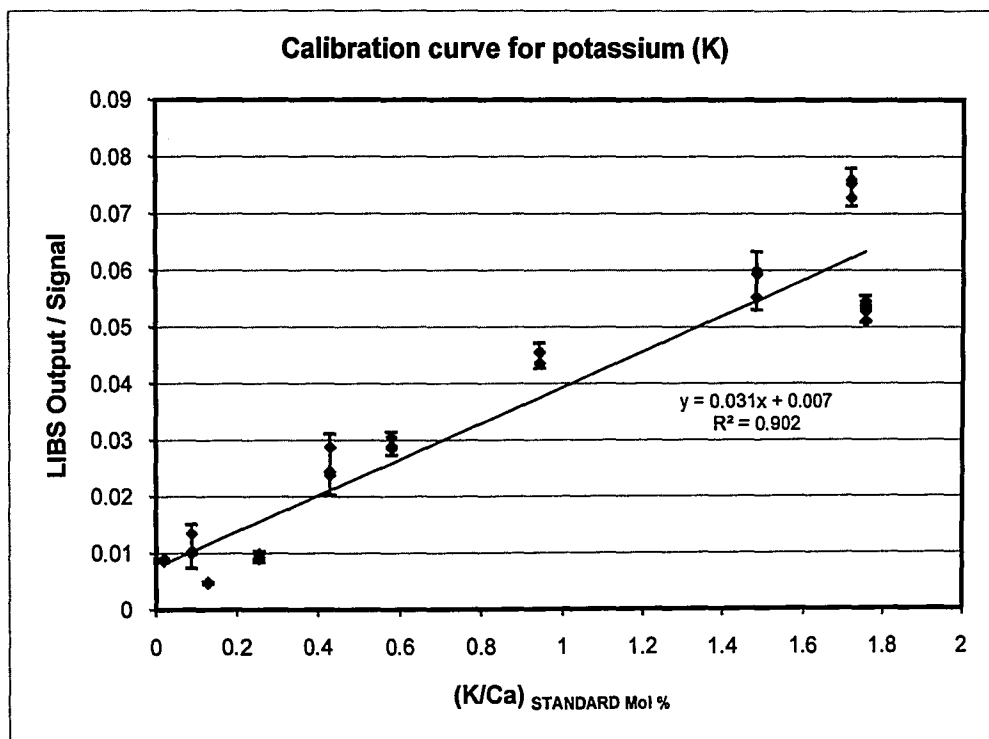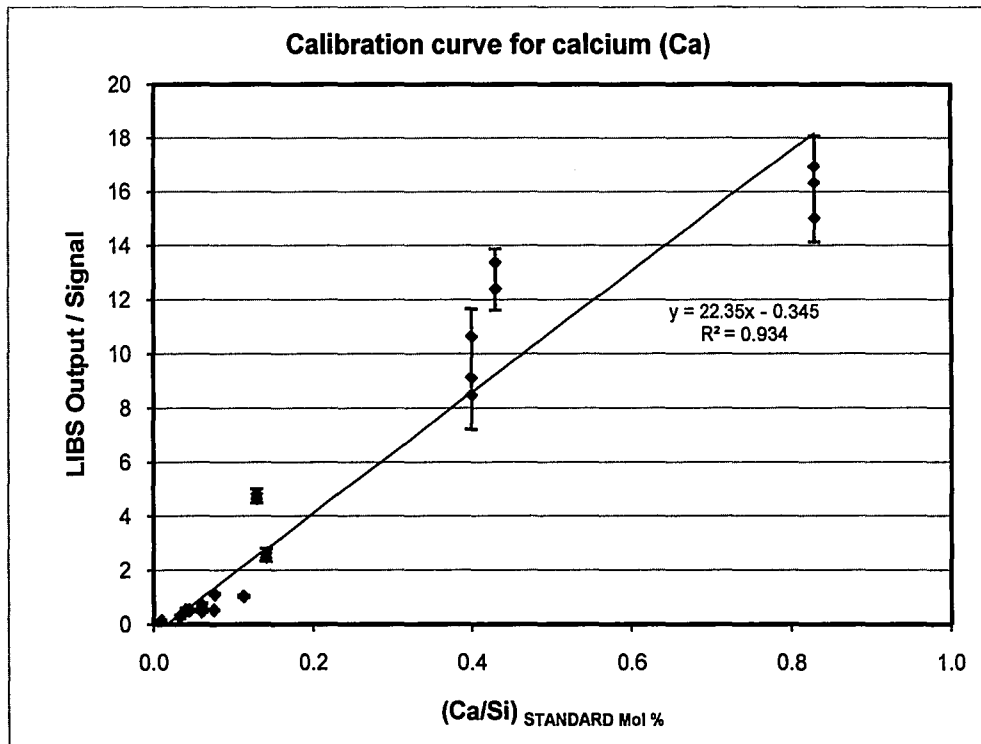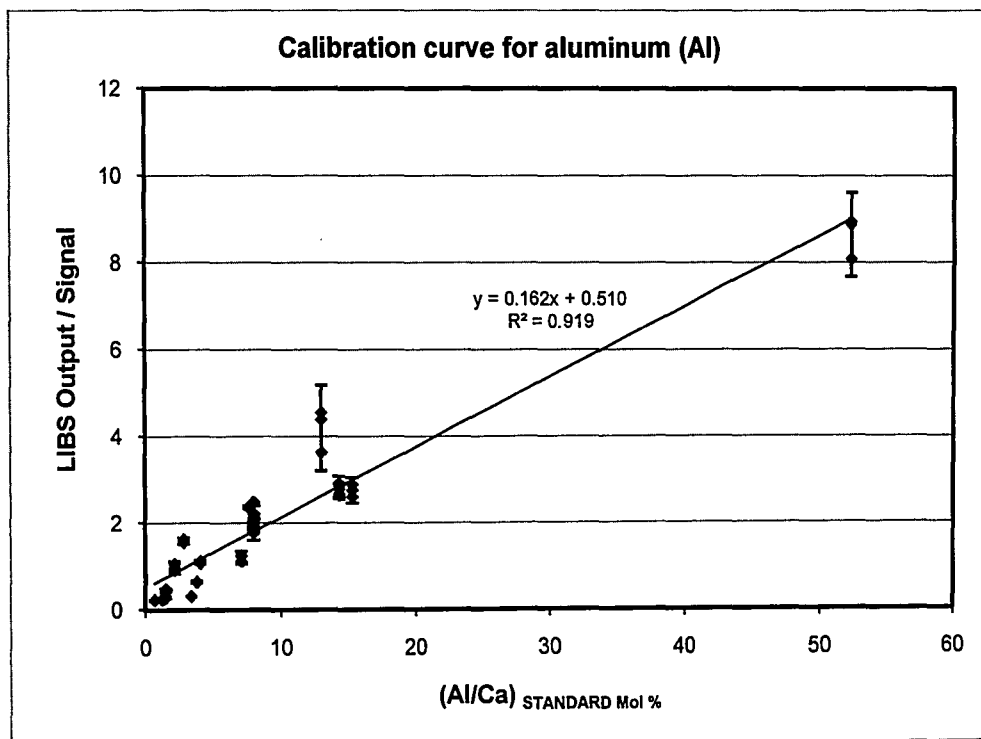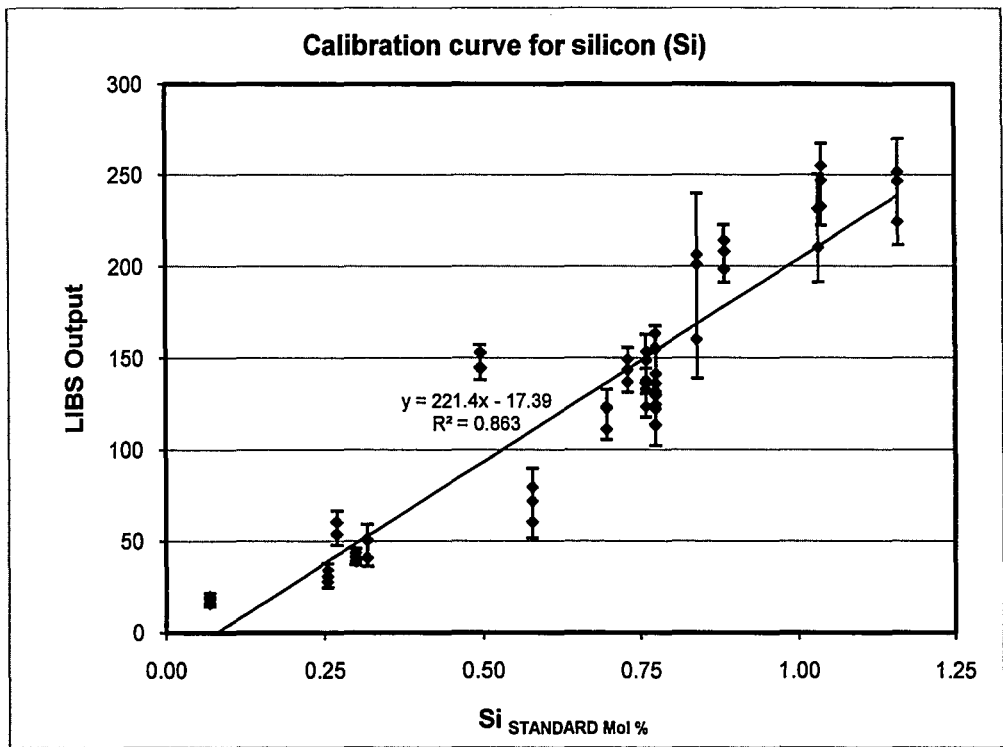**Figure 4-8.** Calibration Curve for Elemental Aluminum.

Figure 4-9. Calibration Curve for Elemental Silicon.
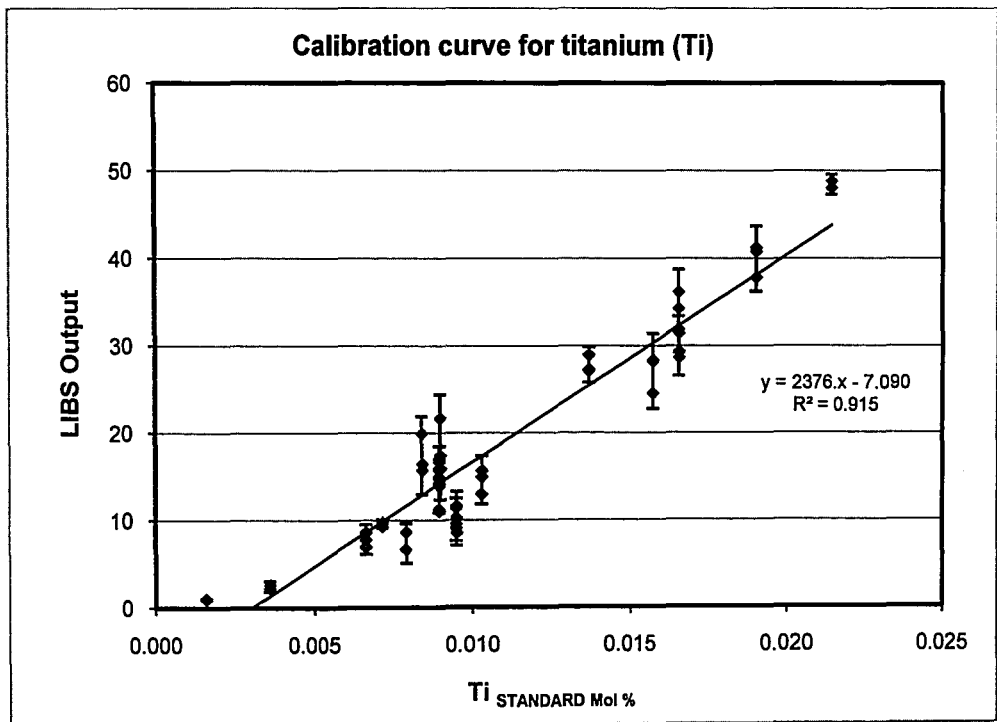
Figure 4-10. Calibration Curve for Elemental Titanium.

71

The calibration curves lead to satisfactory results, considering the broad range of concentrations for each elemental ratio, and the range of coals with dissimilar ranks. Furthermore, the magnitudes of the error bars were not excessive, since large variations in emission intensity would be expected on particle-by-particle basis due to the inherent heterogeneity of coal. The term R^2, which is simply the square of the correlation coefficient (R), on each curve, represents the variation in the data explained by the fitted line. This is commonly used to evaluate the quality of the linear fit, with $R^2=1$ being a perfect linear fit (zero variation). The R^2 terms in the curves range from 0.814 for Mg to 0.994 for Fe. The curves showed that for most of the elements, the correlation quality decreased at larger concentration levels.

The uncertainty and reproducibility of the elemental measurements carried out with the LIBS system were determined from measurements on multiple samples for the Eastern U.S. bituminous coal identified in Table 3-1 as BPD. Uncertainty was defined as the deviation of the average LIBS measurement from the "true" value of each element in the coal, obtained by an independent analytical technique, in this case the ASTM standard method. Reproducibility, or measurement precision, was defined as the percentage that one standard deviation of the set of results represents from the average value.

A total of 18 individual runs were performed through the LIBS measurement cycle for BPD coal, including both atmospheric conditions described elsewhere in this chapter. This led to 9 experimental points with all the elements of interest (aluminum, calcium, magnesium, sodium, iron, silicon, titanium, and potassium). Table 4-3 includes the results of the uncertainty and reproducibility test for each of the eight

elements of interest. Table 4-3 shows results in a mass basis, which was found from the molar basis originally determined by the LIBS system, using the following equation:

$$z_i = x_i \cdot \frac{MW_i}{MW_{coal}}$$

where z_i is the elemental mass fraction of element i, x_j is the elemental mole fraction of element i, and MW_i and MW_{coal} are the molecular weights of element i and coal, respectively.

Table 4-3: Uncertainty and Precision Test Results for BPD Coal.

Sample analysis	wt. % Mg 285.2 nm	wt. % Na 589.0 nm	wt. % K 769.9 nm	wt. % Fe 259.9 nm	wt. % Al 396.2 nm	wt. % Ca 422.7 nm	wt. % Si 288.2 nm	wt. % Ti 323.4 nm
1	0.042	0.074	0.230	0.265	1.012	0.192	2.083	0.055
2	0.042	0.054	0.215	0.260	1.052	0.180	2.087	0.054
3	0.046	0.061	0.241	0.286	1.100	0.200	2.343	0.060
4	0.044	0.063	0.259	0.272	1.144	0.198	2.258	0.058
5	0.049	0.083	0.253	0.297	1.233	0.190	2.444	0.056
6	0.051	0.087	0.260	0.269	1.213	0.199	2.528	0.061
7	0.053	0.067	0.290	0.309	1.262	0.224	2.753	0.054
8	0.045	0.060	0.295	0.349	1.104	0.201	2.342	0.058
9	0.052	0.085	0.310	0.323	1.351	0.213	2.749	0.058
LIBS Mean	**0.047**	**0.070**	**0.261**	**0.292**	**1.163**	**0.200**	**2.398**	**0.057**
SD	0.004	0.012	0.031	0.030	0.109	0.013	0.248	0.003
Precision (%)	*8.7*	*17.4*	*12.0*	*10.3*	*9.4*	*6.5*	*10.3*	*4.6*
ASTM	**0.063**	**0.074**	**0.110**	**0.315**	**1.248**	**0.232**	**2.724**	**0.054**
Uncertainty (%)	*25.3*	*4.8*	*137.4*	*7.1*	*6.8*	*13.8*	*12.0*	*6.1*

The uncertainty test shows agreement within an order of magnitude for the majority of the elements. The average measurement difference between the LIBS and standardized measurements was found to be better than 14 percent (absolute) for all elements, except for magnesium and potassium, which were excessively large. The disparity for the uncertainty found for magnesium could be attributed to the overlapping

nature of the magnesium spectral line with that of iron. On the other hand, the disparity

for the uncertainty found for potassium could be attributed to the performance of the

photodiodes assembly and/or the normalization procedure.

CHAPTER 5

Modeling and Results

The main function of the LIBS system in this application is determining the coal-ash elemental composition. However, this information by itself would be of very limited value in the electric power generation industry. Further use should be given to this information to increase its value and importance. As mentioned in Chapter 2, the ash fusion temperatures are of great importance, more specifically the initial deformation temperature of the coal-ash, because of its capability for determining the slagging propensity of the coal. The main objective of this research work was to estimate the fusion temperature of the coal-ash, based on the elemental composition measured with the LIBS system. This information would be provided to plant operators to mitigate slagging impacts in the boilers. This chapter reports an ANN-based approach and the results obtained in determining initial deformation temperatures of coal-ashes.

The approach proposed in this study aims at utilizing the data produced by the LIBS system for the prediction of coal-ash initial deformation temperature using artificial intelligence (AI) techniques, more specifically ANNs. ANN models were developed to perform the prediction of the initial deformation temperature under reducing conditions. An ANN is an interconnected group of artificial neurons that uses a mathematical or computational model for information processing. They are inspired by the way biological nervous systems, such as the brain, process information (www.en.wikipedia.org). ANNs learn by example, like people. They learn the

relationship between input data vectors and the outpu(s) by a training process. The networks are constructed with processing units or nodes connected together with parameters called weights. A weight indicates how strongly the source unit of the connection affects the value of the destination unit. The units in an ANN are usually arranged in layers, and generally consist of an input layer, one or more internal hidden layers, and an output layer. Each layer can have as many units as necessary for the specific application. In the case of the LIBS modeling architecture, two internal hidden layers were used. As mentioned in Chapter 2, studies have been carried out in developing ash fusion temperature models successfully, using ASTM data and statistical fitting models. The ANN models developed in this study were based on the chemistry of ash fusion temperature and involved key ash elements known to participate in the fusion temperature determination.

The laboratory-derived database based on the LIBS system test results was used to create ANN models using the NeuFrame v.4 software package from Neusciences, UK. The ANN models were used to establish functional relationships (non-linear mapping functions) between LIBS-generated elemental intensity ratios inputs obtained in the laboratory and an output, the coal-ash initial deformation temperature. The elements of interest (aluminum, calcium, magnesium, sodium, iron, silicon, titanium, and potassium) were configured into 13 input parameters: silica value, base, acid, R250, dolomite ratio, silicon, the sum of aluminum and titanium, iron, calcium, magnesium, potassium, sodium, and base to acid ratio (B/A ratio). The inputs were configured using the LIBS elemental intensity ratios, described in Chapter 4. The silica value, base, acid, R250, dolomite ratio, and B/A ratio were defined as:

$$Silica\ value = \frac{Si}{(Si + Fe + Ca + Mg)}$$ Eqn. 5-1

$$Base = Fe + Ca + Mg + K + Na$$ Eqn. 5-2

$$Acid = Si + Al + Ti$$ Eqn. 5-3

$$R250 = \frac{(Si + Al)}{(Si + Al + Fe + Ca)}$$ Eqn. 5-4

$$Dolomite\ ratio = \frac{(Ca + Mg)}{(Fe + Ca + Mg + K + Na)}$$ Eqn. 5-5

$$B/A\ ratio = \frac{Base}{Acid}$$ Eqn. 5-6

The ANN used for this application was a feed-forward network with back-propagation training algorithm. In this type of network, the information flows from the input vector to the output. The back-propagation training algorithm is a generalized form of the Wodrow-Hoff delta rule, which is a gradient-descent algorithm designed to minimize the network error function. In the back-propagation training algorithm, the neurons are trained under the "supervision" of the target data.

77

The back-propagation training algorithm takes a certain amount of epochs to train the network. An epoch is a "training pass", a cycle in which the information flows from the input vector to the output, adjusting the weights through the layers. Each layer inside the network must have a transfer function through which it applies the weights to the different interconnected nodes. These transfer functions are typically linear, sigmoid, and tanh. The learning rate is a parameter that affects the speed at which the ANN arrives at the minimum error solution; it determinates by how much the weights are changed at each step. If the learning rate is too small, the algorithm will take a long time to converge or reach a minimum error. However, if the learning rate is too large, the network may not be able to reach convergence; it may become unstable and diverge. The momentum rate is a parameter used to prevent the algorithm from converging to a local minimum or saddle point. If the momentum rate is too large, it could increase the speed of convergence, but it could also create a risk of overshooting the minimum, which can cause the network to become unstable. On the other hand, if the momentum rate is too small, it cannot reliably avoid a local minimum, and it can also cause considerable computer time loads in the training process of the network (www.chesireeng.com).

The network pre-processes the data by normalizing the complete input vector (each one of the input parameters) to fit a [0, 1] range before the training process. The normalization of the input vector is carried out by first approximating the data to a standard normal distribution, with zero mean and unity standard deviation, as follows:

$$X_1 = \frac{X - \bar{X}}{\sigma} \qquad \text{Eqn. 5-7}$$

where X is the original input data vector, $\bar{X}$ is the mean vector (calculated from the input data vector), σ is the standard deviation vector (calculated from the input data vector), and X_1 is the standard normal approximated input data vector.

The standard normal approximated input data vector is then normalized to fit a [0, 1] range, as follows:

$$X_2 = \frac{X_1 - min(X_1)}{max(X_1) - min(X_1)}$$
<div align="right">Eqn. 5-8</div>

where $min(X_1)$ is the minimum values vector from X_1, $max(X_1)$ is the maximum values vector from X_1, and X_2 is the normalized input vector to be used for the training process. This normalization process limits the functionality of the network to a specific training domain of input parameters. Although the network is capable of extrapolating for certain parameters that may fall outside of this domain, the optimal performance of the network would be limited to the training domain.

Given the large number of input parameters involved in the ANN (thirteen for this application) and the limited number of data points collected in the laboratory (forty eight experimental data points, three for each one of the sixteen coals), the set of input data was repeated four times, to populate the total number of data points provided to ANN to 192 data points. This procedure is typically carried out in the development of ANNs to provide more "robustness" to the network when limited data are available. However, this "trick" should not be over-used because it can cause the network to narrow its extrapolation work domain and/or get over-trained over the provided domain.

The process to obtain the ANN to be used was based on a trial-and-error principle, since there is no defined "recipe" for different applications of the ANNs.

Different combinations of number of internal nodes, type of transfer functions, and learning and momentum rates were tried before reaching the ANN with the lowest root mean square error (RMSE). The resulting architecture for the ANN model is shown in Figure 5-1. The transfer function for the input layer containing the 13 input parameters was set to a linear function. Two internal hidden layers were included with 7 and 3 nodes, respectively, and sigmoid transfer functions for both of them. The transfer function for the output layer, containing the coal-ash initial deformation temperature, was set to a sigmoid function. The network training used 102,045 epochs, with a learning rate of 0.2 and a momentum rate of 0.8. The ANN final RMSE was approximately 12.4 °F.

Figure 5-1. Artificial Neural Network Architecture for Coal-ash Initial Deformation Temperature Prediction.

Different combinations of number of internal nodes, type of transfer functions, and learning and momentum rates were tried before reaching the ANN with the lowest root mean square error (RMSE). The resulting architecture for the ANN model is shown in Figure 5-1. The transfer function for the input layer containing the 13 input parameters was set to a linear function. Two internal hidden layers were included with 7 and 3 nodes, respectively, and sigmoid transfer functions for both of them. The transfer function for the output layer, containing the coal-ash initial deformation temperature, was set to a sigmoid function. The network training used 102,045 epochs, with a learning rate of 0.2 and a momentum rate of 0.8. The ANN final RMSE was approximately 12.4 °F.
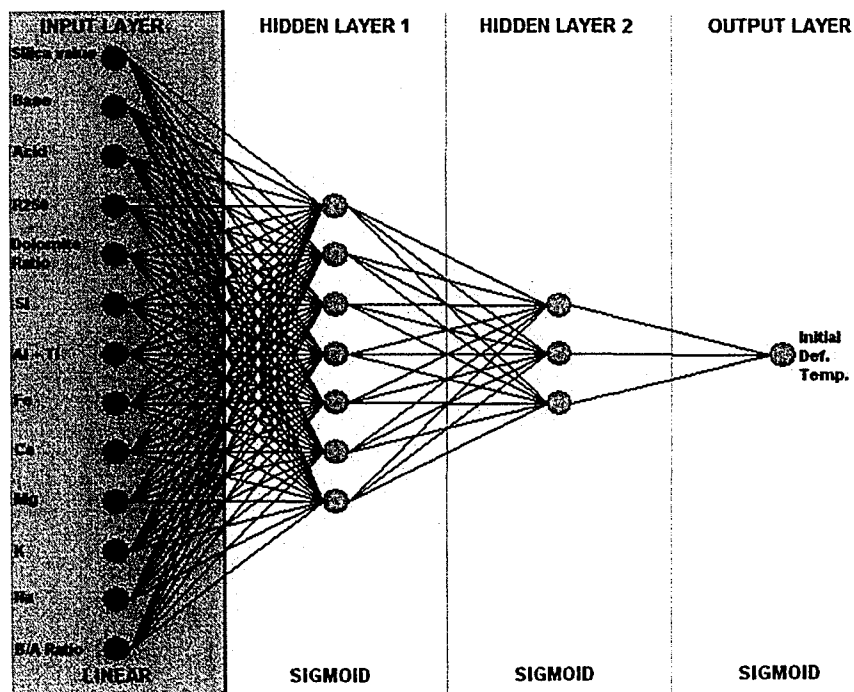

Figure 5-1. Artificial Neural Network Architecture for Coal-ash Initial Deformation Temperature Prediction.

The analytical procedure carried out by the ANN to calculate the output (coal-ash initial deformation temperature) based on the inputs (thirteen input parameters), was performed by using weights assigned in the training process and transfer functions.
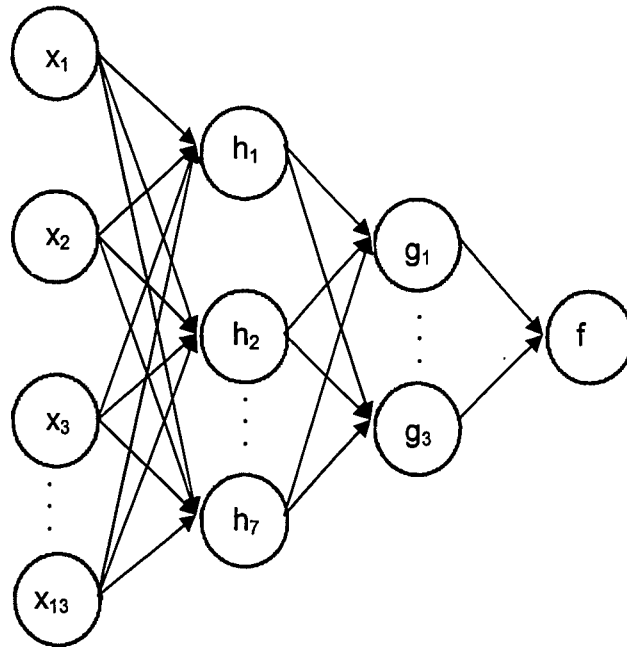
Figure 5-2. Artificial Neural Network Dependence.

Figure 5-2 shows a schematic of a generic ANN configuration. If the nodes in each layer are denoted as i and j, the ANN operation to calculate the vector of values in the second layer can be defined with the following equation:

$$h_j = sigmoid\left(bias_j + \sum_{i=1}^{13} w_{ix} \cdot x_i\right)$$

Eqn. 5-9

where $bias_j$ is a number determined by the training process for node j in layer h, w_{ix} is the weight assigned to the node i in layer x, x_i is the normalized value from node i in

layer x, h_j is the value assigned to node j in layer h (with 7 ≥ j ≥ 1), and the sigmoid

function is defined as:

$$sigmoid(s) = \frac{1}{(1 + e^{-s})}$$ Eqn. 5-10

Furthermore,

$$g_j = sigmoid\left(bias_j + \sum_{i=1}^{7} w_{ih} \cdot h_i\right)$$ Eqn. 5-11

where $bias_j$ is a number determined by the training process for node j in layer g, w_{ih} is

the weight assigned to the node i in layer h, h_i is the value previously found from

Equation 5-9, and g_j is the value assigned to node j in layer g (with 3 ≥ j ≥ 1).

Finally,

$$f = sigmoid\left(bias + \sum_{i=1}^{3} w_{ig} \cdot g_i\right)$$ Eqn. 5-12

where bias is a number determined by the training process for the output node f, w_{ig} is

the weight assigned to the node i in layer g, g_i is found from Equation 5-11, and f is the

value assigned to the output node, the predicted coal-ash initial deformation

temperature. A detailed report, with all the parameters used to characterize the ANN

developed for coal-ash fusion temperature prediction is included in the Appendix at the

end of the thesis.

The results from the ANN model developed with the laboratory LIBS-derived

database are included in Figure 5-3. This figure shows a plot of ASTM fusion

temperatures results versus LIBS-based predicted fusion temperatures. The data

points used to train the network, are shown with blue diamonds. Data that were not used in the training process, and were acquired independently in the laboratory at a later date to test the network, are shown with red squares. The data used to test the network at a later date, were collected with the LIBS system using four coals included in the coal inventory (DRUM, GUA, BPD, and CUCU). These coals were selected because they are commonly fired at the power plant selected for LIBS testing in the field. Given the inherent reproducibility of the ASTM method to determine ash fusion temperatures (up to 176 °F), the large variability of the coal properties present in the coal inventory, and the limited number of coals that were used for development of the training database for the ANN, it can be inferred from the laboratory results shown in Figure 5-3, that an ANN with an acceptable degree uncertainty can be created using LIBS-based coal elemental data and a predicted coal-ash initial deformation temperature.
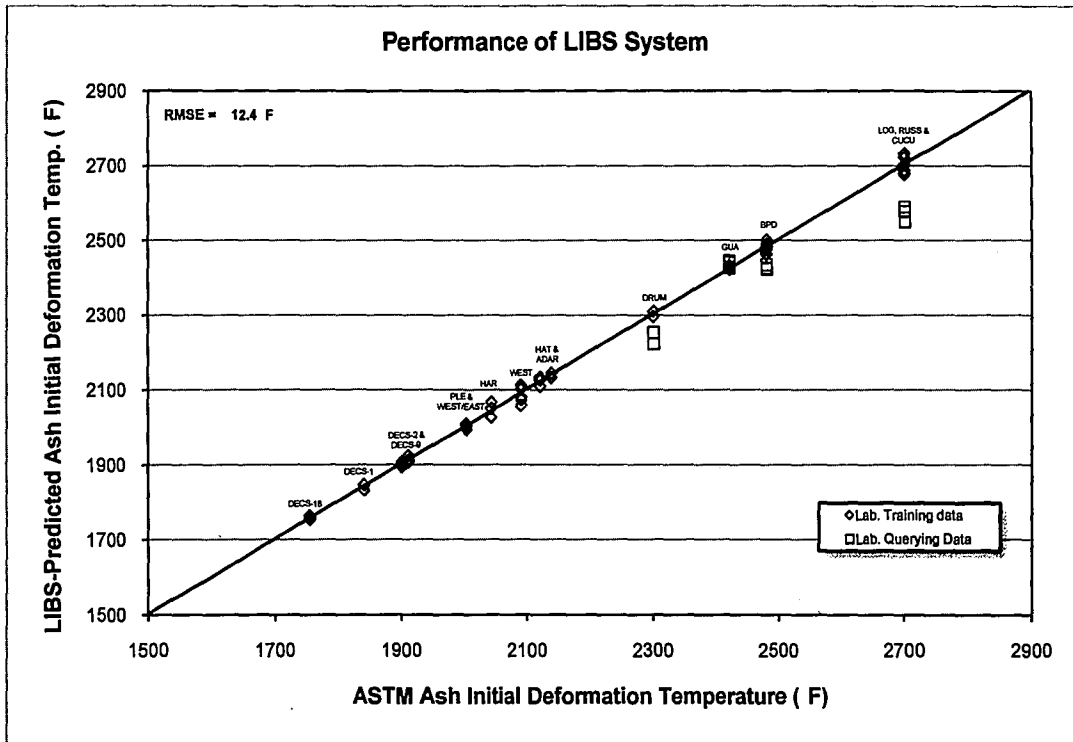
Figure 5-3. Artificial Neural Network Laboratory Results for Coal-ash Initial Deformation Temperature Prediction.

CHAPTER 6

Plant Testing and Results

After obtaining satisfactory results with the LIBS system in the laboratory and developing a sufficiently accurate ANN for the coal-ash initial deformation temperature prediction, the LIBS system was tested in the field, at an electric power generation station. The LIBS system was transported and set-up at a coal-fired power station for testing with the coals fired at the plant. This chapter reports a description of the station, field test procedure, LIBS instrumentation and set-up, and test results obtained at the power station with the LIBS system.

The electric power generation station chosen to carry out the field tests was Brayton Point Station, located in Massachusetts and owned by Dominion Energy. The Brayton Point Station has three coal-fired units and one oil-fired unit, with an installed generating capacity of 1,600 MW (1,150 MW coal-fired), which is the largest coal-fired station in New England. The station burns approximately 400 tons of coal per hour when the coal-fired units operate at full load. The Brayton Point fuel feedstock is composed of Eastern U.S. bituminous coals from Colorado and Pennsylvania, and a variety of South American coals from Colombia and Venezuela. The variability in coal feedstock at Brayton Point poses a significant challenge to the station. Some of the coals at the station have a mineral composition that is susceptible to high-temperature slagging. At times, the station needs to take remedial actions on a retroactive basis, to mitigate the impact of slagging fuels.

The LIBS system field testing was concentrated on the coal supply fired at Brayton Point Unit 3. Unit 3 is a 630 MW_g, supercritical, double reheat unit with a main steam flow rate of 4,050 klb/hr at 3,800 psig and 1,005 °F at the superheater outlet. The high pressure reheater has a design flow of 3,050 klb/hr at 348 psig and 1,055 °F. The temperature set-points for main steam, first and second reheat steam are 1,000; 1,025; and 1,040; respectively. Brayton Point Unit 3 is equipped with five Babcock & Wilcox (B&W) MPS-89K pulverizers that supply coal to 40 burners arranged in four elevations on the front and rear walls, with five burners per wall, per row. These mills have a design capacity of 50 tons/hr of coal, and are retrofitted with B&W rotating dynamic classifiers for on-line fineness adjustment. Brayton Point Unit 3 is also equipped with B&W DRB-XCL low NO_x burners, overfire (OFA) ports, and a selective catalytic reduction (SCR) system for additional NO_x emissions control. Brayton Point Station monitors Unit 3's FEGT with an optical pyrometer, and activate boiler sootblowers to maintain a target FEGT level that does not exceed the predetermined fusion temperature of the ash.

The majority of the samples collected for the LIBS testing were grab samples obtained from the conveyor belt that supplies coal to the 31-Feeder at Brayton Point Unit 3. Figure 6-1 shows a layout of the coal delivery system at Brayton Point and specifies the sampling point during the field testing. The grab samples were collected by Brayton Point personnel on a two hour basis during three days, for each one of three different coals lined up for the LIBS testing, previously arranged with the station. The coals used during the tests were Calenturitas (from Colombia), Central Appalachian (from Eastern U.S.), and Drummond (from Colombia), in that order. Additional coal samples were collected from coal pipes associated to the burners
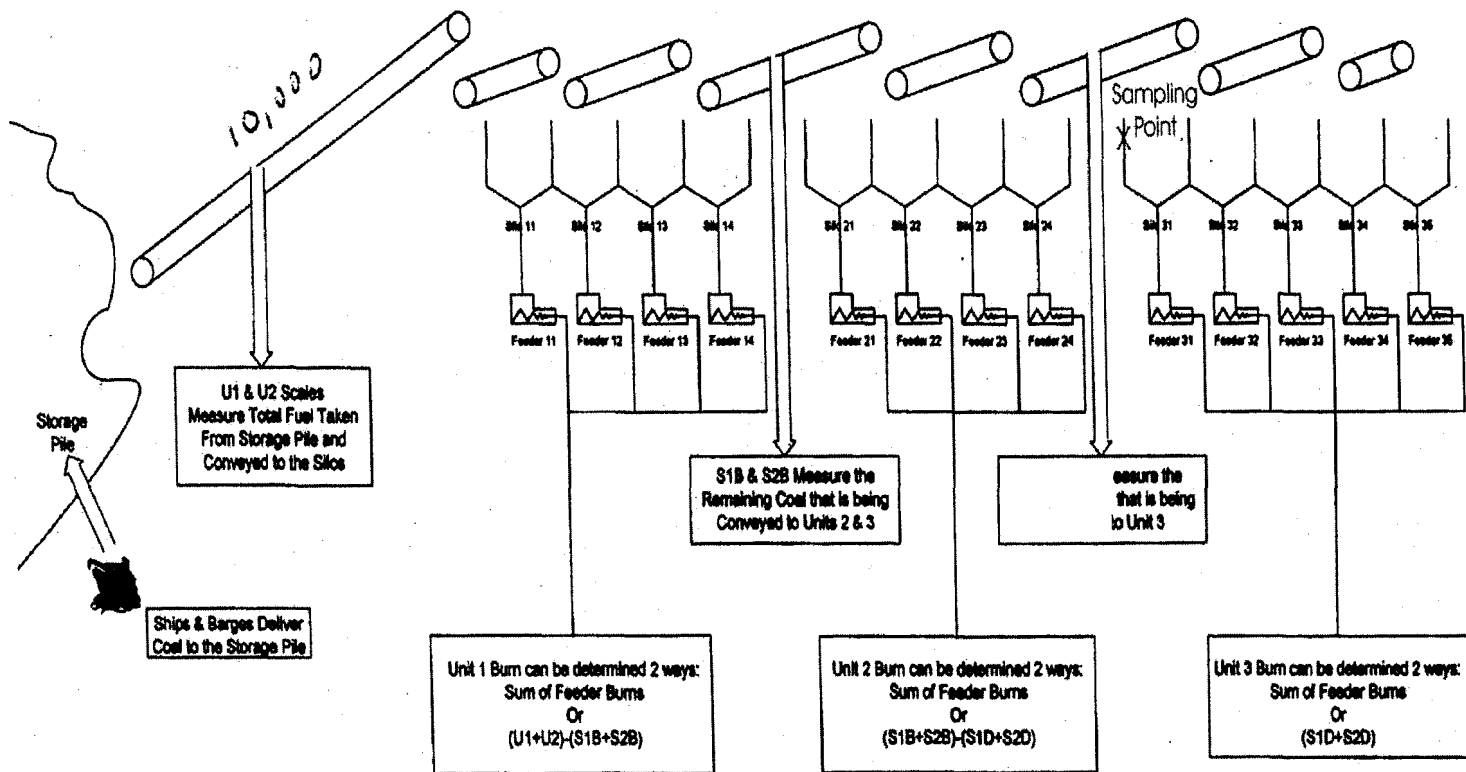
Figure 6-1. Layout of Coal Delivery System at Brayton Point Station.

linked to the 31-Pulverizer. Calenturitas and Drummond coals are known for having relatively low ash fusion temperatures, hence, they are known to cause slagging in the Unit 3 boiler. The Central Appalachian coal is known for having high ash fusion temperature, hence, it is known not to cause any slagging problem at Unit 3. These slagging behaviors from the coals were the main reason for choosing them for the LIBS plant testing.

After daily sample collection by the plant personnel, one of the daily samples was split in two halves. The first half was sent to Consol Energy, in Pennsylvania, for ASTM coal-ash mineral and ash fusion temperatures analyses. The second half, and the rest of the samples collected through the day, were sent to Thielsch Engineering in Rhode Island for grinding and drying. They were ground to 60 mesh (250 µm) and dried in a laboratory furnace for two hours at 110 °C; these samples were returned to Brayton Point for LIBS testing for next day analysis. This preparation procedure was carried out to be compatible with the procedure followed for ASTM laboratory analysis.

The LIBS system, described in Chapter 3, was transported to Brayton Point Station to perform field tests on the coals mentioned in the preceding paragraphs. In general, the set-up for the LIBS system used at Brayton Point was the same as the one used in the laboratory, described in Chapter 3. The experimental set-up consisted of a sample chamber, a flow meter for helium inlet control into the chamber, a pressure gauge for chamber pressure monitoring, and a vacuum pump for chamber purging and atmospheric control inside the chamber; which had to be connected through hoses without any need for further set-up. A helium tank was connected through a hose to the system. The helium tank was provided by the plant. An excitation Nd: YAG

(neodymium-doped yttrium aluminum garnet) laser, an optical spectrometer, a photodiode/amplifier unit, and a controller/processing computer completed the set-up. Figure 6-2 shows a picture of the LIBS system taken after assembly at Brayton Point. The main elements from LIBS system are shown in the photograph, as well as the plant's coal yard and conveyor belt, in the background.

Upon receipt of the ground and dried samples from Thielsch Engineering, LIBS system measurements were performed, following the same procedure described in Chapter 3. The samples collected from the coal pipe, were dried in the Brayton Point Chemical Laboratory for 2 hours in a furnace at 230 °F (110 °C), then prepared and run through the LIBS system following this same procedure. Samples were collected and data was acquired from Wednesday February 27th 2008 through Tuesday March 4th 2008, without interruptions for Calenturitas and Central Appalachian coals, in that order. The sample collection and data acquisition was then suspended to wait for the Drummond coal cargo to arrive at the plant. On Tuesday March 11th 2008, the sample collection and data acquisition continued with Drummond coal until Thursday March 13th 2008.

The results from LIBS elemental intensity measurements for all of the three coals analyzed at Brayton Point, are shown in Figures 6-3 through 6-10. The data processing and normalization applied to these results was the same as described in Chapter 4. These figures also include the ASTM results. The mineral oxides reported on the ASTM results from Consol Energy were converted to a molar basis using Equation 4-1 and the elemental ratios were determined. These ASTM elemental ratios were converted to a LIBS ratio basis using the calibration equations shown in Figures

Figure 6-2. LIBS system set-up at Brayton Point Chemical Laboratory.

4-3 through 4-10. The results obtained by both methods are comparable for some of the elements. Results for magnesium, sodium, silicon, and titanium show good agreement between the LIBS measurements and the ASTM method results. However, results for iron, potassium, calcium, and aluminum do not show good correlation. This might be a consequence of the validity of the calibration curves used for the three coals tested at Brayton Point, from which only one of them (Drummond) was tested in the laboratory and included in the calibration curves. Furthermore, from these four elements, three of them (iron, potassium, and aluminum) were reported as ratios with respect to calcium. The obtained calcium signal was not very good and/or stable, and therefore, affected the behavior of the other three elemental signals (iron, potassium, and aluminum). Additionally, the ASTM-determined average calcium concentration for Central Appalachian coal is lower than for most of the coals included in the calibration
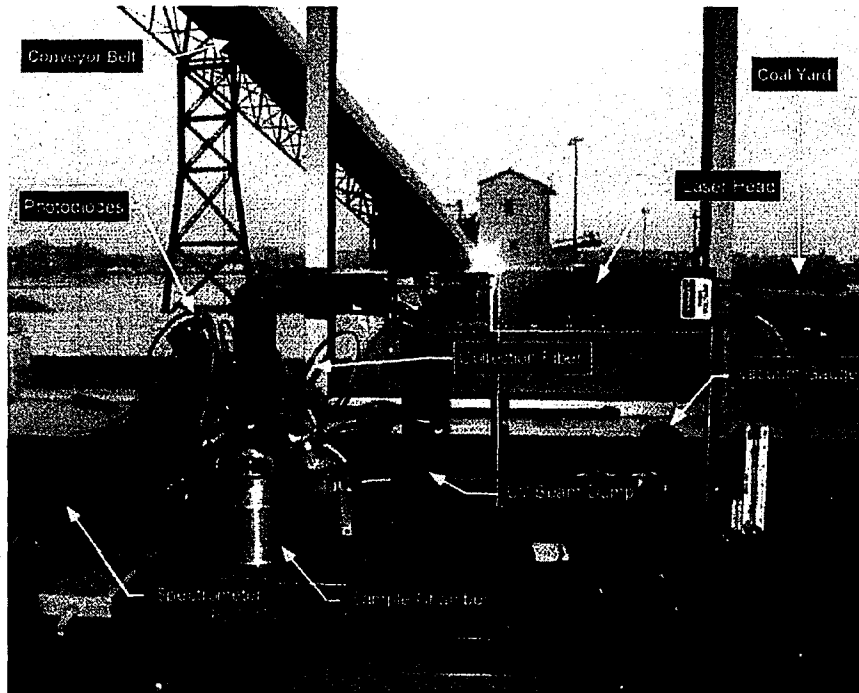
90

Figure 6-2. LIBS system set-up at Brayton Point Chemical Laboratory.

4-3 through 4-10. The results obtained by both methods are comparable for some of the elements. Results for magnesium, sodium, silicon, and titanium show good agreement between the LIBS measurements and the ASTM method results. However, results for iron, potassium, calcium, and aluminum do not show good correlation. This might be a consequence of the validity of the calibration curves used for the three coals tested at Brayton Point, from which only one of them (Drummond) was tested in the laboratory and included in the calibration curves. Furthermore, from these four elements, three of them (iron, potassium, and aluminum) were reported as ratios with respect to calcium. The obtained calcium signal was not very good and/or stable, and therefore, affected the behavior of the other three elemental signals (iron, potassium, and aluminum). Additionally, the ASTM-determined average calcium concentration for Central Appalachian coal is lower than for most of the coals included in the calibration
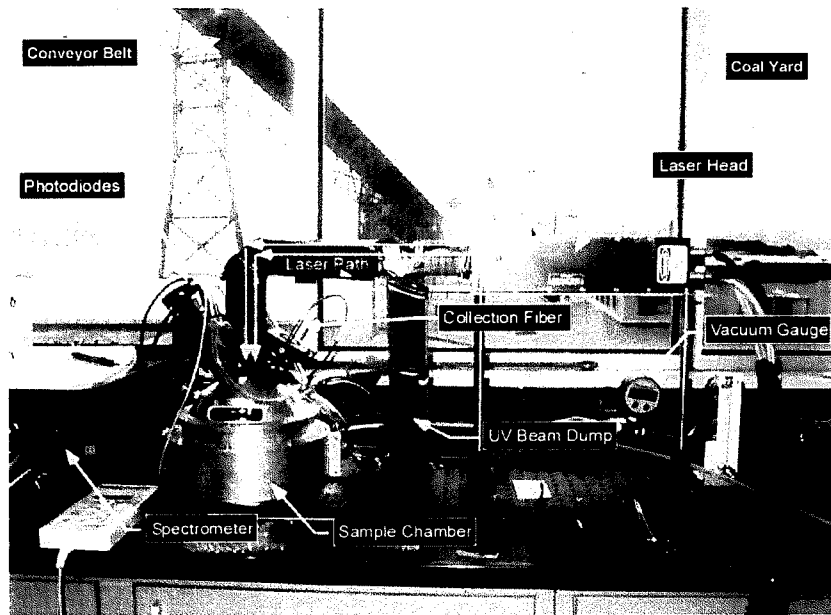
90

curves. Only one of the coals included in the calibration curves (CUCU) had lower calcium concentration than Central Appalachian coal. CUCU had a calcium concentration of 0.007 mol % and Central Appalachian had an average calcium concentration of 0.020 mol %. The next coal with larger calcium concentration than Central Appalachian included in the calibration curves was GUA, with 0.027 mol % of calcium.

Figure 6-3. Results for Fe achieved at Brayton Point Station.

Performance of LIBS System at Brayton Point Station
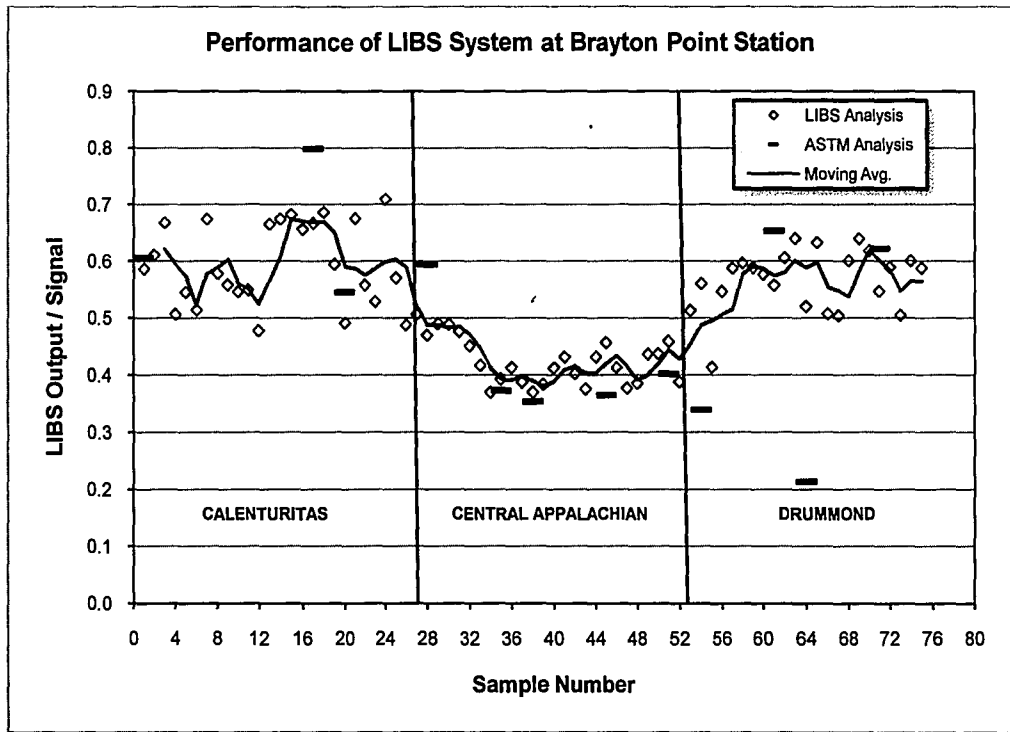
Figure 6-4. Results for Mg achieved at Brayton Point Station.

Performance of LIBS System at Brayton Point Station
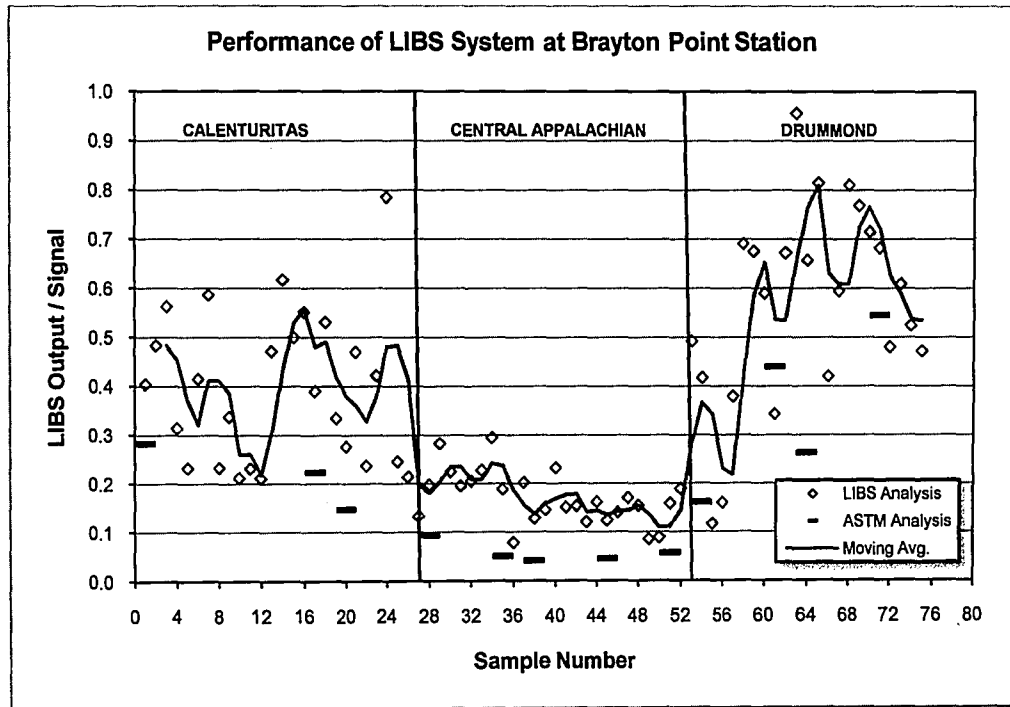
Figure 6-5. Results for Na achieved at Brayton Point Station.
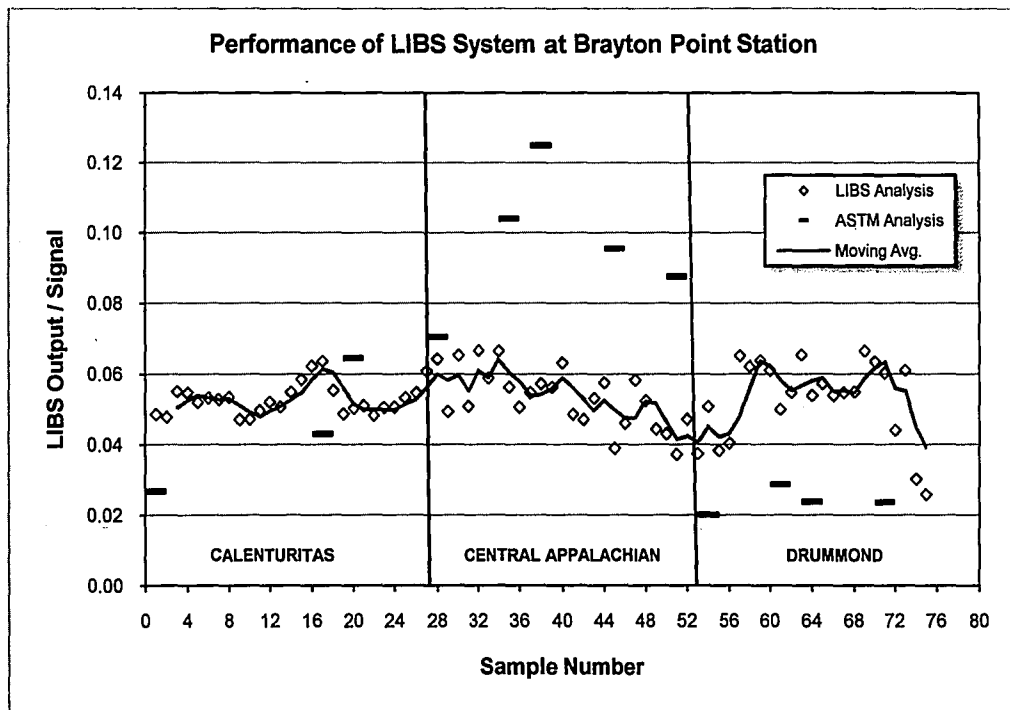
Figure 6-6. Results for K achieved at Brayton Point Station.

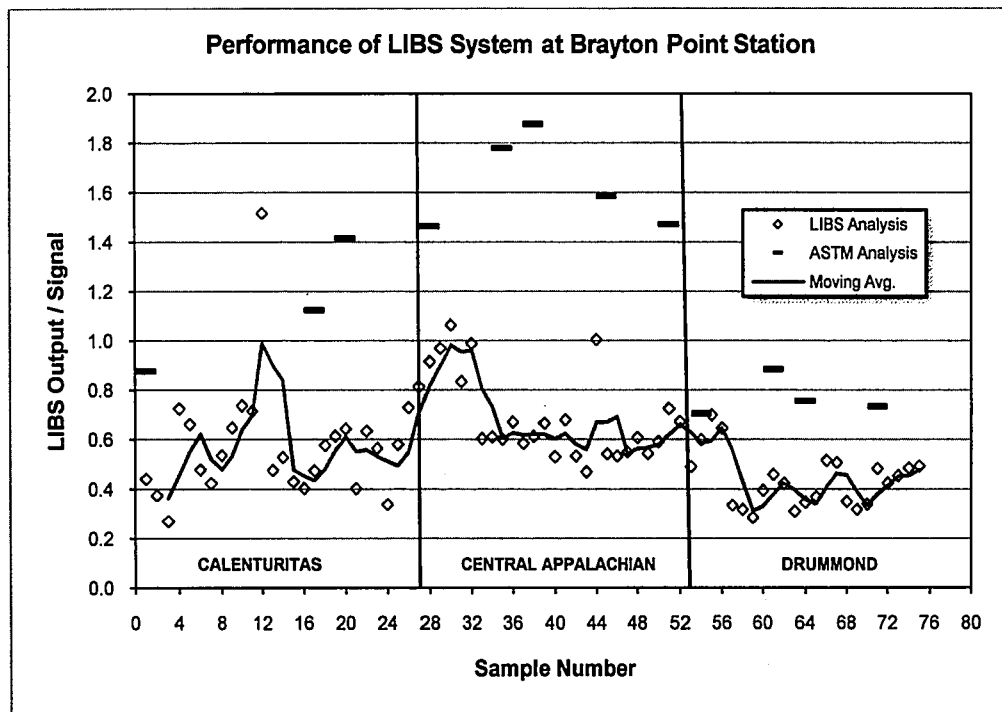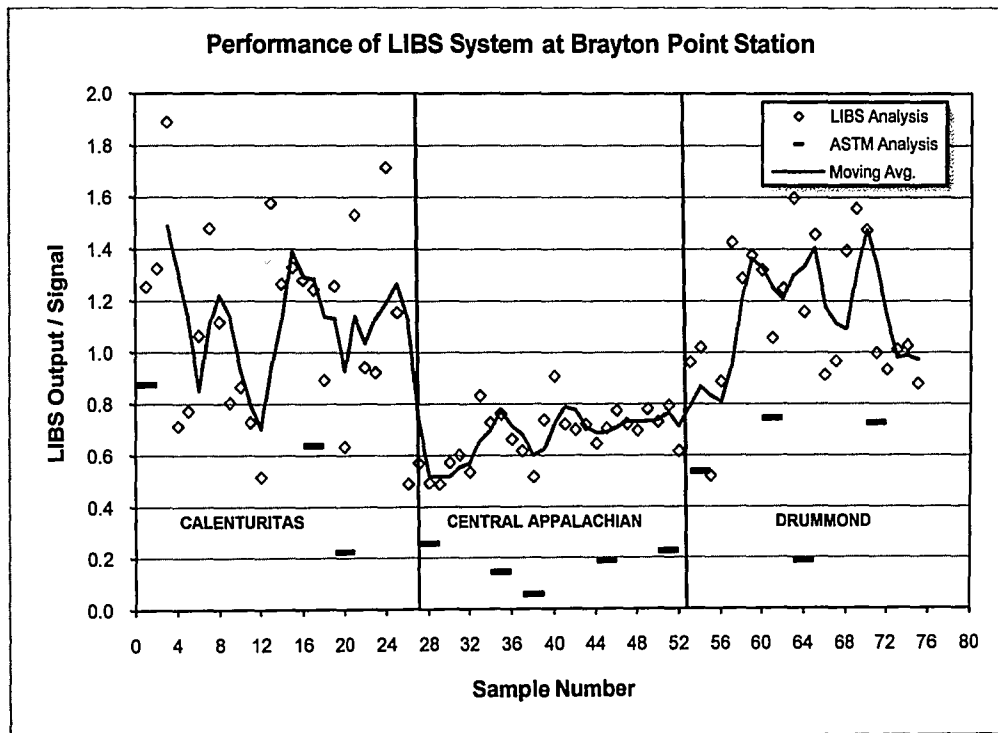**Figure 6-7.** Results for Ca achieved at Brayton Point Station.
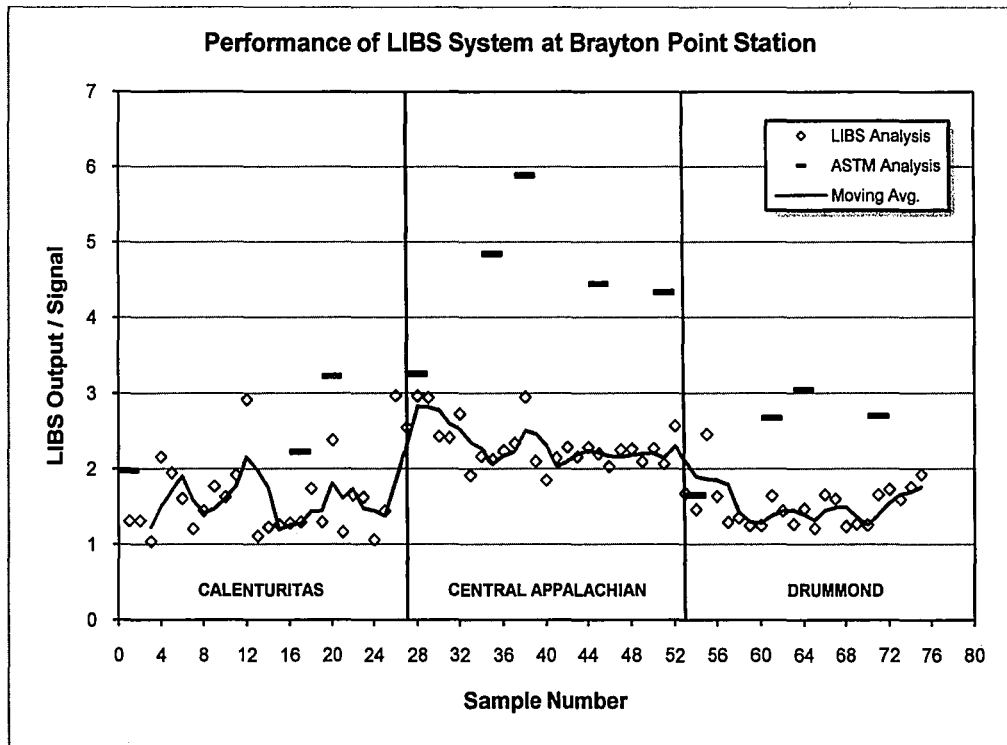
Figure 6-8. Results for Al achieved at Brayton Point Station.
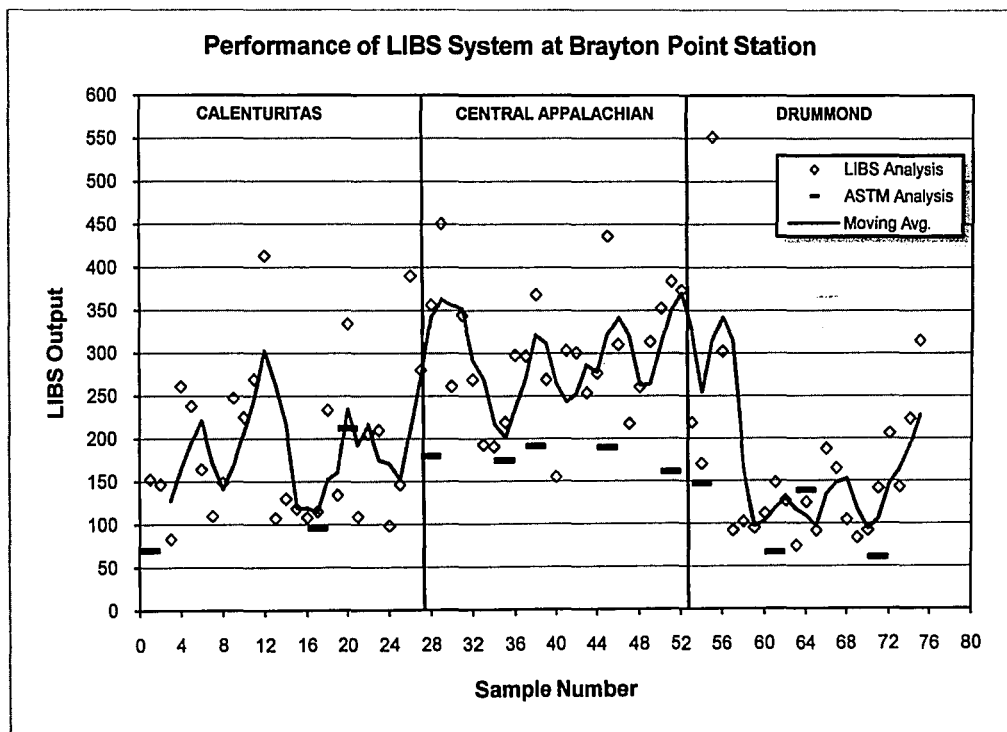
Figure 6-9. Results for Si achieved at Brayton Point Station.

94
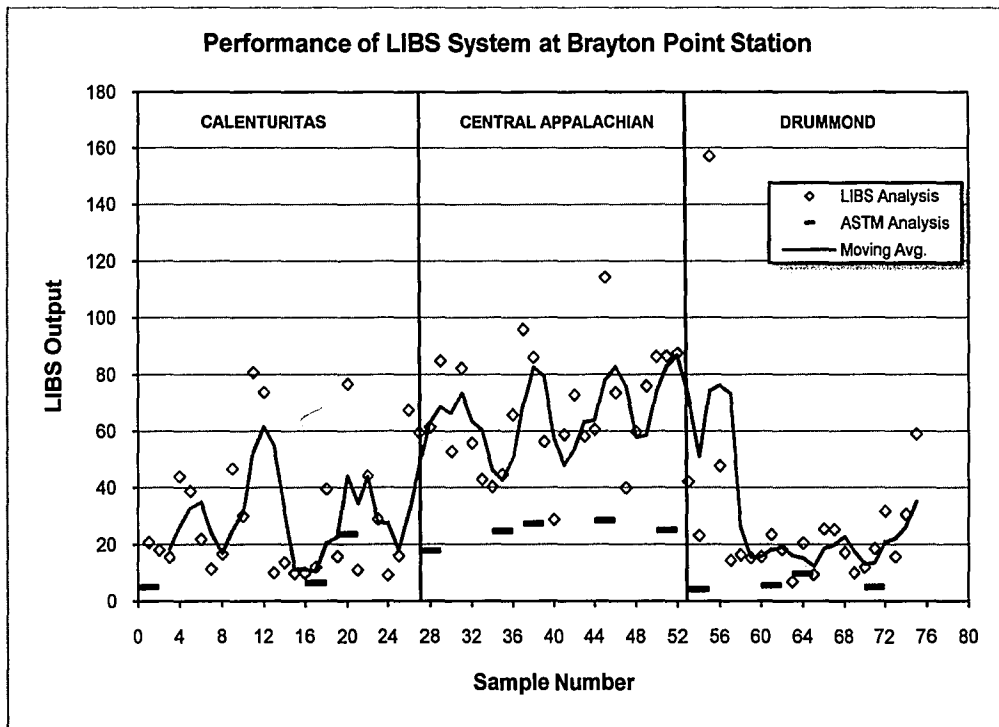
Figure 6-10. Results for Ti achieved at Brayton Point Station.

Table 6-1 includes a summary of the averaged coal-ash mineral composition for the three coals analyzed at Brayton Point with the ASTM methods and LIBS.

Table 6-1. Summary of ASTM and LIBS-based Results for Brayton Point Coal-ash Mineral Composition.

Element	Calenturitas		Central Appalachian		Drummond	
(% mol.)	ASTM	LIBS	ASTM	LIBS	ASTM	LIBS
Si	0.710	0.834	0.888	1.423	0.545	0.804
Al	0.321	0.444	0.525	0.963	0.236	0.418
Ti	0.009	0.013	0.014	0.031	0.006	0.015
Fe	0.060	0.079	0.067	0.120	0.032	0.059
Ca	0.024	0.066	0.020	0.085	0.020	0.063
Mg	0.030	0.034	0.025	0.045	0.016	0.031
Na	0.023	0.060	0.011	0.048	0.031	0.071
K	0.033	0.095	0.059	0.120	0.010	0.087

Using the LIBS elemental intensity ratios, the 13 input parameters described in Chapter 5 were determined. The ANN model developed from laboratory data was used to predict coal-ash initial deformation temperatures for each one of the samples run through the LIBS system. Figure 6-11 shows the results obtained at Brayton Point in terms of the predicted coal-ash initial deformation temperature for all three coals (Calenturitas, Central Appalachian, and Drummond). Figure 6-11 also shows coal-ash initial deformation temperatures determined through the ASTM reducing environment method by Consol Energy, as well as the coal-ash initial deformation temperatures reported in the coal certificate that accompanied Calenturitas and Central Appalachian coals, also determined through the ASTM method. No fuel certificate was available for the Drummond coal.
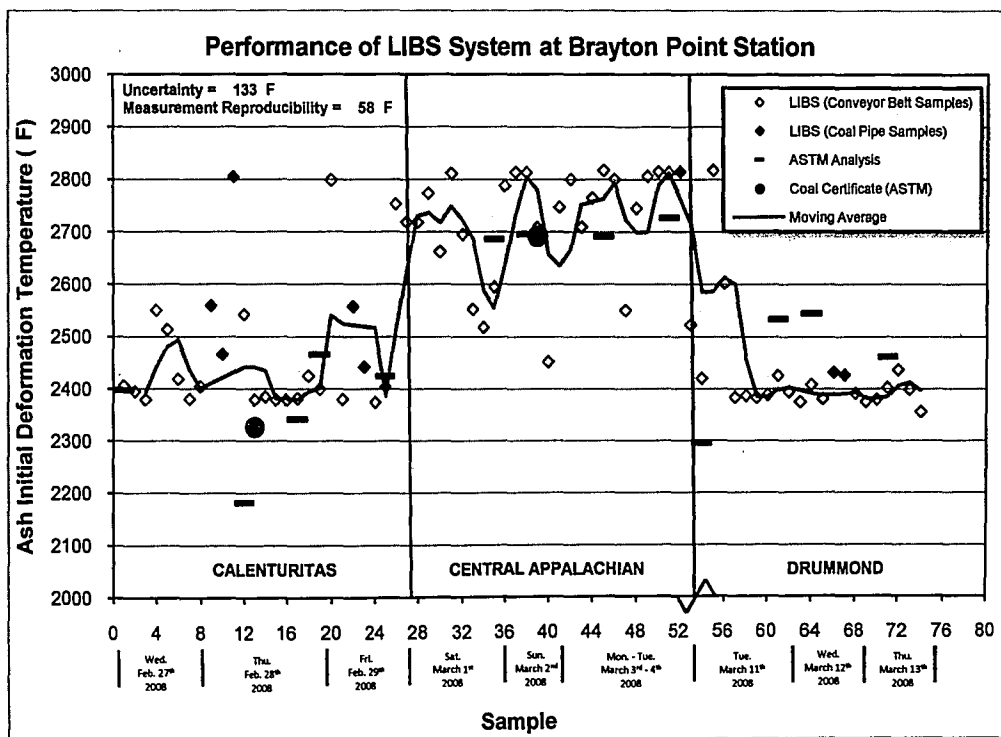
Figure 6-11. Predicted and measured initial deformation temperatures at Brayton Point Station – Feb. 27th through March 13th, 2008.

Twenty conveyor belt Calenturitas samples were analyzed with the LIBS system from February 27th to 29th, 2008. In addition, five Calenturitas samples obtained from Unit 3 coal pipes were analyzed with the LIBS system. Five split samples were provided for analysis by Consol Energy with the ASTM method. The LIBS-based prediction for the initial deformation temperature of Calenturitas coal was 2,434 ± 102 °F. This compares to the average ASTM-based value for initial deformation temperature, which was 2,362 °F ± 110 °F. Twenty five conveyor belt Central Appalachian samples were analyzed from March 1st to 4th, 2008. An additional coal pipe sample was included in the analysis of Central Appalachian coal, and four split samples were analyzed with the ASTM method. The average LIBS-based prediction for the initial deformation temperature of this coal was 2,722 ± 105 °F. This compares to the average ASTM-based determined value for the initial deformation temperature, which was 2,700 °F ± 18 °F. Twenty conveyor belt Drummond samples were analyzed from March 11th to 13th, 2008. Two additional coal pipes samples were included in the Drummond coal analysis, and four split samples were analyzed with the ASTM method. The average LIBS-based prediction for the initial deformation temperature of this coal was 2,432 ± 107 °F. This compares to the average ASTM-based determined value for the initial deformation temperature, which was 2,459 °F ± 115 °F. Table 6-2 shows these results for the three coals tested at Brayton Point. The average LIBS-based results are within approximately 70 °F of ASTM measurements.

Table 6-2. Average Initial Deformation Temperatures for Brayton Point Station Coals.

Coal	ASTM IT (°F)	LIBS IT (°F)
Calenturitas	2,362 ± 110	2,434 ± 102
Central Appalachian	2,700 ± 18	2,722 ± 105
Drummond	2,459 ± 115	2,432 ± 107

Figure 6-11 includes an uncertainty value of ±133 °F, which was calculated using all samples compared with both methods, LIBS and ASTM, for all three coals analyzed at Brayton Point. This error was calculated to evaluate the prediction uncertainty of the LIBS technique as compared to the ASTM reducing environment method through a simple RMSE, given by:

$$RMSE = Uncertainty = \sqrt{\frac{\Sigma(T_{LIBS_i} - T_{ASTM_i})^2}{n}}$$

Eqn. 6-1

where T_{LIBSi} and T_{ASTMi} are the coal-ash initial deformation temperatures evaluated by both methods for sample i, and n is the number of samples used in the comparison. The main reasons for choosing this error for the uncertainty value over others is that it is the same error used for ANN minimization during its training process. The value obtained (±133 °F), seems adequate for the use of LIBS in coal-fired power plants applications to detect changes in slagging propensity of coals, based on their coal-ash initial deformation temperature. This error factors in the variability in the coal sample, and the error and repeatability in the ASTM method.

Figure 6-11 also includes a measurement reproducibility of ±58 °F. This term determines the average prediction precision for the LIBS field measurements performed at Brayton Point for all three coals. It was calculated using the average

relative standard deviation for all three coals, with a 99 percent confidence level, through:

$$Measurement\ Reproducibility = \frac{\sum \left[\frac{2.57 \cdot \sigma_i}{\sqrt{n_i}}\right]}{3} \qquad \textbf{Eqn. 6-2}$$

where σ_i is the standard deviation obtained for the predicted temperatures of coal i, and n_i is the number of samples used for temperature prediction of coal i. The value obtained (±58 °F), is within the tolerance on the measurement for repeatability of the ASTM method for determining coal-ash fusion temperatures.

The LIBS results included in Figure 6-11 are fitted with a 3-sample rolling average. If coal sampling and analysis were performed on an hourly basis, it can be inferred, from Figure 6-11, that the LIBS technology would be capable of providing predicted initial deformation temperature feedback, with enough resolution to advice of changes in fuel quality that may affect the operation of coal-fired boilers to mitigate potential slagging impacts.

Overall, based on results presented in Figure 6-11, there is no distinguishable difference between the initial deformation temperature levels obtained from samples collected from the conveyor belt and samples collected from the coal pipes. Although, the mill pyrite rejection design should contribute to a difference in coal elemental composition and fusion temperatures, sample preparation (grinding, sieving, and drying) used for the grab samples may have precluded noticing the differences between both sample sets.

Figure 6-12 shows the performance of the ANN initial deformation temperature model trained with LIBS data acquired in the laboratory, and queried with additional laboratory data (as shown in Figure 5-2) and data acquired in the field at Brayton Point Station. Figure 6-12 shows a plot of averaged predicted coal-ash initial deformation temperature by the LIBS system versus averaged ASTM coal-ash initial deformation temperature. The temperature values corresponding to the data used for ANN training fall close to the 45 degree line that corresponds to a perfect correlation. Figure 6-12 also shows that predicted temperature from data acquired at a later date in the laboratory, as well as the data acquired in the field could be predicted with a good degree of uncertainty. It should be noticed that the data from two of the fuels tested at Brayton Point, Calenturitas and Central Appalachian, did not participate in the ANN model training. This is an indication that the model may be robust enough to provide predictions of initial deformation temperature for fuels that are not presented to the LIBS system during training and/or calibration process for a particular application. However, these fuels should have an elemental composition close to the composition of the coals used for training.
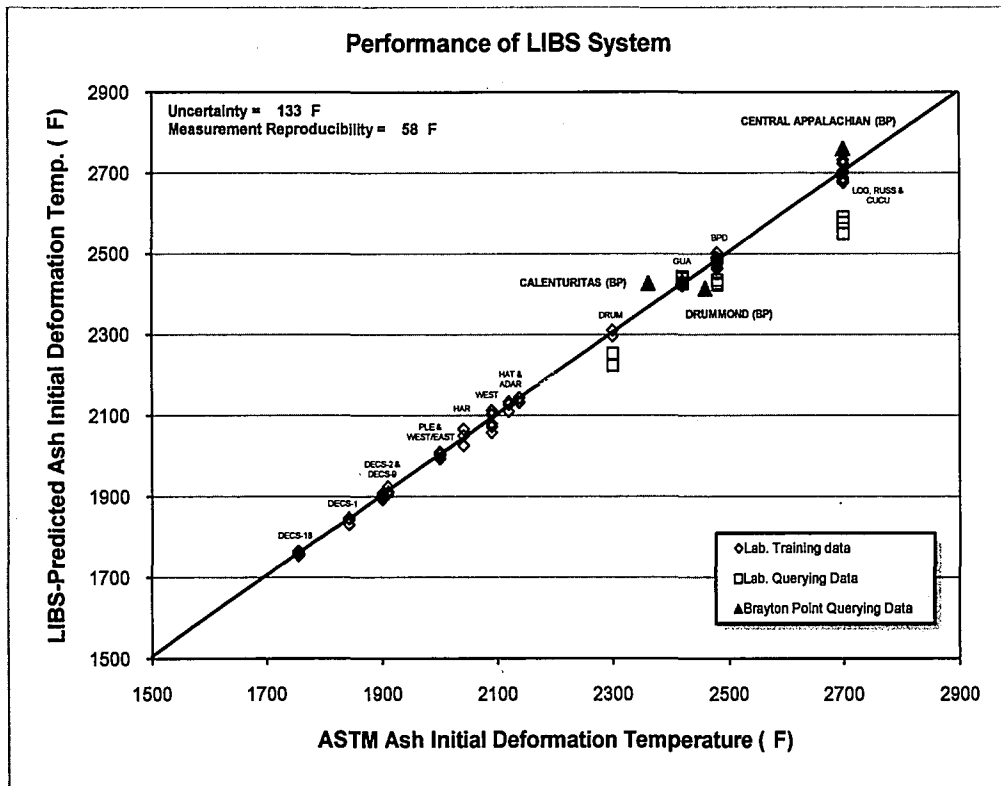
Figure 6-12. Predicted and measured initial deformation temperatures from laboratory tests and field tests (January, February, and March 2008).

CHAPTER 7

Conclusions and Recommendations

Research was performed to assess the feasibility of LIBS to predict coal slagging potential via ANN models, based on LIBS emission intensity measurements and ash fusion temperature predictions. A LIBS measurement system was developed and integrated. The LIBS system was tested in the laboratory using a broad set of coal samples that included U.S. bituminous and sub-bituminous coals, and imported fuels. After development of ANN models, the LIBS system was transported to a power plant and tested in the field. Laboratory and field results showed that the LIBS concept is suitable for use as an advisor for fuel quality change, more specifically for coal slagging potential change, and further mitigation of boiler slagging impacts.

The optical set-up consisted of an excitation Nd: YAG laser, a sample chamber, optical spectrometer, a photodiode/amplifier assembly, and a controller/processing computer. The laser used in the LIBS system was a Q-switched Nd: YAG laser, which yields coincident ultraviolet, visible, and near infrared 7 ns pulses, at a repetition rate of 10 Hz. The spectrometer used was a spectrometer with an Echelle type grating, allowing for high resolution spectra to be collected over a broad wavelength range of 200 to 600 nm. The following elements were measured with the Echelle spectrometer: aluminum, calcium, magnesium, sodium, iron, silicon, and titanium. These elements were chosen because of their participation in the slagging process in coal-fired boilers. The photodiode/amplifier assembly was used to collect intensity traces for the emission

102

line of K at 769.9 nm, as well as the background intensity of the plasma as a function of time.

Laboratory experiments were performed on a coal inventory of sixteen coals collected from different coal-fired power plants and the Pennsylvania State University coal bank. These coals have a broad range of elemental composition and slagging propensity characteristics. The initial deformation temperature for these coal-ashes ranges from 1,755 to 2,700 °F. Samples from each coal were prepared and analyzed independently for ash minerals and fusion temperatures using ASTM Methods 2013, D6349, and D1857. Samples were also analyzed with the LIBS system, collecting emission intensity data for the characteristic emission lines of the elements of interest (Al, Ca, Mg, Na, Fe, Si, Ti, and K). Calibration curves were developed for selected elemental ratios, to relate LIBS intensity ratios to the molar ratio of each element of interest resulting from the standardized analyses. Considering the broad range of concentrations for each elemental ratio, the use of a range of coals with dissimilar ranks, and the very heterogeneous nature of coal, all of the calibration curves exhibited good linear responses. The R^2s of the calibration curves correlations ranges from 0.814 for magnesium to 0.993 for iron. Additionally, uncertainty and reproducibility tests performed on an Eastern U.S. bituminous coal demonstrated that the LIBS instrumentation can yield sufficient repeatability with an acceptable level of uncertainty for commercial LIBS applications. The average measurement difference between the LIBS and the standardized measurements was found to be better than 14 percent (absolute) for all elements; except, for magnesium and potassium. The disparity for magnesium and potassium could be attributed to the overlapping nature of the magnesium spectral line with iron and the performance of the photodiode/amplifier

assembly, as well as the normalization method for potassium emission detection, respectively. The repeatability of the LIBS measurements for one standard deviation was found to be smaller than 18 percent for all the elements.

ANN models were developed to relate elemental intensity ratios measured by the LIBS system to coal-ash initial deformation temperature measured with the ASTM method, under reducing conditions. The type of ANN used for this application was a feed-forward network with back-propagation training algorithm. The elements of interest (aluminum, calcium, magnesium, sodium, iron, silicon, titanium, and potassium) were configured into 13 network input parameters that included their individual concentration ratios and the silica value, base, acid, R250, and dolomite ratio. The initial deformation temperature model predictions using LIBS elemental data were encouraging, demonstrating that the lack of accuracy in the prediction of some of the elemental concentrations may have been compensated by the formulation of the LIBS-based combined parameters and the robustness of the ANN model.

The LIBS system was transported and assembled in the field at Brayton Point Station. The Brayton Point Station has three coal-fired units with a generating capacity of 1,150 MW. The station burns approximately 400 tons of coal per hour, when the coal-fired units operate at full load. The Brayton Point fuel feedstock is composed of Eastern U.S. bituminous coals from Colorado and Pennsylvania and a variety of South American coals from Colombia and Venezuela. The variability in coal feedstock at Brayton Point poses a significant challenge to the station. Some of the coals used at the station have a mineral composition that is susceptible to high-temperature slagging.

Thus, at times, the station needs to take remedial actions on a retroactive basis, to mitigate the impact of slagging fuels.

Static LIBS measurements were performed in the field at Brayton Point Station. Three coals were tested at Brayton Point: Calenturitas (from Colombia), Central Appalachian (from Eastern U.S.), and Drummond (from Colombia), in that order. The Brayton Point field results indicated an average LIBS-based prediction for the Calenturitas fusion temperature of 2,434 ± 102 °F as compared to 2,362 ± 110 °F obtained from the ASTM tests. The corresponding average LIBS-based prediction for Central Appalachian coal was 2,722 ± 105 °F as compared to 2,700 ± 18 °F for the ASTM tests. The corresponding average LIBS-based prediction for Drummond coal was 2,432 ± 107 °F as compared to 2,459 ± 115 °F for the ASTM tests. The field results demonstrated that LIBS coal analyses performed on an hourly basis would be capable of providing predicted initial deformation temperature feedback with enough resolution to advice of changes in fuel quality. The average uncertainty for the initial deformation temperature prediction for all three coals tested at Brayton Point was ± 133 °F. The average precision for the LIBS measurements for all three coals was ± 58°F, which is a value that is within the tolerance on the measurement for repeatability and reproducibility of the ASTM methods for ash fusion temperatures, which is ±176 °F.

The LIBS concept proven in this work aims at determining the coal-ash initial deformation temperature to be used as a slagging index. The coal-ash initial deformation temperature would be ultimately provided to boilers operators and used to coordinate coal yard operations and adjust boiler control settings. The main idea would be to maintain FEGTs below the LIBS-estimated coal-ash initial deformation

temperature and, therefore, mitigate the adverse impact of slagging inside the boiler. The feasibility of using a LIBS system to produce estimated coal-ash initial deformation temperature was demonstrated in this research. However, further development of the LIBS system and its validation needs to be carried out before the system is suitable for on-line deployment in power plants.

Some recommendations on further development needed for LIBS system operation improvement and better suitability for its use in power plants as a compact on-line system, are:

(1) An automated sample collecting procedure should be developed, for an effective on-line operation, by complying with the ASTM standardized methodology (ASTM D-2234, Standard Practice for Collection of a Gross Sample of Coal). There are automated commercially available sampling systems that comply with the ASTM Method D-2234. An example is the cross-belt hammer sampler design (M&W Group), which allows taking out representative raw coal samples from an operating belt conveyor without stopping the belt. The coal is passed through a twin-roll crusher for crushing raw coal to a specified size. The total extracted coal sample is divided into a number of statistically identical but smaller samples by a rotary tube divider in accordance with ASTM D-2013, which ensures that, through a continuous automatic sample division, the divided sample is statistically representative.

(2) The atmospheric conditions inside the testing chamber should be optimized to allow operation of the LIBS system at only one condition for all elements of interest. Further work should be carried to design a sample chamber that

provides satisfactory results for a complete characterization of coal samples in one single run.

(3) The performance for the LIBS-based potassium and magnesium measurements should be improved on their uncertainty. In this study, spectral processing was done using one specific wavelength. However, different elements have different characteristic wavelengths in the spectrum. An increment in the number of wavelengths used for each element would enhance the LIBS-based measurements accuracy as compared to the ASTM-based measurements.

(4) A different approach for predicting coal-ash initial deformation temperature, like Support Vector Machines (or SVM), could be better suited for this application. The SVM uses a more effective analytical methodology for reaching a minimum error, which could offer better repeatability and uncertainty in the prediction of the coal-ash fusion temperatures, having the advantage of working well with reduced data sets.

REFERENCES

[1]   Energy Information Administration. Official Energy Statistics from the U.S. Government, DOE. Electric Power Monthly March 2008 Edition, www.eia.doe.gov/cneaf/electricity/epm_sum.html, downloaded March 20th 2008.

[2]   Painter, P.C., Rimmer, S. M., Snyder, R. W., and Davis A. (1981) "A Fourier Transform Infrared Study of Mineral Matter in Coal: The Application of a Least Squares Curve-Fitting Program" *Applied Spectroscopy*, Society for Applied Spectroscopy, Vol. 35, No. 1, p102.

[3]   Romero, C., Sarunac, N., and Levy, E. (2001) "Swootblowing Optimization in Coal-Fired Boilers." Twenty-sixth Int. Technical Conference on Coal Utilization & Fuel Systems, Clearwater, Florida, March, 2001.

[4]   Couch, G. (1994) "Understanding slagging and fouling in pf combustion." IEA Coal Research, London, United Kingdom.

[5]   Raask, E. (1985) "Mineral impurities in coal combustion: behavior, problems, and remedial measures." Hemisphere Publishing Corporation, New York.

[6]   Singh, J. P., and Thakur, S. N. (2007) "Laser-Induced Breakdown Spectroscopy." Elseiver, Oxford, United Kingdom.

[7]   Wallis, F. J., Chadwick, B. L., and Morrison, R. (2000) "Analysis of Lignite Using Laser-Induced Breakdown Spectroscopy." *Applied Spectroscopy*, Society for Applied Spectroscopy, Vol. 54, No. 8, p1231.

[8]   Body, D., and Chadwick, B.L. (2000) "Simultaneous elemental analysis system using laser induced breakdown spectroscopy." *Review of Scientific Instruments*, American Institute of Physics, Vol. 72, No. 3, p1625.

[9]   Ottesen, D. K., Wang, J. C. F., and Radziemski, L. J. (1989) "Real-Time Laser Spark Spectroscopy of Particulates in Combustion Environments." *Applied Spectroscopy*, Society for Applied Spectroscopy, Vol. 43, No. 6, p967.

[10]   Ottesen, D. K., Baxter L. L., Radziemski, L. J., and Burrows J. F. (1991) "Laser Spark Emission Spectroscopy for in Situ, Real-Time Monitoring of Pulverized Coal Particle Composition." *Energy & Fuels*, American Chemical Society, Vol. 5, No. 2, p304.

[11]   Özbayoğlu, G., and Özbayoğlu, M. E. (2006) "A new approach for the prediction of ash fusion temperatures: A case study using Turkish lignites." *Fuel*, Elsevier, Vol. 85, p545.

[12]   Scheetz, B. E. "Chemistry and Mineralogy of Coal Fly Ash: Basis For Beneficial Use." Materials Research Institute, The Pennsylvania State University, University Park, Pennsylvania, www.mcrcc.osmre.gov/PDF/Forums/CCB5/1.4.pdf, downloaded March 15th 2008.

[13]   Tishmack, J. K. "Bulk Chemical and Mineral Characteristics of Coal Combustion By-Products (CCB)." School of Civil Engineering, Purdue University, West Lafayette, Indiana, www.mcrcc.osmre.gov/PDF/Forums/CCB/3-1.pdf, downloaded March 28th 2008.

[14]   Hatt, R. "Influence of Coal Quality and Boiler Operating Conditions on Slagging of Utility Boilers." Coal Combustion, Inc, Versailles, Kentucky, www.coalcombustion.com/PDF%20Files/UEFInfluenceSlag03.pdf, downloaded March 20th 2008.

[15]   Hatt, R. (1990) "Fireside Deposits in Coal-Fired Utility Boilers." *Progress in Energy and Combustion Science*, Pergamon Press, Vol. 16, p235.

[16]   Jackson, P. J., and Jones A. R. (1983) "Fireside Fouling Experience in Large CEGB Boilers." *Proceedings of the 1981 Conference on Fouling and Slagging Resulting From Impurities in Combustion Gases*, Engineering Foundation, New York, New York, p1.

[17]   Hein, K. (1991) "Deposit Formation Due to Mineral Impurities in Coals." *Proceedings for the Second International Symposium On Coal Combustion*, China Machine Press, Beijing, China, p23.

[18]   Speight, J. G. (2005) "Handbook of Coal Analysis." *Chemical Analysis: A Series of Monographs on Analytical Chemistry and Its Applications*, Wiley-Interscience, Hoboken, New Jersey.

[19]   Gray, R. J., and Moore, G. F. (1974) "Burning the sub-bituminous coals of Montana and Wyoming in large utility boilers." *Paper 74-WA/FU-1*, ASME.

[20]   Sneddon, J., and Lee, Y. (2000) "Application of laser-induced breakdown spectrometry in urban health." *Microchemical Journal*, Elsevier, Vol. 67, No. 1, p201.

[21]   Liangying, Y., Jidong L., Wen, C., Ge, W., Kai, S., and Wei, F. (2005) "Analysis of Pulverized Coal by Laser-Induced Breakdown Spectroscopy." *Plasma Science & Technology*, Vol. 7, No. 5, p3041.

[22]   Winegartner, E. C. (1974) "Coal Fouling and Slagging Parameters." *ASME Research Committee on Corrosion and Deposits from Combustion Gases*, ASME Publications.

[23]   Yueh, F., Singh, J. P., and Zhang, H. (2000) "Laser-induced Breakdown Spectroscopy, Elemental Analysis" *Encyclopedia of Analytical Chemistry*, John Wiley & Sons Ltd, p2066.

[24]   Naumova, N. N., and Khokhlov, V. N. (2006) "A method and an algorithm for rapid computation of the Voigt function" *Journal of Optical Technology*, Optical Society of America, Vol. 73, No. 8, p509.

[25]   Lawrence, A., Kumar, R., Nandakumar, K., and Narayanan, K. (2007) "A Novel tool for assessing slagging propensity of coal in PF boilers." *Fuel*, Elsevier, Vol. 87, p947.

APPENDIX

Back Propagation Network
The network has 4 layers.
Layer 1 has 13 Linear nodes.
Layer 2 has 7 Sigmoid nodes.
Layer 3 has 3 Sigmoid nodes.
Layer 4 has 1 Sigmoid nodes.
Weights:
Layer 2
Node 1 Bias is 0.709434615660173
Node 1 Weight from 1 is   -0.438934652543804
Node 1 Weight from 2 is   -0.409021151025188
Node 1 Weight from 3 is   -0.638170028818858
Node 1 Weight from 4 is   -0.381883559991407
Node 1 Weight from 5 is   0.556959017567289
Node 1 Weight from 6 is   -1.01226412518353
Node 1 Weight from 7 is   -1.17428278660362
Node 1 Weight from 8 is   -0.675008287300382
Node 1 Weight from 9 is   -0.0682738084415549
Node 1 Weight from 10 is   0.0940036701547087
Node 1 Weight from 11 is   -0.29275597025527
Node 1 Weight from 12 is   0.0794807459572662
Node 1 Weight from 13 is   -0.276312808775029
Node 2 Bias is -1.61333722224014
Node 2 Weight from 1 is   -0.486974549242594
Node 2 Weight from 2 is   0.5696318653675
Node 2 Weight from 3 is   0.513012766349723
Node 2 Weight from 4 is   0.0590570333324532
Node 2 Weight from 5 is   1.70851521038405
Node 2 Weight from 6 is   0.855331484103262
Node 2 Weight from 7 is   -0.303976231027773
Node 2 Weight from 8 is   -4.02625261403027
Node 2 Weight from 9 is   1.69995867930812
Node 2 Weight from 10 is   0.106768573955792
Node 2 Weight from 11 is   4.17271525478355
Node 2 Weight from 12 is   -1.10350854274895
Node 2 Weight from 13 is   -1.37092627325191
Node 3 Bias is 1.36643640839952
Node 3 Weight from 1 is   1.04244237631491
Node 3 Weight from 2 is   -1.70566922863182
Node 3 Weight from 3 is   0.423566469176409
Node 3 Weight from 4 is   0.911190259479048
Node 3 Weight from 5 is   -1.0696682569899
Node 3 Weight from 6 is   0.362934443480053
Node 3 Weight from 7 is   1.0206611659887
Node 3 Weight from 8 is   1.47739249923042

111

Node 3 Weight from 9 is   -2.76637073434191
Node 3 Weight from 10 is   -1.14567474345322
Node 3 Weight from 11 is   -1.74698943816803
Node 3 Weight from 12 is   0.165255460603235
Node 3 Weight from 13 is   0.184828140009444
Node 4 Bias is   0.447310086450612
Node 4 Weight from 1 is   0.12104464662551
Node 4 Weight from 2 is   -0.326658473021021
Node 4 Weight from 3 is   -0.869435266580844
Node 4 Weight from 4 is   0.798960496499294
Node 4 Weight from 5 is   0.966961991518112
Node 4 Weight from 6 is   -1.26698912688768
Node 4 Weight from 7 is   -0.356992745266558
Node 4 Weight from 8 is   -1.48765085765933
Node 4 Weight from 9 is   0.294635358647163
Node 4 Weight from 10 is   0.425307651474313
Node 4 Weight from 11 is   1.6876579655814
Node 4 Weight from 12 is   1.13377432470861
Node 4 Weight from 13 is   -0.108433458076621
Node 5 Bias is   -0.203722895657545
Node 5 Weight from 1 is   0.343377655827897
Node 5 Weight from 2 is   -3.85084020682303
Node 5 Weight from 3 is   -0.846975413429581
Node 5 Weight from 4 is   0.891539030389835
Node 5 Weight from 5 is   0.67289472721367
Node 5 Weight from 6 is   -1.82364850668168
Node 5 Weight from 7 is   3.09186178977527
Node 5 Weight from 8 is   -1.11465842097006
Node 5 Weight from 9 is   -2.92593354683847
Node 5 Weight from 10 is   -3.57187313738789
Node 5 Weight from 11 is   0.0375280117244243
Node 5 Weight from 12 is   -2.01884175628045
Node 5 Weight from 13 is   -1.14871073410383
Node 6 Bias is   -2.38530332468881
Node 6 Weight from 1 is   1.08558367674053
Node 6 Weight from 2 is   -0.908775094826169
Node 6 Weight from 3 is   -0.119078648732092
Node 6 Weight from 4 is   1.42929777743578
Node 6 Weight from 5 is   1.70587765836488
Node 6 Weight from 6 is   -0.199777518192946
Node 6 Weight from 7 is   -1.49371688317031
Node 6 Weight from 8 is   0.802808622458271
Node 6 Weight from 9 is   -1.19058869571304
Node 6 Weight from 10 is   -3.33776964938018
Node 6 Weight from 11 is   1.53172386409973
Node 6 Weight from 12 is   2.11979471959807
Node 6 Weight from 13 is   -2.38784292949053
Node 7 Bias is   -0.878613215157914
Node 7 Weight from 1 is   -0.318951407782165
Node 7 Weight from 2 is   0.0640860446665442
Node 7 Weight from 3 is   1.07785975484523
Node 7 Weight from 4 is   -0.342082367935877

Node 7 Weight from 5 is   -0.694963390421251
Node 7 Weight from 6 is   1.04504019183502
Node 7 Weight from 7 is   0.169241330208606
Node 7 Weight from 8 is   1.79423492117223
Node 7 Weight from 9 is   -0.721114786182033
Node 7 Weight from 10 is   -0.215695028021651
Node 7 Weight from 11 is   -1.617775123215914
Node 7 Weight from 12 is   -1.17441800143557
Node 7 Weight from 13 is   -0.361333761298183
Layer 3
Node 1 Bias is -0.415806190230554
Node 1 Weight from 1 is   -2.09709523373361
Node 1 Weight from 2 is   -4.65536031025559
Node 1 Weight from 3 is   0.730538680452332
Node 1 Weight from 4 is   -3.6048596662002
Node 1 Weight from 5 is   3.1217333790664
Node 1 Weight from 6 is   2.58985392638764
Node 1 Weight from 7 is   3.89244290634506
Node 2 Bias is 1.73564804121032
Node 2 Weight from 1 is   1.51961298060351
Node 2 Weight from 2 is   -6.98606636265848
Node 2 Weight from 3 is   4.40390461451378
Node 2 Weight from 4 is   -1.26016078647006
Node 2 Weight from 5 is   -4.96616140386536
Node 2 Weight from 6 is   -7.04715438235208
Node 2 Weight from 7 is   1.75543400603326
Node 3 Bias is -0.302802382971918
Node 3 Weight from 1 is   0.154155484737341
Node 3 Weight from 2 is   -0.662199417532671
Node 3 Weight from 3 is   -1.18110072235361
Node 3 Weight from 4 is   -0.566230554438374
Node 3 Weight from 5 is   0.988226240475782
Node 3 Weight from 6 is   -0.396203279730178
Node 3 Weight from 7 is   -0.142102095421979
Layer 4
Node 1 Bias is 0.317921126949299
Node 1 Weight from 1 is   9.0728587391005
Node 1 Weight from 2 is   -9.88312951246018
Node 1 Weight from 3 is   1.37229147761657

VITA

Ricardo X. Moreno

Date of Birth: December 7th, 1981

Place of Birth: Merida, Venezuela

Name of Parents: Eladio Moreno and Ligia Maldonado

Education:

Lehigh University, Bethlehem, PA, USA
Master of Science in Mechanical Engineering (to be awarded)   09/2008

University of Los Andes, Merida, Venezuela
Bachelor of Science in Mechanical Engineering, graduated first in   10/2004
class of 48 with CUM LAUDE distinction

Professional Experience:

Research Assistant   07/2006 – 05/2008

Energy Research Center, Lehigh University, Bethlehem, PA
Assisted Research Scientists on different projects on power plant unit performance, including laboratory testing, field testing, data processing and analysis, and development of artificial neural networks

Maintenance Resident Engineer   09/2005 – 03/2006

INTEVEN, Caracas, Venezuela
Managed the heavy machinery maintenance workshop, created and followed-up a maintenance database including all the machinery.

END OF TITLE